Biologically Inspired Strategy for the Assembly of Viral Building Blocks with Controlled Dimensions

a dissertation submitted by

Jennifer M. Rego

in partial fulfillment of the requirements for the degree of

Doctor of Philosophy

in

Chemistry

TUFTS UNIVERSITY

February 2012

Adviser: Dr. Hyunmin Yi

Abstract

I demonstrate the assembly of nanoscale viral building blocks of controlled lengths using a biologically motivated strategy. To achieve this I exploit the simple assembly mechanism of *Tobacco mosaic virus* (TMV), whose length is solely governed by the length of its genomic mRNA, using both the wildtype and genetically engineered (displaying cysteine residues) forms of the virus. The observed lengths of the viral building blocks correlate well with the expected lengths. Additionally, I demonstrate the assembly of viral building blocks of controlled length derived from the genetically engineered form of TMV displaying cysteine groups, which signifies that the mutation does not affect viral building block assembly. Next, I examine the application of WT viral building blocks as individual components for the assembly of 1 dimensional nanoarrays via biotin-streptavidin binding. Finally, I examine the application of genetically engineered 1cys viral building blocks as a biological template for the synthesis of metal nanoparticles, functionalization by small molecules and a component of a vertically patterned template. I envision that the biologically inspired assembly strategy to design and construct viral building blocks of controlled dimensions together with the applications explored could be employed to fabricate well-controlled nanoarchitectures and hybrid nanomaterials for a wide variety of applications.

Acknowledgements

First, I would like to express my gratitude for my thesis advisor, Professor Hyunmin Yi. His encouragement and guidance instilled from the moment we first met were instrumental in my fulfillment of this thesis.

Next, I would like to convey my appreciation for my committee members, Professor Krishna Kumar, Professor Charles Sykes and Professor Matthew Panzer. I thank them for their valuable time and helpful insights into this work.

I would also like to thank the past and present members of the Yi lab, especially Christina, Amy, Jihae and Cuixian, for being great friends and making the Yi lab an enjoyable place to work.

Finally, words cannot fully express how grateful I am for my loving family as they supported me throughout the trying process of fulfilling the requirements for this thesis. Their unconditional love and support guided me through every challenge encountered and made me believe I can do anything I dream.

Table of Contents

List of Figures

List of Tables

1 INTRODUCTION

The field of nanotechnology has recently gained substantial attention due to the potential for enhanced performances[1] and novel properties[2] arising from the nanoscale. Specifically, biologically derived supramolecules such as viruses have been extensively implemented as templates or components for functional materials synthesis due to their precisely controlled structures and readily manipulated chemical and genetic properties[3, 4]. Applications of such novel bio-nano hybrid materials range from nanoelectronics[5, 6] energy[7, 8] and catalysis[9, 10]. Despite such advances, the ability to manipulate the dimensions of the virus in the low nanometer scales (i.e.1 – 100 nm) in order to fill the gap between traditional top-down and bottom-up materials synthesis strategies is lacking[11]. Although there have been attempts at fabricating building blocks in the relevant nanoscale using other biological entities such as protein nanotubes[12, 13], these strategies do not allow for the precise and consistent control of the dimensions of the building blocks. As the field of bionanotechnology continues to flourish, a robust and programmable strategy for the synthesis of biologically derived building blocks with precisely defined dimensions is highly desired.

One plant virus that has been extensively employed as a component of nanoscale structures is *Tobacco mosaic virus* (TMV). TMV is a tubular-shaped virus with a length of 300 nm and a diameter of 18 nm. Wildtype

TMV is comprised of about 2130 identical coat proteins helically arranged around a single strand of genomic mRNA of 6300 nucleotides, which forms a 4 nm diameter inner channel as seen in Figure 1.1[14-15]. Additionally, when TMV is visualized by transmission electron micrography (TEM) with negative staining, the inner RNA binding channel is visible in the center of the virus, as seen in Figure 1.1. TMV1cys, a genetically mutated form of TMV, displays 1 cysteine residue on the N-terminus of every coat protein on the exterior of the virus[16]. Each cysteine residue displays a chemically reactive thiol moiety, which can be targeted for chemical modification by maleimide-functionalized molecules[16-17] or the synthesis of metallic nanoparticles[18-19]. TMV is a robust biotemplate, being able to withstand temperatures of up to 90°C, pH values from 3.5 – 9 and exposure to organic solvents without deleterious effects to the structural integrity of the virus[20].

In addition, the assembly mechanism of TMV is well understood. For assembly, the viral coat proteins aggregate to form the 20S disk structure. Initiation of viral assembly occurs with the binding of a 20S coat protein disk to a sequence of RNA termed the origin of assembly (OA), a stem-loop structure located 876 nucleotides from the 3' end of the RNA[21-22]. The stem-loop structure of the OA sequence is predicted to be introduced into the center of the 20S disk[23]. Elongation of the virus occurs in both directions of the RNA by the addition of coat proteins or protein disks. At

the 5’ end, the 5’ end of the RNA is pulled up through the central hole of the evolving viral helix with the addition of 20S coat protein disks to the expanding nucleoprotein structure[24-26]. At the 3’ end, assembly occurs more slowly and is considered to incorporate the addition of single coat protein subunits or small coat protein aggregates (A protein)[27]. Importantly, the length of the virus is entirely governed by the length of RNA; the key underlying principle enlisted in this study.

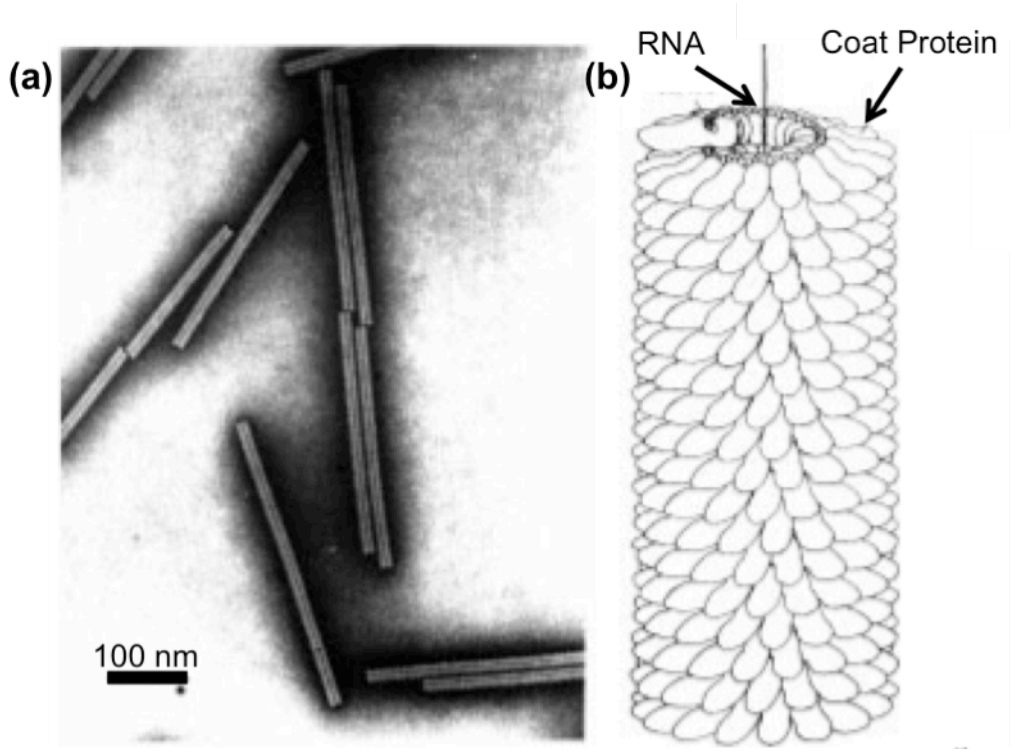

Figure 1.1 TEM image and schematic representation of TMV[14]. (a) Negatively stained TEM image of TMV. (b) Schematic depiction of the structure of TMV. Arrows highlight the viral coat protein helically assembled around a single strand of RNA

1.1 My Approach

In this work, I have examined the fabrication of viral building blocks of controlled lengths via the *in vitro* assembly of short mRNA strands with precise lengths and both WT and 1cys coat proteins. Additionally, I have examined the application of WT and 1cys viral building blocks of controlled dimensions as the individual components implemented in the bottom-up assembly of nanoarchitectures.

Specifically, I first examined the synthesis of viral building blocks from precise lengths of mRNA and viral coat proteins. In Chapter 3, I show the assembly of WT and 1cys viral building blocks of controlled lengths, which is achieved by combining equilibrated 20S coat protein disks with the desired length of RNA. The observed lengths of the viral building blocks correlate well with the expected lengths based on the length of RNA transcript employed, confirming the hypothesis that the lengths of the viral building blocks can be manipulated and is solely governed by the length of the RNA.

Next, I studied the application of WT viral building blocks of controlled dimensions for the assembly of one dimensional (1D) nanoarrays, using viral building blocks assembled with RNA biotinylated at both ends and streptavidin. In Chapter 4, I show the 5' and 3' biotinylation of RNA. RNA transcripts were biotinylated at the 5' end by the incorporation of 5'-Biotin-

GMP to the *in vitro* transcription reaction. For biotinylation of the 3' end of RNA, purified RNA transcripts were selectively oxidized at the 3' end and then conjugated with hydrazide-functionalized biotin. Additionally, the results in this chapter show the synthesis of doubly biotinylated viral building blocks with controlled dimensions from equilibrated coat proteins and RNA that is biotinylated at the 5' and 3' ends. Upon the addition of streptavidin to the doubly biotinylated viral building blocks, the results show the assembly of higher order oligomers, but the formation of 1D nanoarrays due to the presence of streptavidin was not conclusive.

Finally, I investigated the application of 1cys viral building blocks of controlled dimensions for use as a template and component of the bottom-up assembly of nanoarchitectures. In Chapter 5, I show the use of 1cys viral building blocks as a biological template for the synthesis of metal nanoparticles. In addition, I examined the exploitation of the number of cysteine residues displayed by the 1cys viral building blocks, which should be directly dependent upon the length of the 1cys viral building blocks, for functionalization by small molecules. The results in Chapter 5 establish the foundation of studies toward the functionalization of 1cys viral building blocks with the small molecules Nanogold and green fluorescent protein, by exploiting the reactive thiol moieties displayed on the 1cys viral building blocks. Additionally, the results show the length dependent functionalization of viral building blocks with fluorescein, such that longer

viral building blocks interact with more fluorescein than do viral building blocks of shorter dimensions.

Together, the results presented in this thesis demonstrate the synthesis of biologically derived building blocks whose dimensions are readily controlled and easily tuned. Also demonstrated in this work is the length dependent functionalization of the viral building blocks as well as the foundation for alternative applications of the viral building blocks with controlled dimensions. I envision that the controlled nanoscale building block fabrication strategy via biomolecular techniques and TMV's unique self-assembly mechanism in conjunction with the applications explored here could be enlisted toward the synthesis of precisely defined components for the bottom-up fabrication of nanodevices under mild aqueous conditions in many applications such as nanoelectronics[28-29] and catalysis[30].

2 VIRUSES AS NANOBUILDING BLOCKS

In this chapter, I briefly review the characteristics and applications of readily available plant and bacteria viruses for the synthesis of novel nanomaterials by the chemical functionalization and higher order assembly of the viral systems. By harnessing and manipulating the exquisite control that nature has provided, the overarching goal for the research endeavors in the emerging field of nanobiotechnology has been to achieve features and performances that transcend what is possible from inorganic, man-made methods. Viruses and virus-like protein assemblies in particular have attracted substantial attention as building blocks and templates for nanomaterials synthesis during the past two decades. Materials and applications arising from this novel bottom-up assembly approach vary widely from metal and metal oxide nanoparticles and nanowires for catalysis and nanoelectronics, high surface area electrodes for energy applications, and sensing or tissue engineering scaffolds for biomedical applications. While most early studies were limited to the demonstration of the concepts, an increasing number of recent developments are showing signs of reaching the goal; performances and capabilities that are beyond or impossible to achieve in traditional materials, top-down approaches and inorganic devices. This array of unprecedented advancements largely stems from the increasing understanding and better manipulation of the unique advantages that viral

assemblies offer, including precisely defined structure, genetic modifications and chemical functionality.

I focus on three categories of viruses, specifically the rod-shaped plant virus Tobacco Mosaic Virus (TMV), the icosahedral plant viruses Cowpea Mosaic Virus (CPMV) Cowpea Chlorotic Mottle Virus (CCMV) and the bacteria virus M13 phage. I first highlight the structure and characteristics of each virus, which promote its application as a biological template and component of higher order assemblies. For each virus, I then highlight several studies, which demonstrate the application of the viruses as nanobuilding blocks for the assembly of novel materials using a biologically-templated bottom-up assembly approach.

2.1 Tobacco Mosaic Virus

From a materials science perspective, tobacco mosaic virus (TMV) represents biologically derived nanotubes. As the first virus to be discovered, TMV has been most widely studied for its structure, assembly/disassembly mechanism, and host-guest interactions in the broad biology fields. In-depth understanding of its properties from such extensive studies along with its many advantages has enabled TMV to be widely employed for nanomaterial synthesis.

2.1.1 Characteristics of TMV

TMV is a cylindrical, rod-shaped plant virus belonging to the *Tobamovirus* genus. The length of the virion is 300 nm and the diameter measures 18 nm. The virion encompasses the entire structure of the virus as it exists outside of a host cell, while maintaining its ability to infect. TMV is composed of a single strand of positive strand RNA enclosed around 2130 identical coat proteins with three nucleotides binding to the inner groove of each protein subunit. The RNA is helically arranged along the entire length of the virus forming an inner RNA-binding channel whose diameter is 4 nm[14-15].

The TMV coat protein subunit exists as a right-handed anti-parallel helical bundle made from four α-helices. Both the N-terminus and C-terminus of the coat protein are exposed on the exterior surface of the assembled virus. TMV coat protein exists in three predominant forms, based on the pH and ionic strength of the environment as seen in Figure 2.1. Coat protein monomers or low number aggregates of subunits, termed 4S or A-protein, exist at basic pH and low ionic strength. Coat protein monomers transition to form an aggregate of 38 coat protein subunits arranged in a disk shape. This class of coat protein is termed 20S disk. The third form of coat protein, the virion-like structure, is the arrangement of coat protein monomers in the cylindrical shape of the fully assembled virus but without the presence of RNA[15, 31].

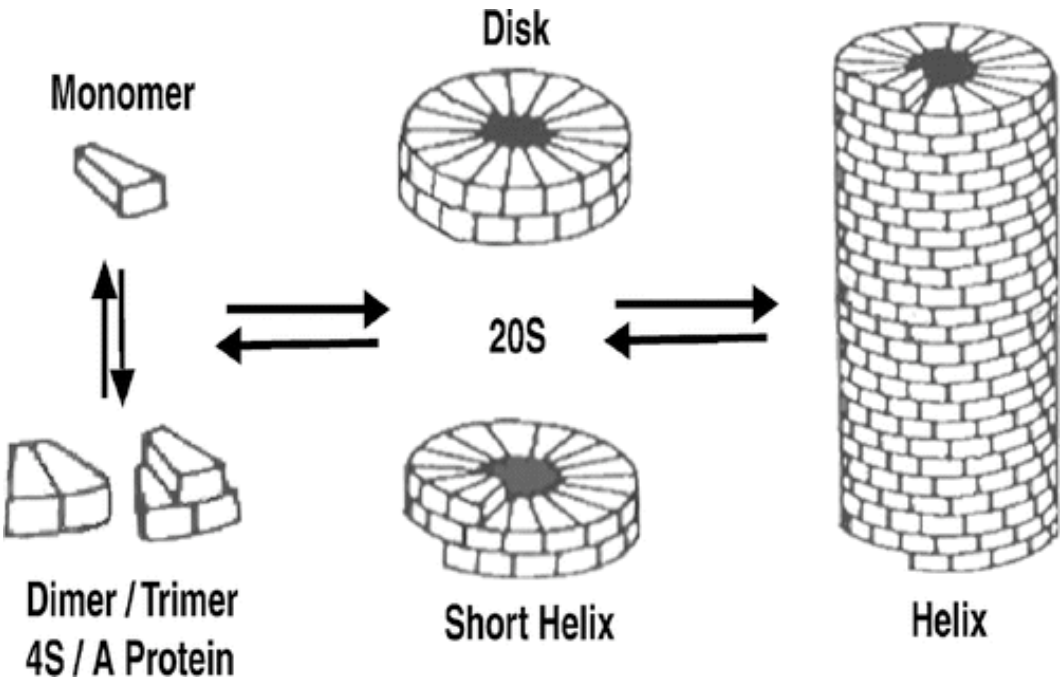

Figure 2.1 TMV coat protein assemblies[15]

The exterior surface of TMV is negatively charged and each coat protein subunit contains charged residues that are exposed on both the interior and exterior surface of the virus[32]. Understanding the chemical properties of TMV allows for probing the virus for chemical conjugation with the appropriate reactive reagents. TMV maintains its structural integrity at temperatures above 90°C and between the pH range of 3.5-9 demonstrating the robust nature of the virus[33]. The assembly mechanism of TMV has also been established[14-15]; briefly, a coat protein disk binds to a segment of RNA termed the origin of assembly and elongation of the virus occurs in both directions of the RNA by addition of coat protein.

2.1.2 Application of TMV as Nanobuilding Blocks

Sites for the covalent coupling of small molecules at consistently placed intervals on the surface of the coat proteins make TMV an advantageous biotemplate. For this, several amino acid side chains have been targeted for chemical modification, such as the side chains of tyrosine and glutamic acid, as well as genetically inserted cysteines. The Francis group has utilized chemical conjugation to synthetically introduce functional groups by covalently attaching small molecules to the interior and/or exterior of TMV, which can subsequently be targeted for further modification[34]. First, to chemically modify the exterior surface of TMV, Tyr139 was targeted on the surface of the coat protein by reaction with diazonium salts which

possess electron-withdrawing moieties. The resulting azo adducts retained the structural integrity of the assembled virus and it was determined that more than 90% of the coat protein monomers had been functionalized. Modifying the exterior of TMV with the diazonium salt derived from *p*-aminoacetophenone generated an azo adduct with a ketone, which could be targeted for further conjugation. This procedure for exterior surface modification of TMV yields rod-shaped viral particles displaying over 2000 copies of the desired functionality with a uniform periodicity of 3.3 nm.

Additionally, the interior surface of TMV coat proteins was altered by targeting Glu97 and 106 for the formation of amide bonds to be modified by additional chemical reactions. Activated glutamic acid residues of intact WT TMV were reacted with various amine substrates, including bulky dye molecules, resulting in 21-86% of the coat protein monomers to be singly or doubly modified with no change in the assembled structure of the virus. The preservation of the ability of the interior-functionalized coat proteins to self-assemble was successfully tested by disassembling intact interior-modified TMV and reassembling the modified coat protein monomers into higher ordered structures upon introduction into specific pH and ionic strength buffers. These findings suggest that the addition of small molecules to the interior of the virus particles do not provide enough steric hindrance to prevent interior-modified coat protein monomers from

self-assembling into coat protein oligomers. Furthermore, dual-modified virus particles were synthesized by chemically conjugating rhodamine to the interior of exteriorally azo-modified TMV. In summary, the advantage of using TMV as a biotemplate for nanomaterial synthesis has been expanded by the chemical modification of the interior and/or exterior of the virus.

Expanding on the work by Francis and coworkers to target tyrosine residues on the exterior of TMV for chemical conjugation, Wang and coworkers have utilized copper-catalyzed azide-alkyne 1,3-dipolar cycloaddition, or “click chemistry”, in combination with the diazonium coupling to modify the surface of the virus as shown in Figure 2.2[35]. Implementing click chemistry to further functionalize the surface of the azo adduct of TMV may broaden the range of potential chemical structures of starting materials which can be incorporated onto the surface of the virus. Using this methodology, it was possible to covalently attach small molecules, peptides and polymers to the exterior surface of TMV. Most notably, this approach allows for the display of an azide functionality so that a second click chemistry reaction can be carried out, which significantly improves the pool of potential molecules that can be utilized to derivatize TMV. As an application of this approach, the authors demonstrated that TMV modified via click chemistry to display moieties intended to either inhibit or promote cellular growth exhibited their

predicted properties on cellular metabolism. In conclusion, the disadvantages of targeting tyrosine residues on TMV exclusively with diazonium salts to incorporate uniformly spaced functionalities has been overcome by combining this approach with copper-catalyzed azide-alkyne 1,3-dipolar cycloaddition to expand the range of small molecules, peptides or polymers available that can be covalently coupled to the surface of TMV.

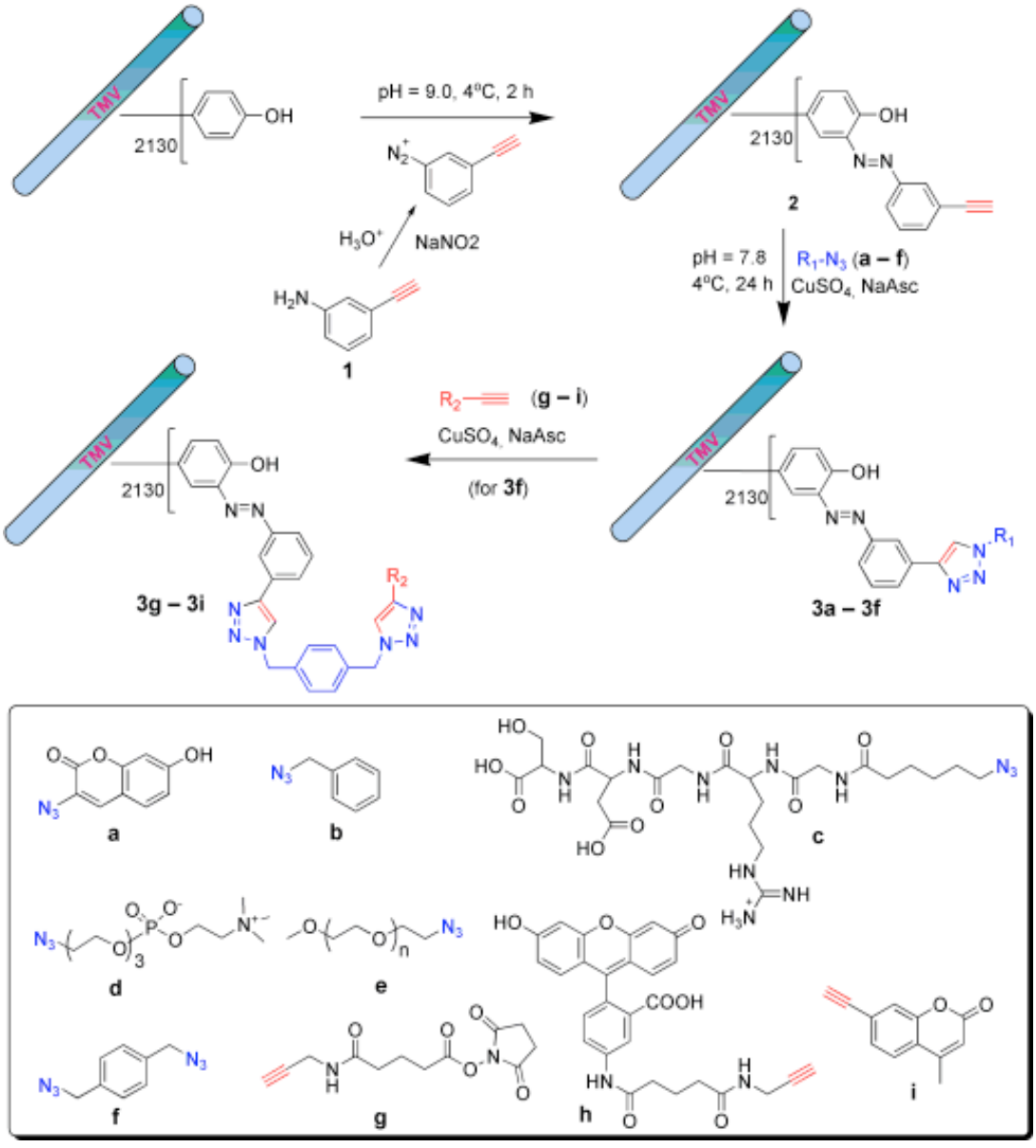

Figure 2.2 Schematic illustrating the functionalization of TMV by click chemistry[35]

Wang and coworkers have also exploited the precise, rod-like structure of TMV and employed chemical modifications to synthesize conductive polyaniline (PANi) nanowires using the virus particles as a biotemplate[36]. As depicted in Figure 2.3, the combination of TMV, polyaniline, poly(sulfonated styrene) and ammonium persulfate resulted in the formation of biotemplated nanofibers whose length was dependent upon the length of the virus. Adjusting the pH influenced the arrangement of polymerized polyaniline on the virus to assemble either non-conductive, branched oligoaniline or conductive PANi nanowires. Initial preparation of the TMV templated PANi nanowires at neutral pH resulted in the arrangement of viral particles end-to-end to form nanofibers longer than the 300 nm length of TMV. The electronic properties of these longer TMV/PANi nanowires were probed to yield a conductivity measurement of ~1 x 10^{-5} $\Omega^{-1}cm^{-1}$. In conclusion, Wang and coworkers have demonstrated the construction of water soluble, conductive PANi nanowires of controllable length using native TMV as a biotemplate in conjunction with a facile ordered assembly and polymerization process. These conductive PANi nanofibers have the potential to be implemented in optical, electronic or sensing applications.

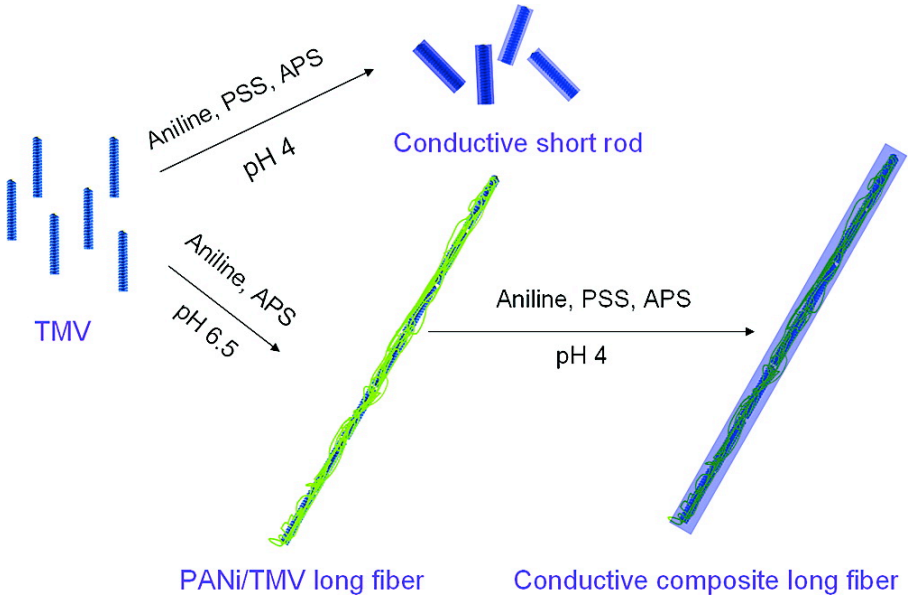

Figure 2.3 Schematic illustrating the assembly of TMV templated polyaniline fibers[36]

The exterior coat protein surface of TMV displays various charged amino acid side chains at uniform intervals, which could serve as potential nucleation sites for the controlled layering of inorganic materials to synthesize biotemplated nanomaterials. Exploiting the evenly spaced functionalities on the surface of TMV, in conjunction with the robust stability of the virus, Mann and coworkers were the first to utilize TMV as a template for the synthesis of metallic nanoparticles[20]. By incubating native TMV with metal salt solutions and hydrogen sulfide, an evenly dispersed coating of CdS or PbS nanocrystals were observed on the exterior of the virus, yielding hollow nanotube complexes of metallic nanoparticles.

Building upon this initial study, Mann and coworkers further explored various conditions for the preferential synthesis of metallic nanoparticles on the exterior or interior of TMV[37]. By adjusting the pH of the reaction conditions and relying on the difference in pKa's of the exposed amino acid functionalities within the interior RNA binding channel or the exterior of the virus surface, the interior or exterior electrostatic charge was chemically and selectively tuned to discriminate between interior or exterior viral templated metal nanoparticle deposition. Utilizing this strategy, at acidic pH where amino acid side chains on the surface of TMV are positively charged, the formation of discrete platinum and gold nanoparticles upon the exterior surface of native TMV could be achieved

from reaction with negatively charged metal salt precursor as seen in Figure 2.4a. Similarly, at neutral or slightly alkaline pH, silver nanoparticles were observed in the interior of native TMV, as seen in Figure 2.4b, due to the preferential interaction between the negatively charged inner channel of the virus and silver cation precursor.

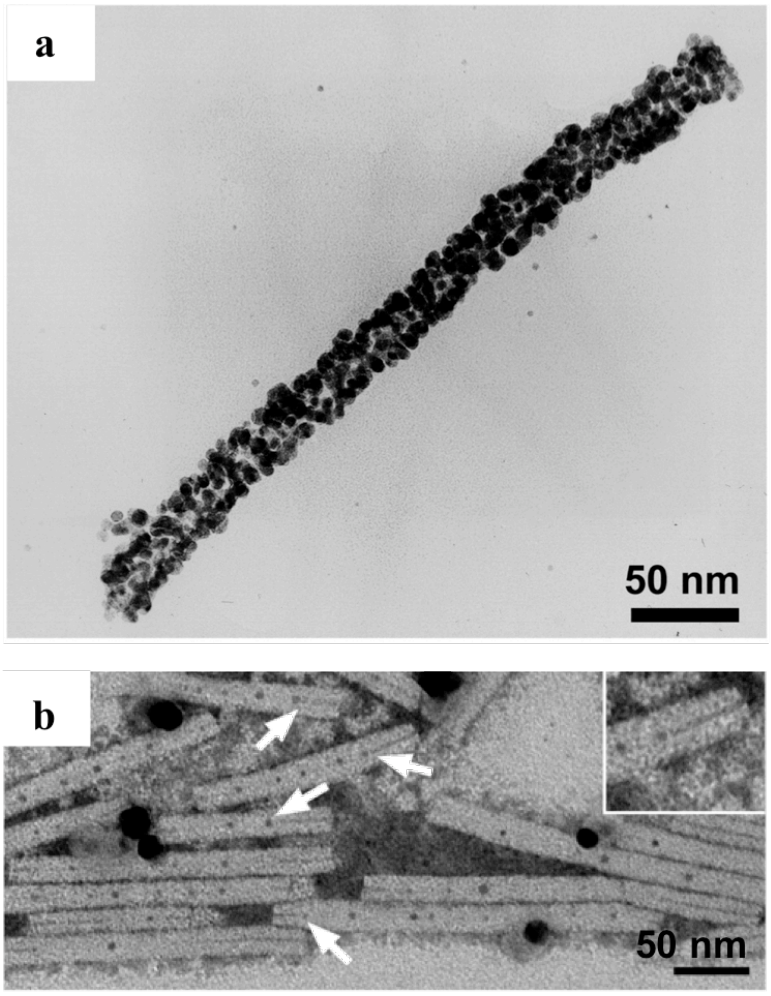

Figure 2.4 TEM Images of metallized TMV[37]. (a) TEM image of TMV selectively coated with discrete gold nanoparticles. The viral templates nanoparticles with diameters of 8.6 ± 3 nm were formed by incubating TMV with $HAuCl_4$ at pH 2.9 for 30 minutes with stirring in the dark followed by reduction with hydrazine at pH 2.3. (b) TEM image of negatively stained uranyl acetate of silver nanoparticles selectively formed within the RNA binding channel of TMV. To form silver nanoparticles, whose diameters measured less than 5 nm, TMV was incubated with Ag (I) benzoate of $AgNO_3$ at pH 7 overnight with stirring. Reduction of silver ions was achieved by irradiation with 254 nm light. As specified by the arrows, the presence of silver nanoparticles within the RNA binding channel of TMV was an obstacle that prevented the uranyl acetate stain from completely entetering the interior of TMV.

Kern and coworkers have also explored controllable, uniform metal deposition by employing TMV as a biotemplate. In their studies, the addressable amino acid side chains that function as metal nucleation sites are first activated with a metal complex, followed by incubation with the desired metal for metallization and its subsequent chemical reduction to form metal nanoparticles.[38-39] By employing this approach of electroless deposition, discrete nickel, silver and cobalt nanoclusters were selectively formed on the interior or exterior of the virus by controlling the pH and the activation complex used in the reaction. In addition to synthesizing distinct nanoparticles templated by native TMV, Kern and coworkers have also exploited the nucleation sites present within the interior RNA binding channel of the virus to construct continuous nanowires[33, 40]. Specifically, electroless deposition using metal activation complexes that selectively bind to the amide residues located within the interior of TMV together with the reductant dimethylamine borane (DMAB) were employed to synthesize uninterrupted nickel, cobalt and copper nanowires within the RNA binding channel of the virus. The wires exhibited a dimater of ~3 nm and in some instances the length of the wires exceeded the length of an individual virus particle due to the ability of TMV to spontaneously form dimers.

Although the advantage of using native TMV as a biotemplate for the synthesis of metallic nanomaterials has been demonstrated, genetically modifying the coat protein of the virus to display an accessible thiol group greatly increases the metal binding affinity of TMV. Using site-directed mutagenesis, Culver and coworkers have engineered a mutated form of TMV, termed TMV2cys, to include two additional cysteine residues at the N-terminus of the coat protein[41]. TMV2cys efficiently biotemplated the formation of discrete silver and gold nanoparticles. Most notably, the deposition of palladium on the surface of native TMV resulted in a highly dispersed layer of metal over the exterior of the virus, whereas TMV2cys facilitated the synthesis of discrete palladium nanoparticles with diameters of less than 5 nm. The ability of TMV2cys to successfully act as a biotemplate for the formation of palladium nanoparticles in direct contrast to native TMV suggests that TMV2cys exhibits a higher metal binding affinity and therefore is a more efficient biotemplate for metal nanoparticle synthesis. Similarly, another genetically engineered version of TMV, TMV1cys, which displays only one additional thiol functionality due to the inclusion of one cysteine residue at the N-terminus of the coat protein, has been exploited for its preferential metal binding nucleating sites to template the synthesis of metallic nanomaterials. Yi and coworkers have exploited the increased metal binding affinity of TMV1cys to form palladium nanoparticles whose dimensions are easily controllable[17]. By adjusting the concentration of the reducer sodium hypophosphite, it was

possible to tune the size of the metallic nanoparticles that preferentially formed on the surface of TMV1cys. Some examples of applications for the metallic nanomaterials synthesized with the assistance of the genetically engineered TMV include implementation as nanocatalysts[42] and battery electrodes[5].

2.2 Icosahedral Viruses

The second category of the viral templates discussed here are spheroidal plant viruses, most of which have icosahedral symmetry. In this section, I first describe the fundamental characteristics of two representative viruses that have been widely enlisted; cowpea mosaic virus (CPMV) and cowpea chlorotic mosaic virus (CCMV). I then discuss endeavors to functionalize the surfaces of these viral nanoparticles by both chemical and genetic modifications that mirror the ones utilized for TMV. Finally, efforts to harness a range of inner cavity sizes, perhaps the most unique feature of this class of viral assemblies, from various spheroidal viruses and protein cages for the synthesis of precisely controlled nanoparticles are described.

2.2.1 Characteristics of Icosahedral Viruses

Cowpea mosaic virus (CPMV) belongs to the *Comoviridae* plant virus family. CPMV is an icosahedral virus with a diameter of 28 nm. The structure of CPMV consists of a single strand of positive sense RNA enclosed by capsid protein subunits. The CPMV genome exists as two

unique strands of RNA with each of the two strands of RNA encapsulated separately into identical viral particles. A mixture of viral particles with the two different strands of RNA is necessary for CPMV to infect whole plants[43-45].

There are two different coat protein subunits that compose the structure of CPMV. Each CPMV particle is comprised of 60 of each of the two different coat protein subunits. The smaller coat protein subunit, the S subunit, has a mass of 23.7 kDa and adopts a jelly roll β sandwich tertiary structure. The other coat protein subunit, the L subunit, is the larger of the two. The mass of the L subunit is 41.2 kDa and folds into two jelly roll β sandwiches[43-45]. The thickness of the protein shell of the assembled CPMV particles is 3.9 nm[44].

CPMV affords several properties which make it advantageous for use as a viral template in nanostructure assemblies and material synthesis. First, CPMV can be readily obtained in gram quantities from the infection of black-eyed peas. Second, CPMV has been extensively studied so the general properties and the structure of the virus are well known, which may permit facile manipulation of the virus. In addition, CPMV viral particles are stable over the pH range of 3 to 9 and maintain their structural integrity when heated to 60°C for an hour[45].

Another icosahedral plant virus used as a viral template is cowpea chlorotic mosaic virus (CCMV), a member of the *Bromoviridae* family. CCMV has a diameter of 28.6 nm and is comprised of a coat protein shell encapsulating a single strand of positive-sense RNA. Like CPMV, the genome of CCMV is comprised of multiple strands of RNA, with the 3 unique strands of RNA packaged individually into virus particles. The individual coat protein capsids of CCMV are composed of 190 amino acid residues and have a total mass of 19.8 kDa. The protein shell of the virus is composed of 180 identical coat protein subunits. In contrast to CPMV, CCMV particles are stable at pH 5 but swell up to 10% in size when the pH is increased to 7. When the virus is swollen, pores are created within the protein shell, which permit the interior of the virus particles to be penetrated by small molecules. The transition back to stable, unswollen viral particles is achieved by decreasing the pH to 5.0 or increasing calcium and magnesium ion concentration to 0.05 M. This unique property of CCMV to transition from stable to swollen states offers another advantage for viral templated material synthesis[46].

2.2.2 Application of Icosahedral Viruses as Nanobuilding Blocks

To determine the validity of exploiting exposed chemical moieties on the surface of CPMV to yield functionalized virus particles, Finn and coworkers investigated the chemical reactivity of native CPMV and developed a genetically modified CPMV which would display free thiol

groups that could be targeted for derivitization by maleimide-functionalized small molecules[47]. By probing for the presence of free sulfhydryl groups in the form of cysteine residues displayed on the coat protein of native CPMV, it was determined that reactive thiol groups reside within the interior of the virus particles and can only be targeted by small molecules that can easily traverse through the coat protein shell to reach the interior. To increase the chemical reactivity of CPMV, the native virus was genetically engineered to incorporate a cysteine residue to be displayed on the exterior surface of the capsid. Due to the addressable thiol functionality presented on the exterior surface of the mutated virus, genetically altered viral particles demonstrated increased reactivity toward maleimide functionalized chromophores and Nanogold, in comparison to native CPMV. In addition, genetically modified CPMV retained the capability to be derivatized internally by labeling of the cysteine residue exposed within the interior of the virus as with native CPMV, resulting in viral particles that could be dually labeled at two positions under suitable conditions. Finn and coworkers also examined the chemical reactivity of lysine residues exposed on the exterior of the native CPMV capsid[33]. Fluorescent native CPMV was fabricated by reacting native viral particles with the lysine-selective N-hydroxysuccinimide (NHS) ester and isothiocyanate derivatives of fluorescein. In addition, biotinylated CPMV was synthesized from the reaction of native CPMV with biotin-NHS ester and aggregated in the presence of avidin; this implies that the reactive

lysine residues are indeed displayed at the exterior surface of the viral particles.

Furthermore, solvent-exposed tyrosine residues were successfully targeted for functionalization and to conjugate dye molecules to CPMV and to form cross-linked viral particles[48]. As an application for the chemical modification of CPMV, Finn and coworkers covalently modified the exterior of CPMV with DNA oligonucleotides to form virus-DNA conjugates[49]. As illustrated in Figure 2.5, when CPMV-DNA conjugates with complementary sequences were incubated together, the viral conjugates behaved as nanobuilding blocks to form a self-assembled array. The binding of complementary oligonucleotides drives the formation of the self-assembled CPMV aggregation, which can be reversed by the addition of an excess of competing unconjugated complementary DNA. Moreover, the extent of assembly is temperature dependent. At 4°C, the most preferential interactions between complementary strands of DNA are unable to be achieved resulting in the formation of smaller arrays (Figure 2.5b). At room temperature, more interactions between complementary strands of DNA yield more extensive arrays of CPMV-DNA conjugated viral particles than observed at a lower temperature due to the increased kinetic energy available. But the interactions between the complementary strands of DNA at room temperature are still not strong enough to prevent the viral arrays from succumbing to the forces of TEM sample preparation

and appear as a two-dimensional array in the resulting TEM image seen in Figure 2.5c. Finally, at 40°C, complementary strands of DNA are able to orient themselves to provide maximum overlap for hybridization resulting in the formation of a stronger viral array. These stronger interactions between CPMV-DNA conjugated viral particles result in the appearance of a three-dimensional network (Figure 2.5d). These studies conducted by Finn and coworkers demonstrate for the first time the capability of CPMV to be chemically modified by the covalent attachment of small molecules, which signifies the potential of these viral particles to be employed as biotemplates or biological building blocks for nanomaterial synthesis.

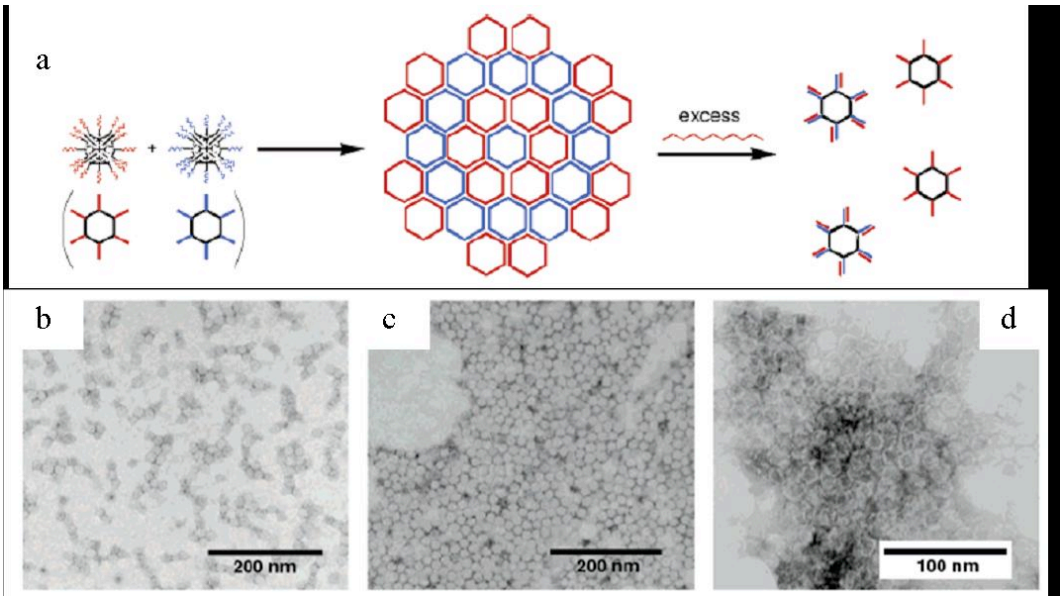

Figure 2.5 Formation of a self-assembled CPMV array by oligonucleotide hybridization[49]. (a) Schematic depicting the formation of CPMV aggregation to form an array of viral particles. CPMV particles functionalized with complementary strands of DNA were incubated together. (b) TEM image of DNA-hybridized CPMV aggregates formed at 4°C for 16 h. (c) TEM image of DNA-hybridized CPMV aggregates formed at room temperature for 16 h. (d) TEM image of DNA-hybridized CPMV aggregates formed at 40°C for 16 h.

Expanding on the work of Finn and coworkers, Evans and coworkers have also exploited CPMV as a biological scaffold for the functionalization and synthesis of biotemplated nanomaterials. The chemical reactivity of additional amino acid side chains of native CPMV was explored by selectively probing the carboxylate groups of glumatic and aspartic acids present on the exterior of the viral particles[50]. A carbodiimide-functionalized fluorescent dye was shown to selectively react with the carboxylate groups displayed by the glutamic and aspartic acid residues presented on the exterior surface of CPMV without altering the structural integrity of the viral coat proteins. Furthermore, the carboxylate functionalities on CPMV were targeted as anchors for the attachment of organic, redox-active methyl(aminopropyl)viologen, which yielded electrochemically active viral nanoparticles. Evans and coworkers have also employed native CPMV as a biological scaffold to construct another variation of redox-active nanoparticles by the selective targeting of solvent-exposed lysine residues for the covalent conjugation of the organometallic ferrocenecarboxylate[51]. Analysis of the ferrocene derivatized viral particles determined that multiple ferrocene molecules were covalently coupled to a single coat protein asymmetric subunit and each ferrocenyl moiety functioned as an individual, electronically active entity.

In addition to functionalizing native CPMV for electrochemical applications, Evans and coworkers utilized the exterior of CPMV as a biological template for the synthesis of inorganic nanoparticles[52]. Silica nanoparticles were synthesized from a genetically mutated version of CPMV, which included the insertion of a 12 amino acid peptide sequence previously determined to initiate the nucleation of silica mineralization. The introduction of a short peptide into the viral capsid did not alter the assembly or morphology of the virus and successfully templated the silica mineralization of viral nanoparticles by chemical solution deposition. The silica nanoparticles that formed were monodisperse and exhibited a diameter of approximately 32 nm, suggesting that the layer of silica deposited on the viral particles was about 2 nm. Collectively, the studies by Evans and coworkers further expanded the application and utilization of CPMV as a biological template for functionalization and nanomaterial synthesis.

Trevor Douglas and Mark Young have employed another icosahedral plant virus to facilitate the synthesis of nanomaterials. In their initial study, cowpea chlorotic mottle virus (CCMV) was utilized as a host for the mineralization of paratungstate and decavanadate[53]. Douglas and Young, exploiting the pH-dependent gating mechanism of native CCMV, encapsulated inorganic, metallic precursor ions at pH values greater than 6.5. By subsequently lowering the pH, the structure of the capsid was

altered as the pores in the viral protein shell closed and the crystallization of either paratungstate or decavanadate was achieved within the interior of the viral particle. The resulting metallic nanoparticles were only observed in the presence of CCMV and exhibited the same monodisperse diameter as the viral particles. The nucleation of the metallic crystals was presumed to be induced by the electrostatic attraction between the negatively charged precursor metal ions and the positively charged amino acid side chains displayed within the interior of the viral capsid at the N-terminus of each coat protein. In another study, Douglas and coworkers employed the same strategy to synthesize titania nanoparticles as well as amorphous titania[54]. Using anionic titanium salts in conjunction with the pH dependent gating mechanism of CCMV, a composite of β-TiO_2 was formed which possessed the same diameter of the viral capsid and demonstrated photocatalytic activity in the presence of methylene blue.

Collectively, the work by Trevor Douglas, Mark Young and coworkers demonstrates the ability to utilize an additional icosahedral virus for the encapsulation of reagents to spatially control inorganic nanomaterial synthesis within the cavity of a viral template. More importantly, this series of work illustrates an elegant means to exploit the in-depth understanding of the physicochemical properties as well as highly controlled dimensions of viral nanoparticles for the synthesis of inorganic nanomaterials with precise sizes and functionalities.

2.3 Filamentous Viruses

While most of the plant viruses discussed in the previous two sections are rod or icosahedral shaped, bacterial viruses come in various shapes including spheres, satellites and filaments. Owing to the rapid turnover cycle (i.e. infection, replication and recovery with fast-growing bacterial hosts) and the seminal work of phage display by Smith[55], a combinatorial affinity screening (a.k.a. biopanning) procedure using the filamentous M13 bacteriophage has revolutionized the field of biotemplate-based materials synthesis. While such display libraries have been proposed for other viruses (e.g. TMV), M13 phage display-based biopannng remains as the most potent system with infinite possibilities.

2.3.1 Characteristics of M13 Bacteriophage

M13 phage is a filamentous bacteriophage belonging to group Ff of the class I of filamentous bacteriophage, which infect *E. coli*. M13 is composed of a single strand of circular DNA containing about 6400 nucleotides encapsulated by a coat protein shell. The diameter of the phage is 6 nm, while the length of the phage is dependent upon the length of its DNA and measures ~1 μm for the native strain of M13. There are 5 different coat proteins that comprise the protein shell of M13. The predominant form of coat protein that composes M13 is the gene-8 major coat protein, termed pVIII. pVIII exists with ~2,700 copies covering the length of M13. The remaining forms of coat protein present

on the phage particles are minor coat proteins and only about 5 copies of each are present. Protein-7 and protein-9 (pVII and pIX) exist at one end of the phage while protein-3 and protein-6 (pIII and pVI) are found at the other end of the phage[56].

The ability of M13 bacteriophage to incorporate foreign DNA into its genetic core and subsequently display foreign peptides makes M13 an advantageous viral template. Although the DNA of the native strain of M13 has about 6400 nucleotides, foreign DNA with a length of up to 12,000 nucleotides can be successfully incorporated[57]. When the foreign DNA is spliced into a gene encoding for the synthesis of the viral capsid, the phage is able to display foreign peptides or proteins on its exterior surface. The fusion of foreign peptides to native phage coat proteins has been achieved for the pIII, pVIII and pVI forms of phage coat proteins. Exploiting this technique of phage display has facilitated the formation of phage display libraries that can be implemented to discover peptides or proteins with high binding affinity to small molecules or inorganic materials of interest. First, the phage library is allowed to interact with the target. Phage bound to the target are isolated by elution and subsequently amplified by bacterial amplification. This strategy is repeated several times to enhance the phage library with phage displaying peptides that bind to the target with the greatest affinity. Unique to this system is the link between the selected peptide or

protein displayed on the phage and the DNA sequence encoding for the peptide found within the core of the phage. Analysis of the phage DNA will yield the peptide sequence(s) that exhibits the greatest binding affinity toward the target[58-59].

2.3.2 Application of M13 Bacteriophage as Nanobuilding Blocks

By employing the strategy of combinatorial phage display, Belcher and coworkers have selected a sequence of peptides that selectively bind with high affinity to semiconductor single-crystals based on their identity or crystal structure[60]. A library of random peptides for phage display was incorporated into the pIII coat protein of M13 phage and were probed for their selective binding affinity towards five different semiconductors. For each single-crystal semiconductor studied, a single discriminatory peptide sequence was determined which differentiated among the range of semiconductors examined based on their composition or crystalline face structure. This work has yielded the basis for binding organic peptides, arranged as a spatially controlled template on the surface of the M13 phage virus, to inorganic semiconductors for the synthesis of nanomaterials using a bottom-up approach. Belcher and coworkers have also exploited M13 phage as a biotemplate to synthesize quantum dot nanowires[61]. Specifically, genetically engineered M13 phage were employed to display a previously determined peptide sequence in the pVIII M13 coat protein that specifically facilitates the nucleation and growth of

ZnS or CdS nanocrystals with preferential alignment guided by the peptide template. By lowering the temperature of the system, water dispersed from the viral particles and single-crystalline quantum dot layered nanowire structures were synthesized. Additionally, Belcher and coworkers were also able to demonstrate the versatility of M13 phage to display more than one genetically engineered peptide sequence to nucleate the growth of two different quantum dots to facilitate the construction of multi-component materials.

As another example to demonstrate the versatility of applying genetically engineered M13 phage system for nanomaterial synthesis, Belcher and coworkers have recently utilized M13 phage as a biological scaffold to construct a photochemical catalyst[62]. Genetically mutated M13 phage displaying a peptide sequence exhibiting selective binding for iridium oxide in conjunction with the chemical attachment of zinc porphyrins to the phage coat protein to act as photosensitizers functioned as a photocatalytic nanoarchitecture capable of oxidizing water.

While the chemical functionalization of M13 phage has been extensively studied to form metal nanowires and nanocatalysts, Belcher and coworkers have also employed M13 phage as nanobuilding blocks in the fabrication of programmable assemblies[63]. Figure 2.6a details the strategy used to employ M13 phage as components of a nanoassembly.

First, two types of phage libraries were constructed. The first intended to isolate peptides displayed by the pVIII protein along the axis of the phage for binding gold nanoparticles. The second phage library was aimed at discovering a peptide sequence displayed at the end of the phage by the pIII protein for binding streptavidin. Once the respective peptides for binding gold nanoparticles and streptavidin were established, the genes for these peptides were fused into the genome of the M13 phage for display by the pVIII and pIII coat proteins, respectively. The resulting genetically engineered M13 phage successfully expressed the foreign peptides without inhibiting their ability to bind to their respective target. As seen in Figure 2.6b, the genetically engineered M13 phage were used to assemble higher order nanoarchitectures. The pVIII coat protein bound gold nanoparticles along the length of the M13 phage in an ordered 1 dimensional array. Additionally, the pIII coat protein bound streptavidin-coated nanoparticles at one end of the virus. The streptavidin-coated nanoparticles facilitated the assembly of the gold nanoparticle coated M13 phage into various heterostructures (Figure 2.6b Images C & D). This approach of employing genetically engineered viruses for the assembly of nanostructures could easily be applied to other materials and structures.

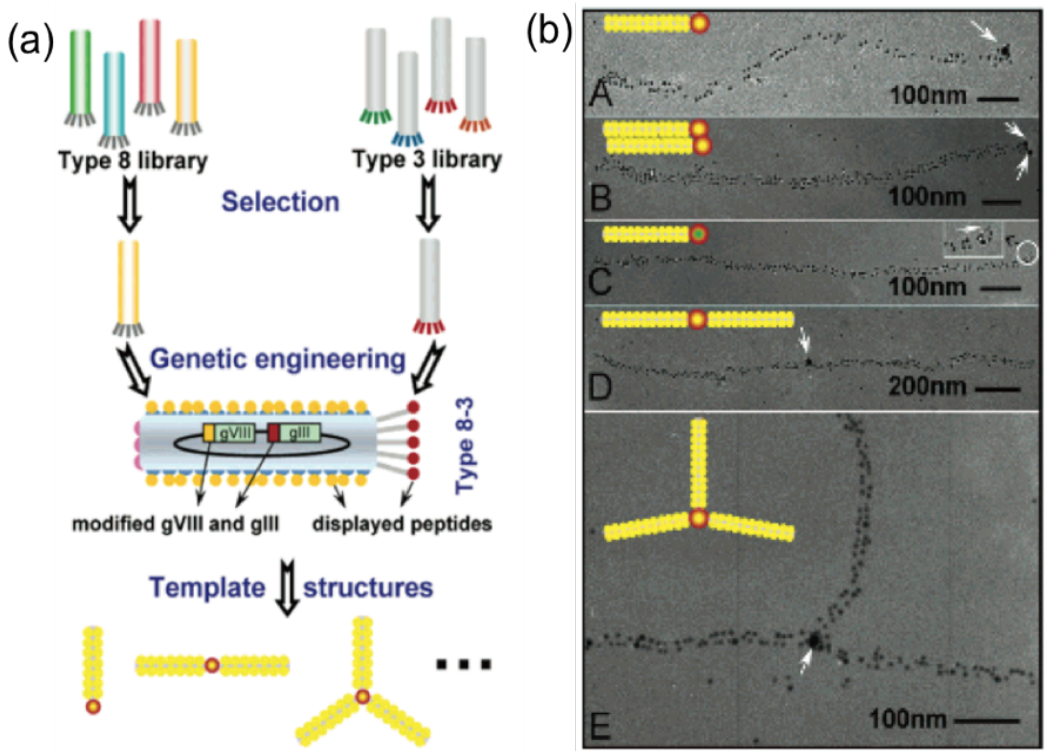

Figure 2.6 Genetic engineering and assembly of phage to form nanoarchitectures[63]. (a) Schematic depicting the engineering of the pVIII and pIII proteins of the phage. The engineered phage include insertions added to the genome for pVIII and pIII phage coat proteins, resulting in the display of additional peptides on pVIII and pIII proteins. The corresponding expressed motif and their inserted genes are highlight in yellow (pVIII) and red (pIII). Engineered phage are utilized to template the assembly of nanoarchitectures. (b) TEM images of various nanoarchitectures. Engineered phage displaying streptavidin binding peptides on the pIII coat proteins bind streptavidin-coated nanoparticles while gold nanoparticles (~5 nm) simultaneously bind to pVIII proteins along the viral axis. The streptavidin-conjugated gold nanoparticles (~15 nm) and streptavidin coated CdSe quantum dots bound on pIII coat proteins are highlighted with arrows. In the schematic depiction, the virus structure is represented in white, the gold nanoparticles bound to pVIII are represented by yellow, the CdSe quantum dot is represented by a green dot, and the streptaividn coating on gold or CdSe particles is represented in red. (c, inset) Enlarged image of CdSe quantum dot bound to pIII coat proteins at end of virus.

While variations of M13 phage have successfully been employed as templates for the synthesis of metallic nanomaterials and the assembly of nanoarchitectures, Lee and coworkers have exploited genetically modified M13 phage for the biological application of tissue regeneration[64]. M13 bacteriophage were genetically altered to display the peptide sequence RGD, which promotes cell adhesion integrin binding, or the peptide sequence IKVAV, for promoting the adhesion of neural cells and the growth of neurites. The addition of the RGD or IKVAV peptides to the coat protein of the phage capsid resulted in increased interaction between the phage and hippocampal neural progenitor cells and had no deleterious effects on the viability of the cells. Cells grown and differentiated into neurites in the presence of genetically altered phage matrices aligned their growth with the orientation of the phage and exhibited an increased length of neurites in comparison to cells not exposed to genetically engineered phage matrices. Building on the findings in this fundamental study, Lee and coworkers have used a shearing strategy to construct liquid crystalline films of genetically modified phage to align the growth of a series of cell types[65]. Genetically altered phage displaying the integrin binding peptide RGD were self-assembled into 2-D matrices by shearing a solution of RGD-displaying phage on a substrate. The linearly aligned phage matrices exhibited no adverse effects on cell viability. The RGD-displaying 2-D phage films were also observed to guide the direction of growth of differentiated cells such that over 80% of the elongated cells were aligned

within a 20° angle of the oriented phage after 4 days of incubation. Collectively, the work by Lee and coworkers demonstrates the ability of genetically modified phage to easily self-assemble into aligned matrices. These genetically altered phage films are able to interact with cells to facilitate the controlled directional growth of the cells. The results of these studies could find applications in medical therapies for tissue engineering or as a mock-system for the study of cell-signaling pathways.

2.4 Conclusions

In this chapter, I described the fundamental characteristics, chemical modification schemes, and the evolution of three virus shape categories into unique directions in bottom-up assembly approaches for novel nanomaterials development. A growing pool of chemical toolkits, such as click chemistry, often combined with a small genetic modification of rod-shaped TMV viruses have led to exciting systems with precisely spaced chemical functionality. TMV's simple structure and precise dimensions have also been exploited for the fabrication of higher order assemblies to form conducting nanowies. Moreover, the precise dimensions along with the readily functionalized side chains displayed by the coat proteins renders the icosahedreal virus CPMV easily modified with small molecules or applied to the formation of nanoassemblies. Potent affinity selection (i.e. biopanning) based on M13 phage display combined with larger scale fabrication strategies is

increasingly enlisted in a wide range of biomedical and catalytic applications and furthermore can be adapted to facilitate the programmable assembly of higher order architectures. Collectively, the studies highlighted in this chapter showcase the exciting developments achieved in the use of viruses as chemically functionalized biological nanotemplates and nanobuilding blocks for the fabrication of programmable assemblies using a bottom-up approach toward the synthesis of novel materials and more enhanced device performances that can be readily deployed in real applications in the near future.

3 SYNTHESIS OF VIRAL BUILDING BLOCKS OF CONTROLLED DIMENSIONS

In this chapter, I examine the assembly of nanoscale viral building blocks of controlled length. To achieve this, the simple assembly mechanism of TMV is exploited. TMV is an ideal virus to employ in the assembly of viral building blocks because the length of the virus is solely dependent upon the length of the viral genetic material (mRNA), the key underlying principle enlisted in this study. Both WT TMV and a mutated form of TMV, TMV1cys, which displays one cysteine residue by every coat protein, are employed in this study. It should be noted that a recent publication by Wege and coworkers has demonstrated the application of a similar strategy for the assembly of TMV particles of a defined length, but the resulting viral nanotubes were synthesized attached to a substrate, their length was greater than 100 nm and only the native form of the virus was employed[66].

As seen in Figure 3.1, I began with full-length TMV and separated the virus into its two components, coat protein and mRNA. The coat proteins were equilibrated to form the disk structures necessary for viral building block assembly, as depicted in the left side of Figure 3.1a. To synthesize the viral RNA of desired length, reverse transcription followed by polymerase chain reaction (RT-PCR) was performed on the full-length viral RNA to produce DNA templates of desired lengths as illustrated in

the right side of Figure 3.1a. Figure 3.1b shows the relationship of primer binding with respect to the full-length TMV RNA sequence for RT-PCR to yield RNA transcripts of desired lengths. Specifically, both the forward (FP) and reverse primers (RP) bind to sequences which flank the OA sequence necessary to initiate assembly of the viral building blocks. In addition, RNA transcripts of different lengths were synthesized by changing the position that the forward primer binds on the DNA template upstream of the OA sequence region. Assembly of the viral building blocks of controlled length is achieved by combining the equilibrated 20S coat protein disks with the desired length of viral RNA.

My results show the reliable synthesis of DNA templates and RNA transcripts of desired lengths upon RT-PCR and *in vitro* transcription respectively. In addition, my results show the *in vitro* assembly of viral building blocks of three defined lengths (i.e. 16, 28 and 56 nm) using WT TMV coat protein or 1cys TMV coat protein, such that the mutated form of the viral coat protein does not inhibit the assembly of viral building blocks. The observed lengths of the viral building blocks correlate well with the expected lengths based on the length of RNA transcript employed, confirming the hypothesis that the lengths of the viral building blocks can be manipulated and is solely governed by the length of the RNA. In addition, assembly of the viral building blocks is consistent and reproducible, with only building blocks of uniform dimensions observed.

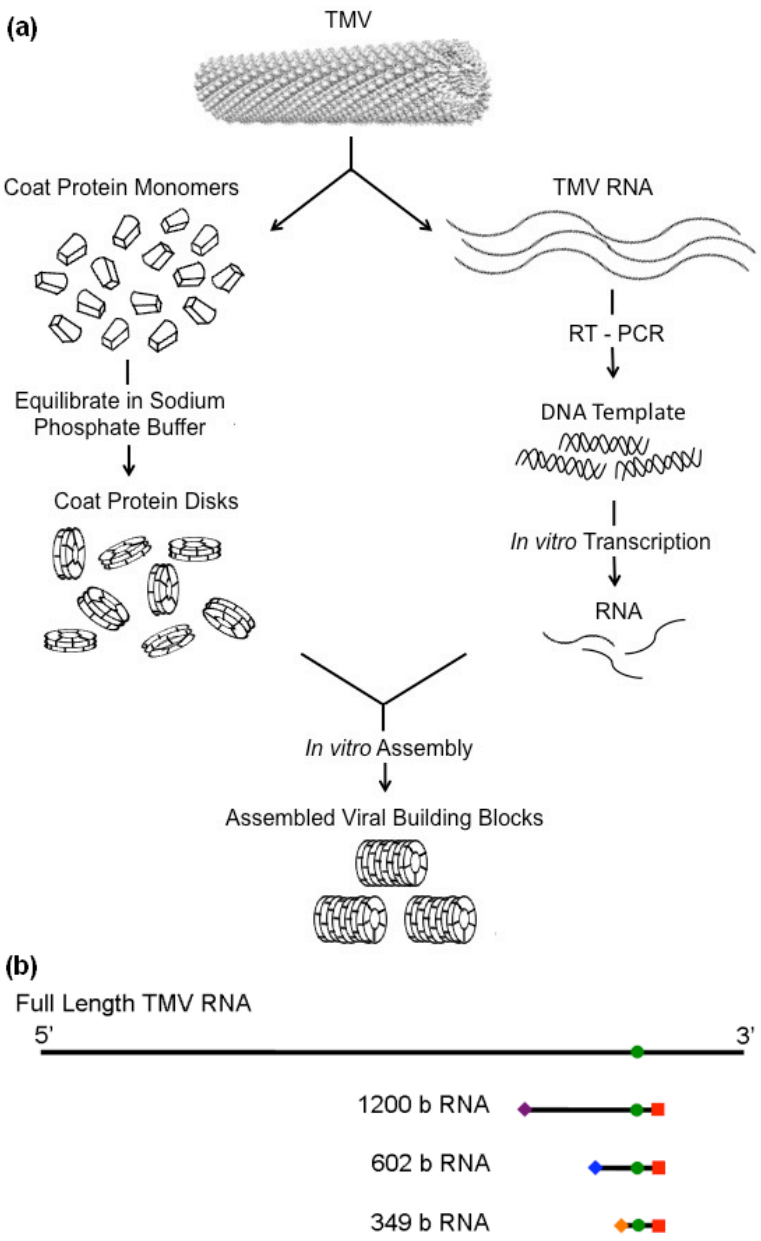

Figure 3.1 Assembly of viral building blocks. (a) Schematic illustration of the biologically inspired assembly strategy for the assembly of viral building blocks. (b) Schematic depiction of the full-length TMV RNA and the synthesized RNA transcripts employed for the assembly of the viral building blocks. The location of the OA is designated in green. The sequence complementary to the RP is designated in red. The sequence complementary to the FP is designated in purple for the 1200 b transcript, blue for the 602 b transcript and orange for the 349 b transcript

3.1 Materials and Methods

3.1.1 Materials

Wildtype TMV was a generous gift from Dr. Gerald Stubbs at Vanderbilt University (Nashville, TN). TMV1cys was generously provided by Dr. James Culver at the University of Maryland. Primers utilized for RT-PCR (Table 1) were purchased from Integrated DNA Technologies (Coralville, IA) and used without further purification. M-MulV Reverse transcriptase and T7 RNA Polymerase were purchased from New England Biolabs (Ipswich, MA). PCR Master Mix was purchased from Promega (Madison, WI). The QIAquick PCR Purification Kit was purchased from QIAgen (Valencia, CA). The gels used in polyacrylamide gel electrophoresis (PAGE) for the purification of *in vitro* RNA transcripts were prepared from the Sequagel – Ureagel System from National Diagnostics (Atlanta, GA). The Elutrap Elution System and its accessories used for the electroelution of the RNA transcripts from the PAGE gel were purchased from Whatman (Piscataway, NJ). Vivapure diethylamine high capacity (D-H) mini ion exchange spin columns utilized for purification of coat protein from the intact virus were purchased from Sartorius Stedim Biotech (Carlsbad, CA).

3.1.2 Design and Preparation of DNA Templates and RNA Transcripts

Full-length TMV RNA was prepared by phenol/chloroform extraction from full-length wildtype TMV. To establish the desired lengths of RNA, reverse transcription (RT) was performed on the full-length TMV RNA followed by the polymerase chain reaction (PCR) to amplify the DNA templates used for *in vitro* transcription. Primers were designed for RT-PCR, which flanked the origin of assembly (OA) sequence necessary for initiation of viral assembly, to establish the length of the resulting RNA transcript. The reverse primer (RP) was designed to bind downstream of the OA sequence (Figure 3.2). The RP (*m*C*m*UA TTT TTC CCT TTG CGG A) binds between nucleotides 5562 and 5580 of the TMV mRNA sequence. The RP was synthesized with a 2'-O-methyl modification on the first two bases of the sequence to decrease the primer's susceptibility of degradation by RNase[67-68]. For RT, approximately 1.5 ug of full-length TMV RNA was denatured at 75°C for 5 min. The denatured RNA was added to a solution of dNTP's (1 mM), $MgSO_4$ (1 mM), reverse primer (0.7 uM), 1x M-MulV Reverse Transcriptase Reaction buffer and 200 units of M-MulV Reverse Transcriptase. The reagents were incubated at 42°C for 50 min, then 95°C for 5 min to denature the reverse transcriptase.

Amplification and the final length of the DNA templates were established by PCR. For PCR, forward primers (FP) were designed to bind upstream of the OA sequence (Figure 3.2) on the complementary DNA template

resulting from RT. The location of FP binding determined the length of the resulting RNA transcript. Each FP contains the T7 RNA Polymerase promoter sequence[69] (represented in italics) and the complementary sequence for binding to the product of RT for amplification by PCR (Table 3.1). For the 349 b RNA transcript, the FP (*GCG TAA TAC GAC TCA CTA TAG* GAG CAG CTG CAA AGA AAA GAT TT) binds between nucleotides 5232 and 5254 of the full-length TMV mRNA sequence. For the 602 b RNA transcript, the FP (*GCG TAA TAC GAC TCA CTA TAG* CGA TGT TTA CCC CTG TAA AG) binds between nucleotides 4979 and 4998 of the full-length TMV mRNA sequence. For the 1200 b RNA transcript, the FP (*GCG TAA TAC GAC TCA CTA TAG* GCA TCT GGT ATC AAA GAA AG) binds between nucleotides 4381 and 4400 of the full-length TMV mRNA sequence. For the PCR reaction, the RT product was added to a solution of RP and the respective FP at a final concentration of 0.56 uM each. Upon addition of PCR Master Mix to 1x, the reagents were incubated at 94°C for 55 s, 54°C for 40 s then 72°C for 40 s for 30 cycles with a final elongation step of 7 min at 72°C. The amplified PCR products were concentrated and purified using the QIAquick PCR Purification Kit. The lengths of the purified DNA templates were verified by resolution on a 1.5% agarose gel and visualization by ethidium bromide staining (Figure 3.3).

4381…GCATCTGGTATCAAAGAAAGAGCGGGGACGTCACGACGTTCATTGGAAACACTGTGATCATTGCTGCATGTTT
GGCCTCGATGCTTCCGATGGAGAAAATAATCAAAGGAGCCTTTTGCGGTGACGATAGTCTGCTGTACTTTCCAAAGG
GTTGTGAGTTTCCGGATGTGCAACACTCCGCGAATCTTATGTGGAATTTTGAAGCAAAACTGTTTAAAAAACAGTATG
GATACTTTTGCGGAAGATATGTAATACATCACGACAGAGGATGCATTGTGTATTACGATCCCCTAAAGTTGATCTCGA
AACTTGGTGCTAAACACATCAAGGATTGGGAACACTTGGAGGAGTTCAGAAGGTCTCTTTGTGATGTTGCTGTTTCGT
TGAACAATTGTGCGTATTACACACAGTTGGACGACGCTGTATGGGAGGTTCATAAGACCGCCCCTCCAGGTTCGTTT
GTTTATAAAAGTCTGGTGAAGTATTTGTCTGATAAAGTTCTTTTTAGAAGTTTGTTTATAGATGGCTCTAGTTGTTAAAG
GAAAAGTGAATATCAATGAGTTTATCGACCTGACAAAAATGGAGAAGATCTTACCGTCGATGTTTACCCCTGTAAAGA
GTGTTATGTGTTCCAAAGTTGATAAAATAATGGTTCATGAGAATGAGTCATTGTCAGAGGTGAACCTTCTTAAAGGAGT
TAAGCTTATTGATAGTGGATACGTCTGTTTAGCCGGTTTGGTCGTCACGGGCGAGTGGAACTTGCCTGACAATTGCA
GAGGAGGTGTGAGCGTGTGTCTGGTGGACAAAAGGATGGAAAGAGCCGACGAGGCCACTCTCGGATCTTACTACAC
AGCAGCTGCAAAGAAAAGATTTCAGTTCAAGGTCGTTCCCAATTATGCTATAACCACCCAGGGACGCGATGAAAAAC
GTCTGGCAAGTTTTAGTTAATATTAGAAATGTGAAGATGTCAGCGGGTTTCTGTCCGCTTTCTCTGGAGTTTGTGTCG
GTGTGTATTGTTTATAGAAATAATATAAAATTAGGTTTGAGAGAGAAGATTACAAACGTGAGAGACGGAGGGCCCATG
GAACTTACAGAAGAAGTCGTTGATGAGTTCATGGAAGATGTCCCTATGTCGATCAGGCTTGCAAAGTTTCGATCTCGA
ACCGGAAAAAAGAGTGATGTCCGCAAAGGGAAAAATAG…5580

Figure 3.2 Abbreviated TMV RNA sequence presenting locations of RT-PCR primer binding. Green = origin of assembly sequence. Red = location of reverse primer binding. Orange = location of forward primer binding on corresponding DNA template for synthesis of 349 bp DNA template. Blue = location of forward primer binding on corresponding DNA template for synthesis of 602 bp DNA template. Purple = location of forward primer binding on corresponding DNA template for synthesis of 1200 bp DNA template

Primer Name	Binding Site on TMV	Primer Sequence (5' to 3')
Reverse Primer	5562	TCC GCA AAG GGA AAA ATA G
349 b Forward Primer	5232	*GCG TAA TAC GAC TCA CTA TAG* GAG CAG CTG CAA AGA AAA GAT TT
600 b Forward Primer	4979	*GCG TAA TAC GAC TCA CTA TAG* CGA TGT TTA CCC CTG TAA AG
1200 b Forward Primer	4381	*GCG TAA TAC GAC TCA CTA TAG* GCA TCT GGT ATC AAA GAA AG

Table 3.1 Primers utilized for RT-PCR. The promoter sequence for T7 RNA Polymerase in each forward primer is highlighted in italics

To synthesize RNA transcripts of desired lengths, *in vitro* transcription was employed. DNA template (2 pmoles) was mixed with 1x T7 RNA Polymerase Reaction buffer, ribonucleotides (1.5 mM each), DTT (5 mM) and 200 units T7 RNA Polymerase. The reagents were incubated at 42°C for 2 hours. The transcription reaction product was purified by resolution on a 4% native PAGE gel in 0.5x TBE running buffer. The bands of RNA were cut from the gel and electroeluted using the Elutrap electroelution system. The RNA was then concentrated by ethanol precipitation and stored at -20°C. The lengths of the purified RNA transcripts were verified by resolution on a 1.5% agarose gel and visualization by ethidium bromide staining (Figure 3.3).

3.1.3 Preparation of Coat Proteins

Both WT TMV and 1cys TMV coat proteins were prepared from the full-length virus using the alkaline method described by Richards and Williams[70] with minor modifications. For the purification of 1cys TMV coat proteins, 100 mM tris (2-carboxylethyl) phosphine (TCEP) was included in all the buffers used for purification[71]. Briefly, to degrade the full-length virus, 0.5 – 1.0 mL of a 10 – 15 mg/mL solution of TMV was dialyzed against 100 mM ethanolamine-5mM HCl (pH 11) at 4°C overnight. The TMV was then dialyzed against 12 mM Tris – 10 mM HCl (pH 7.6) at 4°C for 4 hours. To separate undegraded TMV, the solution was centrifuged at 54,000 *x g* for 4.25 hrs at 4°C. To remove the RNA, the supernatant was passed through an equilibrated D-H ion exchange mini spin column.

The column was washed with 12 mM Tris – 10 mM HCl and the purified coat proteins were eluted with 120 mM Tris – 100 mM HCl. The purified coat protein sample collected was then dialyzed against 100 mM sodium acetate buffer (pH 5) at 4°C to convert the protein to the stable, helical rod form. For use in *in vitro* assembly reactions, the coat protein was further dialyzed against 40 mM sodium phosphate buffer (pH 7) at 4°C. Concentration of coat protein was determined by A_{280} = 1.28 mg/mL.

3.1.4 Assembly of Viral Building Blocks

To prepare the coat proteins for assembly into viral building blocks, a sample of purified coat protein was equilibrated in 40 mM sodium phosphate buffer overnight at 20°C. To assemble the viral building blocks, RNA transcripts (~ 10 pmol) were added to equilibrated coat proteins in a ratio of 1:20 RNA:coat protein by mass in 40 mM sodium phosphate buffer (pH 7). The mixture was then incubated at 20°C for 2 hours.

3.1.5 Transmission Electron Microscopy

The assembled viral building blocks were prepared for analysis by transmission electron microscopy (TEM). A ~ 1.0 mg/mL viral building block sample was placed on a 300 mesh formvar/carbon coated copper grid and then stained with uranyl acetate solution. TEM analysis was carried out on a JEOL 2100 TEM at 200 kV at the Center for Nanoscale Systems (CNS) at Harvard University (Cambridge, MA).

3.2 Results and Discussion

3.2.1 RNA Synthesis

As shown in Figure 3.3, I first examined the synthesis of specific length DNA templates followed by the generation of RNA transcripts of corresponding lengths. For this, RT was performed on full-length TMV mRNA to produce DNA templates of specified lengths. The DNA templates were then amplified via PCR. Importantly, the sequences of the RT-PCR primers were designed so that the resulting DNA templates include the region of the OA sequence near their 3' end. Specifically, the reverse primer for RT-PCR binds downstream (i.e. 3' end) of the OA sequence to establish the length of the DNA templates at the 3' end. The forward primers for PCR bind upstream (i.e. 5' end) of the region of the OA sequence to establish the length of the DNA templates at the 5' end. The relationship between the location of primer binding and the OA sequence is further detailed with the abbreviated TMV RNA sequence depicted in Figure 3.2. Table 3.1 shows the sequences of the primers employed for RT-PCR to yield the DNA templates with desired lengths. I then used *in vitro* transcription to generate RNA strands of desired lengths from the amplified DNA templates. Figure 3.3a shows purified RT-PCR DNA template products resolved by agarose gel electrophoresis. Lanes 1-3 show DNA templates that were synthesized by RT-PCR from full-length TMV RNA with lengths of 349 bp, 602 bp and 1200 bp respectively, while lane 4 shows the DNA size marker. For each DNA product a single band

is observed at the correct corresponding length, demonstrating the generation of monodisperse DNA templates of specific lengths from the full-length TMV RNA using RT-PCR.

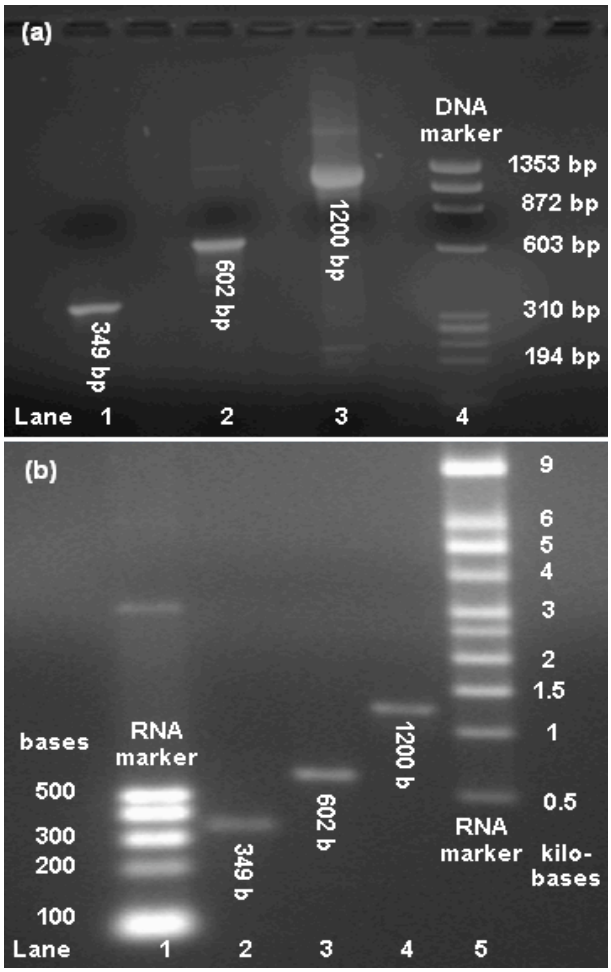

Figure 3.3 Resolution of (a) purified DNA templates and (b) RNA transcripts by agarose gel electrophoresis

Next, Figure 3.3b shows the resolution by agaorse gel electrophoresis of purified RNA transcripts synthesized by *in vitro* transcription of the amplified DNA templates. Lane 1 shows the resolution of a lower molecular weight RNA marker, while lane 5 shows the resolution of a higher molecular weight RNA marker. Lanes 2-4 show purified RNA transcripts of 349 b, 602 b and 1200 b respectively. For each length of RNA transcribed, only one band of RNA corresponding to the correct length is visible. These results in Figure 3.3b illustrate the generation of specific size, monodisperse RNA products produced from *in vitro* transcription of the DNA templates. In conclusion, Figure 3.3 validates my strategy to employ molecular biology to produce RNA transcripts of desired lengths from the full-length genomic RNA of TMV.

3.2.2 Assembly of Viral Building Blocks

As shown in Figure 3.4 and Figure 3.5, I next examined the assembly of viral building blocks, derived from WT TMV with controlled lengths as governed by the length of RNA transcripts. For this, purified coat protein monomers were equilibrated to yield 20S coat protein disks necessary for the assembly reaction[23]. Next, I assembled viral building blocks of controlled lengths by incubating equilibrated coat protein disks with RNA transcripts of desired lengths. Importantly, the length of the viral building blocks is entirely governed by the length of the RNA transcripts. Figure 3.4a shows a transmission electron microscope (TEM) image of WT TMV 20S coat protein disks produced by equilibrating coat protein monomers.

In this image, coat protein disks of the expected 18 nm diameter are visible[72]. The presence of a substantial population of coat protein disks demonstrates the consistent assembly of coat proteins to the 20S form necessary for the assembly of viral building blocks.

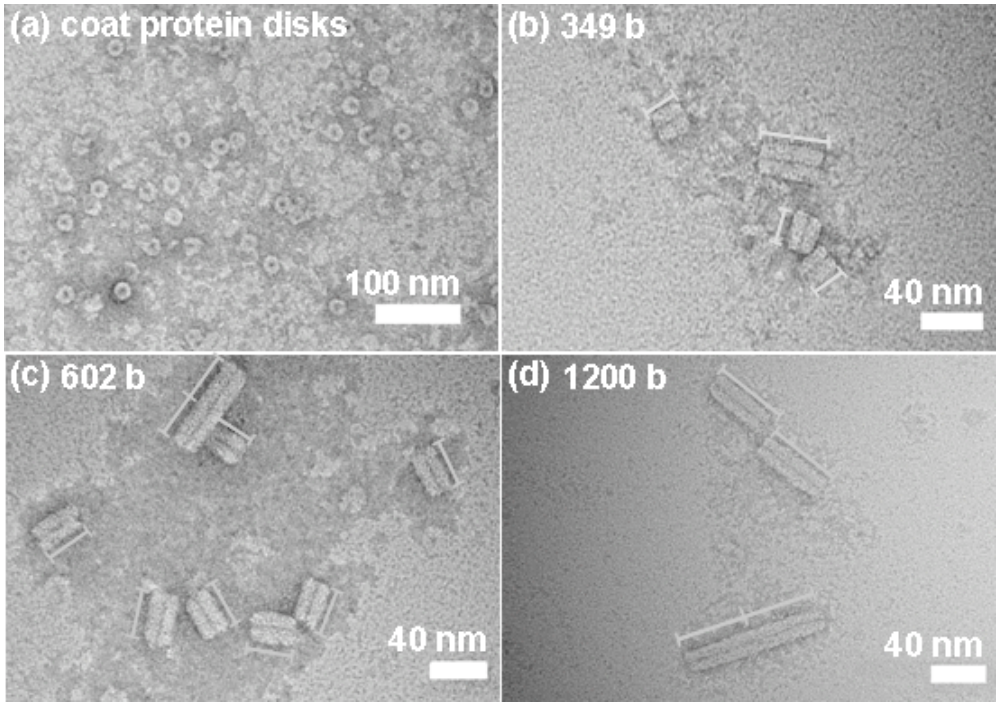

Figure 3.4 TEM images of assembled WT viral building blocks. (a) 20S coat protein disks. (b) 349 b viral assembled building blocks. (c) 602 b viral assembled building blocks. (d) 1200 b viral assembled building blocks. Brackets have been placed in the image to facilitate the distinction of monomer and dimer assemblies of the viral building blocks

Next, Figures 3.4b-d show TEM images of WT viral building blocks assembled from specific length RNA transcripts and WT coat protein disks. Figure 2b shows WT viral building blocks of the expected length of 18 nm constructed from 349 b RNA, while Figure 2c shows WT viral building blocks with the expected length of 28 nm constructed from 602 b RNA. Finally, Figure 2d shows WT viral building blocks of the expected length of 56 nm constructed from 1200 b RNA. Additional TEM images of each WT viral building block length further confirm the consistency of these results (Figure 3.5). For each length of WT viral building blocks assembled, the length of WT viral building blocks is uniform and correlates well with the expected length, with no assembled products of other lengths observed. This demonstrates that the assembly of WT viral building blocks is consistent and reproducible. Additionally, several dimers due to the end-to-end aggregation of two individual nanobuilding blocks in solution or as a result of the TEM sample preparation are observed. This phenomenon is well expected and known to occur spontaneously due to hydrophobic interactions between both ends of the virus[23]. Collectively, these results illustrate that the assembly of WT viral building blocks of controlled lengths is governed by the length of RNA.

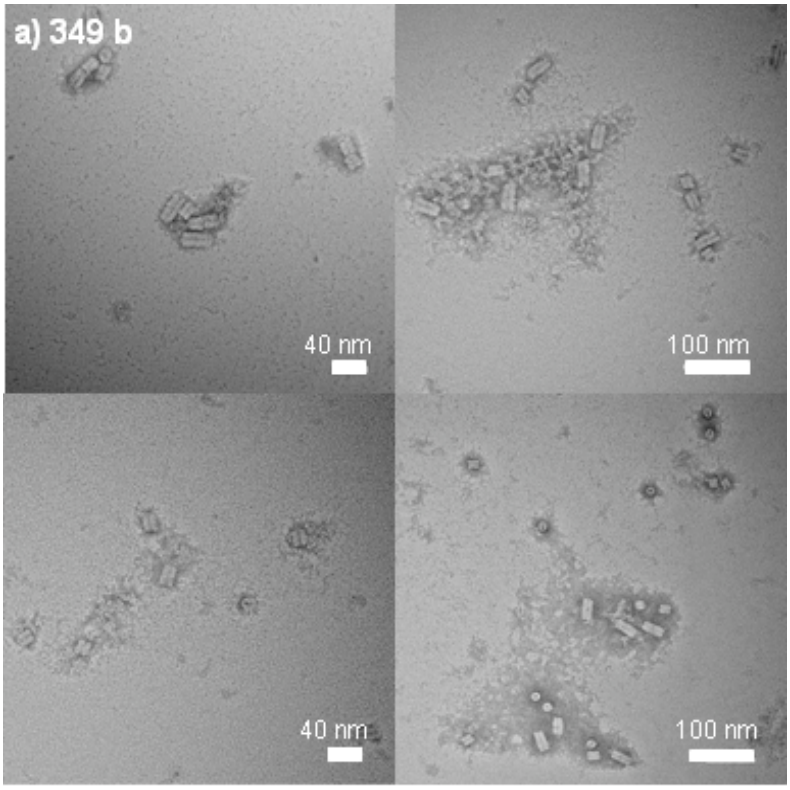

Figure 3.5a Additional TEM images of 349 b WT viral building blocks

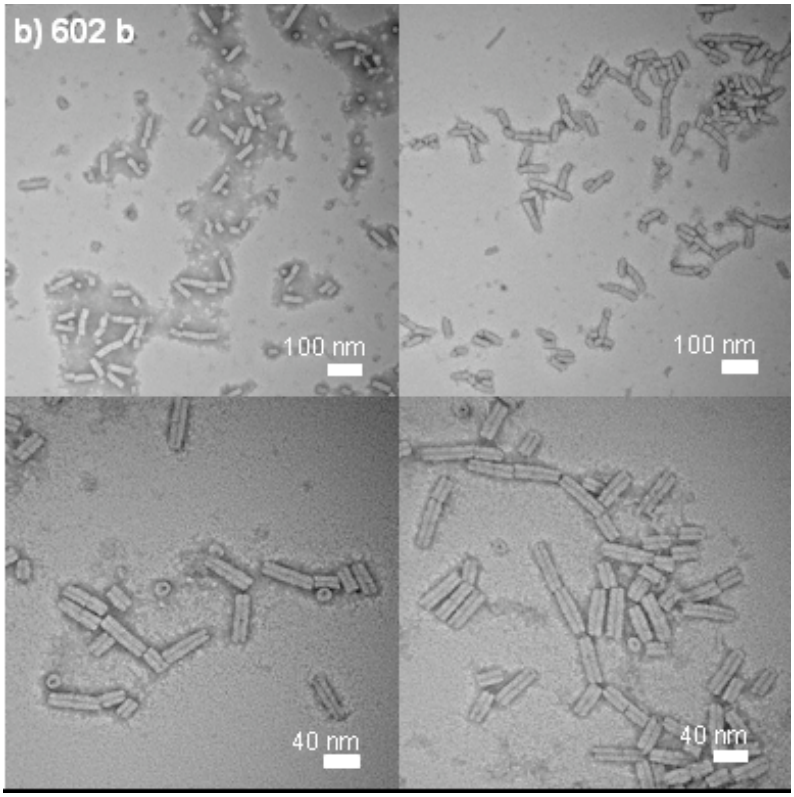

Figure 3.5b Additional TEM images of 602 b WT viral building blocks

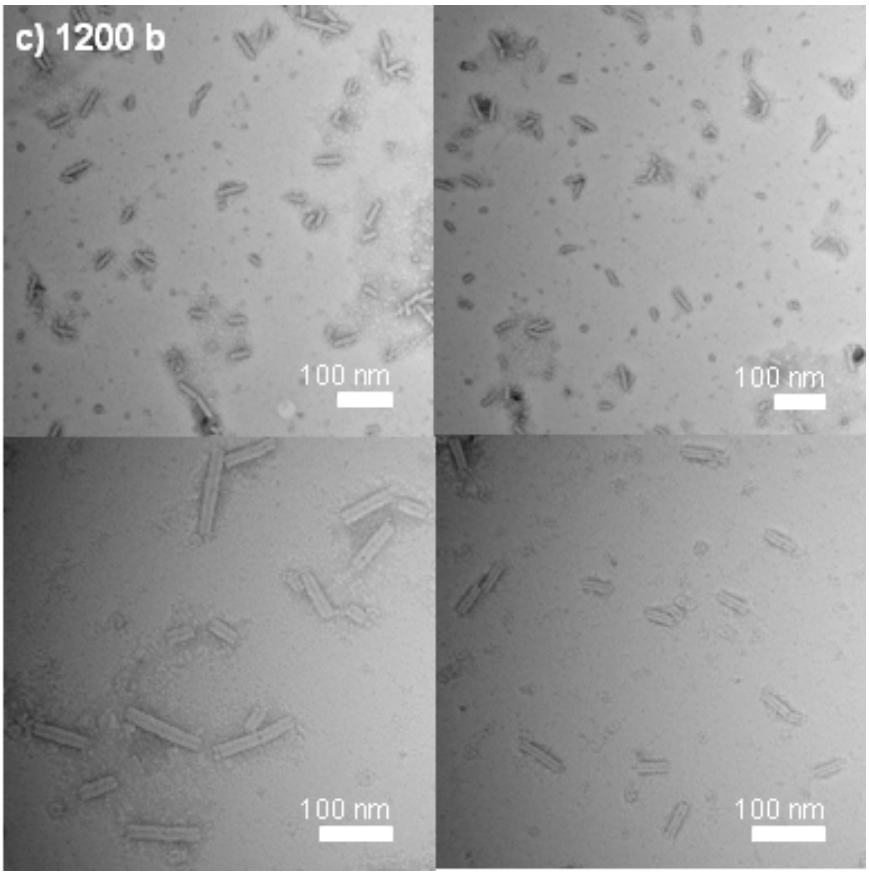

Figure 3.5c Additional TEM images of 1200 b WT viral building blocks

Next, Figure 3.6 and Figure 3.7 show the assembly of 1cys viral building blocks of controlled length from mRNA of desired length and equilibrated 1cys coat protein. For this, 1cys coat protein monomers were equilibrated to yield the 20S coat protein aggregates necessary for the assembly of the viral building blocks. The equilibrated 1cys coat protein 20S disks were then incubated with RNA transcripts of desired lengths to form 1cys viral building blocks. As with the WT viral building blocks, the length of the 1cys viral building blocks is entirely dependent upon the length of the RNA transcripts employed in assembly. More importantly, the reactive thiol moieties displayed by the genetically engineered 1cys viral building blocks do not inhibit the formation of viral building blocks of controlled dimensions.

Figure 3.6a shows a TEM image of 1cys TMV 20S coat protein disks produced by equilibrating coat protein monomers. As expected, coat protein disks of 18 nm are observed as with the equilibrated WT coat proteins. Despite the addition of the chemically reactive cysteine residues displayed by the coat proteins, a significant population of coat protein disks necessary for assembly of viral building blocks is observed. Figures 3.6b-d show TEM images of 1cys viral building blocks assembled from specific length RNA transcripts and equilibrated 1cys coat proteins. Figure 3.6b shows 1cys viral building blocks of the expected length of 18 nm synthesized with 349 b RNA. Figure 3.6c shows 1cys viral building

blocks of the expected length of 28 nm constructed from 602 b RNA. Finally, Figure 3.6d shows 1cys viral building blocks of the expected length of 56 nm constructed from 1200 b RNA. As seen in Figure 3.7, additional TEM images of each length of 1cys viral building blocks substantiate these results. As observed with the assembly of WT viral building blocks, the lengths of the 1cys viral building blocks are uniform. These results demonstrate that the reactive thiol groups displayed on the mutated coat protein does not inhibit the consistent and reproducible assembly of 1cys viral building blocks. In addition, these results signify that the length of 1cys viral building blocks is dependent upon the length of RNA employed.

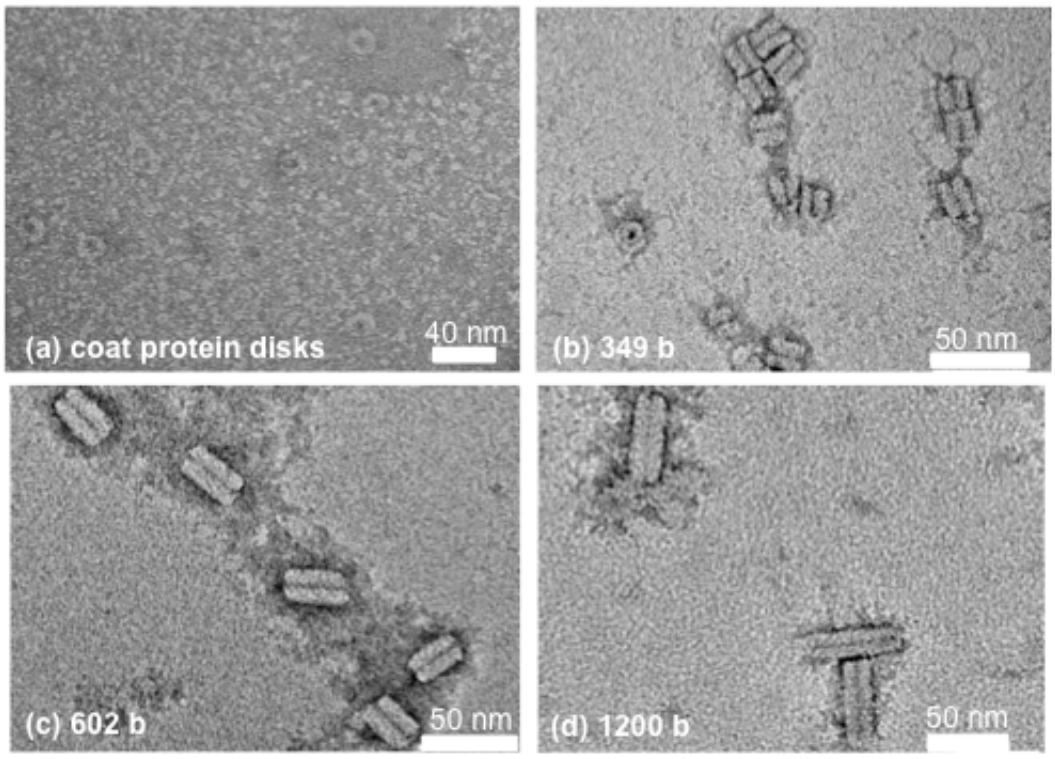

Figure 3.6 TEM images of 1cys assembled viral building blocks. (a) 20S coat protein disks. (b) 349 b viral assembled building blocks. (c) 602 b viral assembled building blocks. (d) 1200 b viral assembled building blocks.

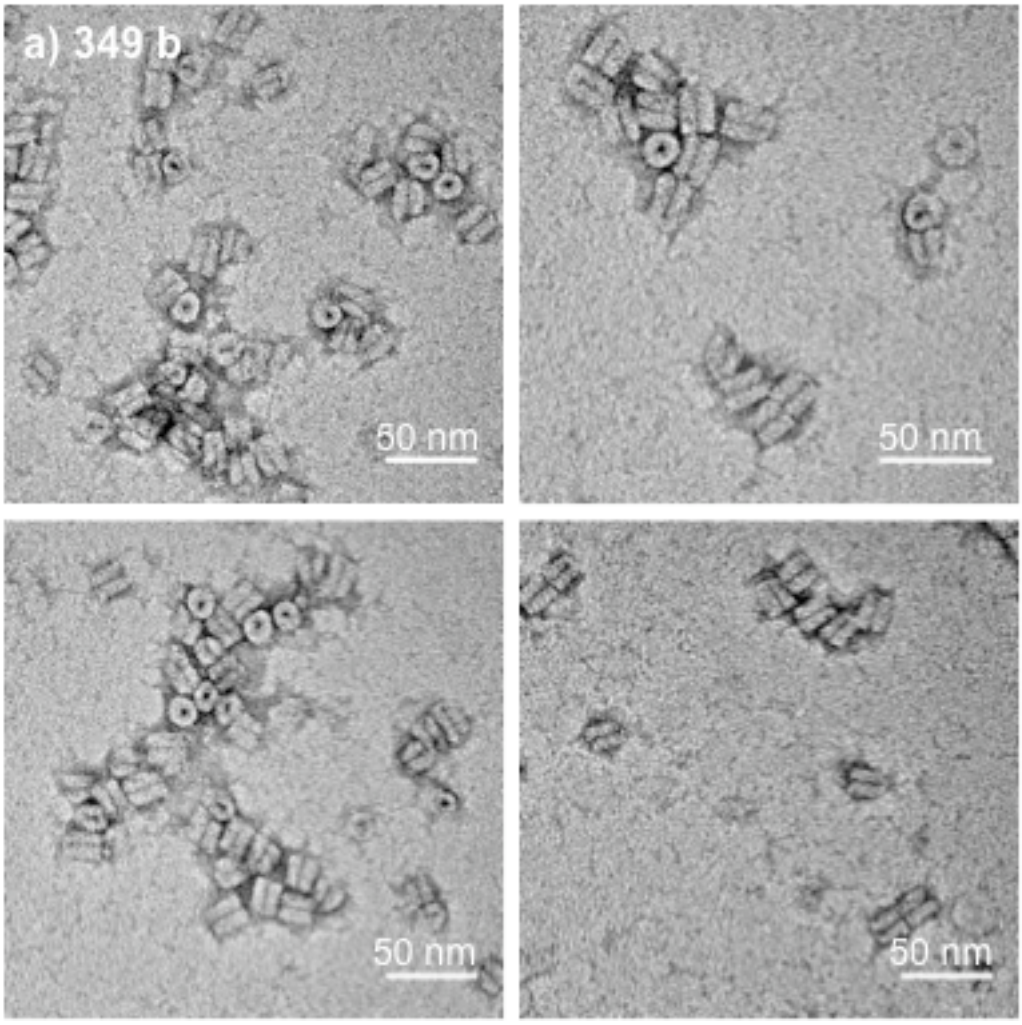

Figure 3.7a Additional TEM images of 349 b 1cys viral building blocks

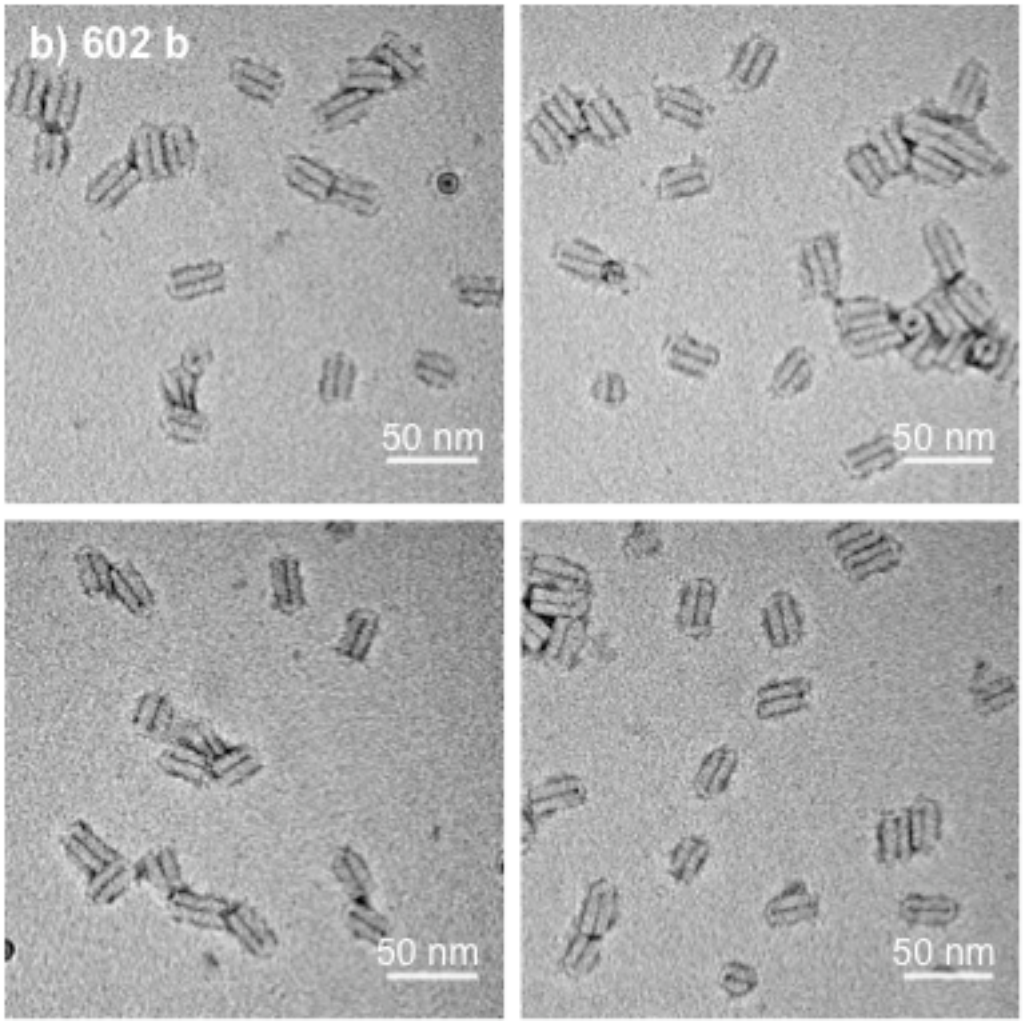

Figure 3.7b Additional TEM images of 602 b 1 cys viral building blocks

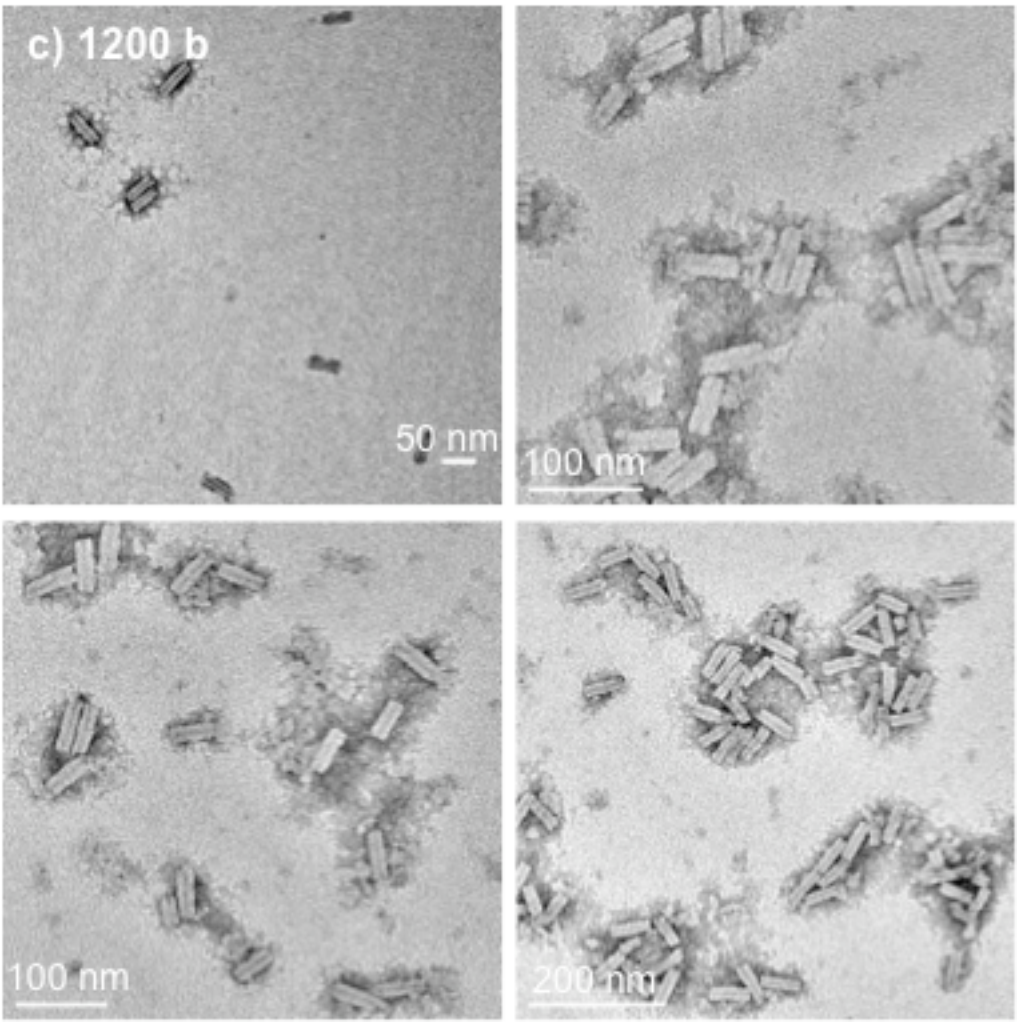

Figure 3.7c Additional TEM images of 1200 b 1cys viral building blocks

As shown in Figure 3.8, I further examined the assembly of the WT viral building blocks and found it to be highly consistent and reproducible throughout the entire population observed for each length of RNA transcript utilized. For this, I measured the length of each WT viral building block observed from 10 or more TEM images collected so that populations of at least 50 building blocks were analyzed for each monomeric and dimeric form of viral building blocks assembled. Additionally, only three 602 b trimers were observed throughout the entire population of 602 b assembled WT viral building blocks. From these data, I then calculated the mean length for each WT monomer, dimer and trimer observed for each length of the RNA transcripts employed. Figure 3.8a shows the number of bases in the RNA transcripts utilized in the assembly of the WT viral building blocks plotted against the calculated mean length of each viral building block. Despite the limited resolution of the TEM-based length measurements under the conditions enlisted in this study, the RNA lengths and the lengths of the assembled WT viral building blocks correlate well, with R^2 values greater than 0.99. This illustrates that the assembly of the WT viral building blocks is governed and readily controlled by the length of the RNA transcript employed for each of the RNA lengths examined. Additionally, as seen in Figure 3.8b, the calculated average lengths of the WT viral building blocks throughout the entire population observed correlate well with the expected values calculated from the RNA lengths. This demonstrates that the length of the

assembled viral building blocks is predictable and consistent. Collectively, these results illustrate that the assembly of the WT viral building blocks is consistent and reproducible for each specified length, which is readily controlled by the length of the RNA transcripts utilized for assembly.

a)

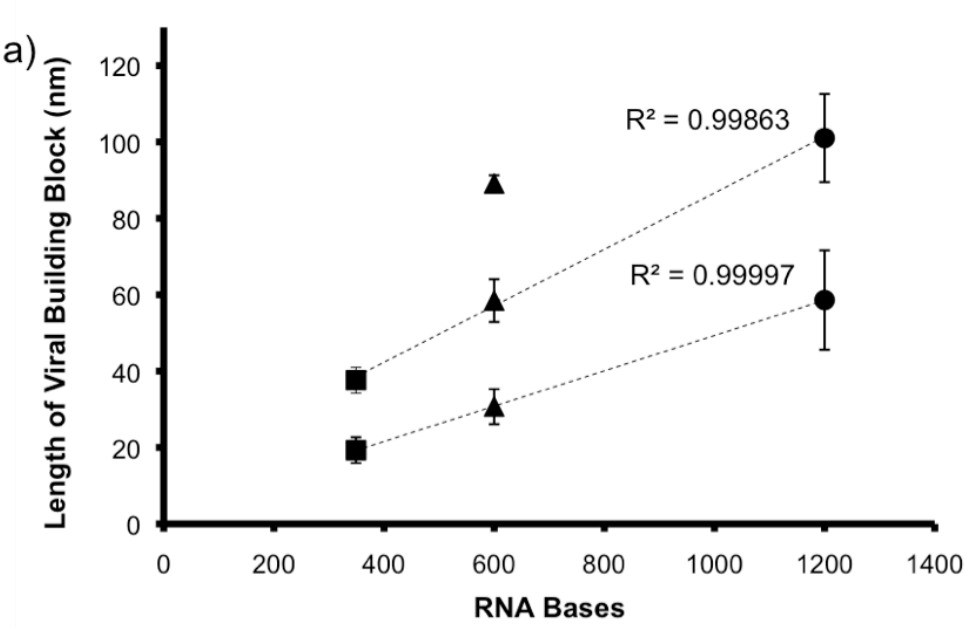

b)

Viral Building Block	Expected Length	Measured Length	N
349b monomer	18 nm	19.3 nm	85
349b dimer	36 nm	37.6 nm	77
600b monomer	28 nm	30.7 nm	153
600b dimer	56 nm	58.4 nm	118
600b trimer	84 nm	89.1 nm	3
1200b monomer	56 nm	58.6 nm	168
1200b dimer	112 nm	101.1 nm	52

Figure 3.8 Analysis of the lengths of the WT viral building blocks (a) Graph of the number of bases in the RNA transcripts employed vs. the length of the WT viral building blocks. (b) Table displaying the expected length, the average measured length and the number of WT building blocks analyzed for each length of WT building block assembled and its oligomers.

Figure 3.9 shows further analysis of the lengths of 1cys viral building blocks observed, demonstrating that the length of the 1cys viral building blocks is also reproducible and consistent for every length of RNA transcript employed. I measured the length of each 1cys viral building block observed from 10 or more TEM images collected so that more than 100 building blocks were analyzed for each length studied. Using these data, I calculated the mean length for each 1cys viral building block observed for each length of the RNA transcripts utilized. Figure 3.9a shows the number of bases in the RNA transcripts employed in the assembly of 1cys viral building blocks plotted against the calculated mean length of each 1cys viral building blocks. As observed with the WT viral building blocks, there is a significant correlation between the length of the 1cys viral building blocks and the length of RNA used in the assembly, with an R^2 value greater than 0.99. This result demonstrates that the assembly of 1cys viral building blocks is dependent upon and controlled by the length of RNA transcript used in the assembly of 1cys viral building blocks for each length of RNA transcript examined. Additionally, Figure 3.9b shows that the calculated average lengths of the observed population of 1cys viral building blocks correlate well with the expected values calculated from the lengths of RNA. As observed with the WT building blocks, this result illustrates that the length of the 1cys assembled viral building blocks is consistent and predictable. Together, these results demonstrate that the assembly of the 1cys viral building blocks is

governed by the length of RNA transcripts employed for assembly and is consistent and reproducible for each specified length. These findings are in accordance with the results obtained for the assembly of WT viral building blocks of different lengths. Importantly, this demonstrates that the addition of cysteine groups in the mutated form of the coat protein does not influence the uniform and predictable assembly of 1cys viral building blocks.

a)

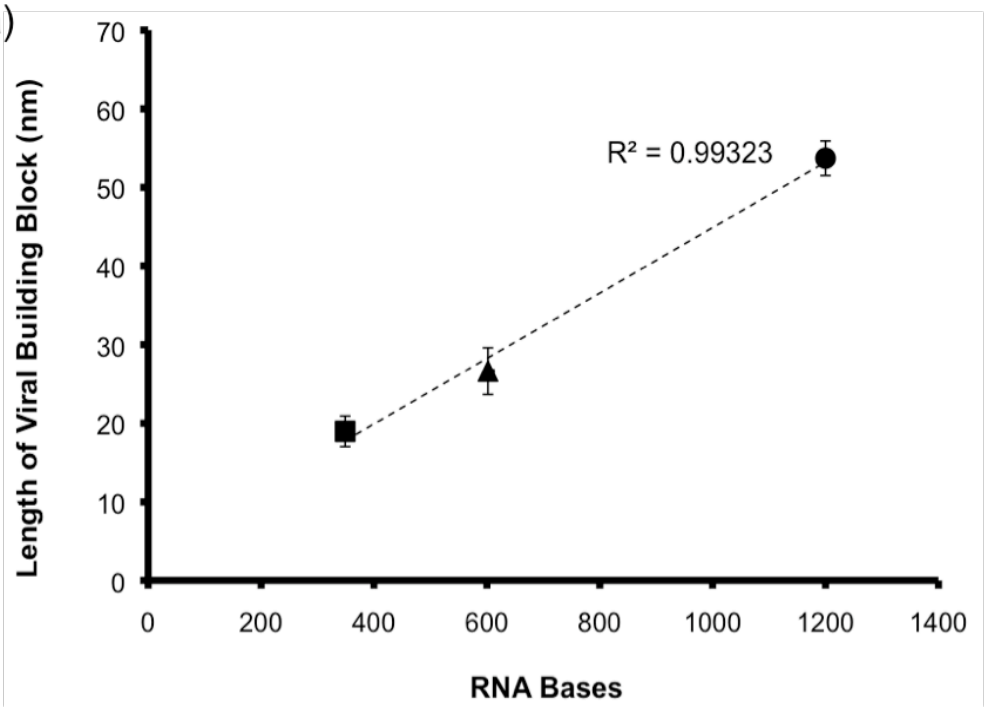

b)

Viral Building Block	Expected Length	Measured Length	N
349 b monomer	18 nm	18.9 nm	120
602 b monomer	28 nm	26.6 nm	138
1200 b monomer	56 nm	53.7 nm	202

Figure 3.9 Analysis of the lengths of the 1cys viral building blocks (a) Graph of the number of bases in the RNA transcripts employed vs. the length of the 1cys viral building blocks. (b) Table displaying the expected length, the average measured length and the number of 1cys building blocks analyzed for each length of 1cys building block assembled and its oligomers

3.3 Conclusions

In this chapter, I studied the assembly of viral building blocks of controlled dimensions using a biologically inspired assembly strategy. To achieve this, I first synthesized DNA templates and *in vitro* RNA transcripts of desired lengths as seen in Figure 3.3 via molecular biology techniques. Assembling the RNA transcripts with TMV coat protein disks yielded viral building blocks of controlled lengths as directed by the lengths of the RNA transcripts employed, as seen in Figures 3.4 and 3.6. Importantly, using either WT coat proteins or the mutated form of the coat protein, which displays a cysteine residue, resulted in the controlled assembly of viral building blocks as governed by the length of RNA transcript used in assembly. This finding illustrates that the addition of a reactive thiol moiety on the coat protein surface does not affect the assembly of 1cys viral building blocks. Further analysis of the assembled viral building blocks, as seen in Figures 3.8 and 3.9, demonstrated that the observed lengths of the WT and 1cys viral building blocks correlate well with the expected lengths as controlled by the length of the RNA transcript utilized. Additionally, both the assembly of WT and 1cys viral building blocks is consistent and reproducible, yielding only building blocks of uniform dimensions.

4 ASSEMBLY OF ONE DIMENSIONAL VIRAL ARRAYS

In this chapter, I investigate the application of WT viral building blocks to assemble one dimensional (1D) arrays via streptavidin-biotin binding. Once established, this strategy could be applied to utilizing doubly biotinylated viral building blocks of controlled dimensions to bind streptavidin coated quantum dots to study the energy transfer between quantum dots arranged at uniform periodicity[73-74]. For this study, viral building blocks assembled with RNA biotinylated at both the 3' and 5' ends are incubated with streptavidin to assemble the 1D nanoarrays, as seen in Figure 4.1. The high affinity binding between biotin and streptavidin (K_D = 10^{-14})[75] makes this interaction an ideal method by which to combine individual viral building blocks to form 1D nanoarrays[76].

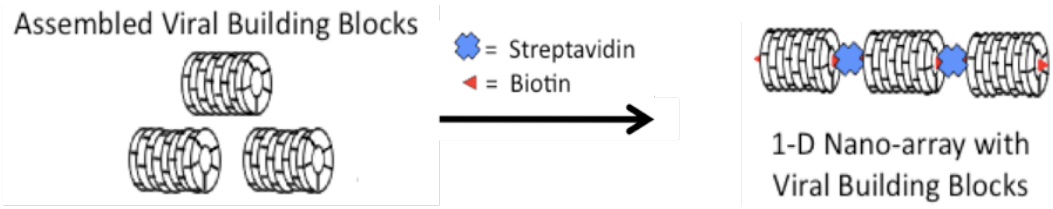

Figure 4.1 Schematic representing the synthesis of a one dimensional nanoarray using doubly biotinylated viral building blocks with streptavidin

To produce doubly biotinylated viral building blocks for use in the assembly of 1D arrays with streptavidin, I first synthesized doubly biotinylated RNA transcripts to be assembled with equilibrated coat proteins. The 5' end of the RNA transcript is biotinylated by the incorporation of 5'-Biotin-GMP (Figure 4.2a) in the *in vitro* transcription reaction of the RNA transcript of specified length. To biotinylate the 3' end of the RNA transcript, the purified RNA transcript is selectively oxidized at the 3' end with sodium meta-periodate to yield hydrazide-reactive dialdehydes. The 3' oxidized RNA is reacted with a biotinylated hydrazide (Figure 4.2b) resulting in the biotinylation of the 3' end of the RNA transcript. Assembling equilibrated coat protein disks with RNA transcripts biotinylated at both the 5' and 3' ends results in the synthesis of doubly biotinylated viral building blocks. To form 1D nanoarrays, the doubly biotinylated viral building blocks are incubated with streptavidin as seen in Figure 4.1.

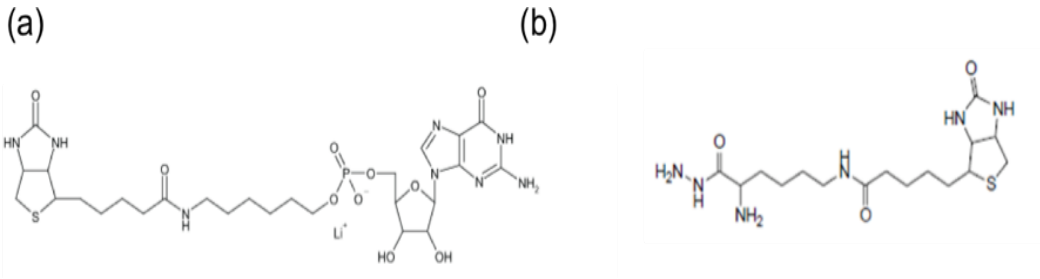

Figure 4.2 Molecules employed in the biotinylation of RNA transcripts. (a) 5'-Biotin-GMP is employed in the transcription reaction of viral building block RNA to biotinylate the 5' end of RNA (b) Biocytin hydrazide used to biotinylate 3' of RNA via periodate oxidation.

My results of this study show the successful synthesis of 3' and 5' biotinylated RNA that is able to bind streptavidin. Additionally, the assembly of doubly biotinylated RNA transcripts and equilibrated coat proteins results in the synthesis of doubly biotinylated viral building blocks, confirming the hypothesis that the functionalization of the ends of the RNA transcript does not prevent the assembly of doubly biotinylated viral building blocks. As with unbiotinylated viral building blocks, the length of the doubly biotinylated viral building blocks is consistent and correlates well with the expected lengths. Finally, my results show that dimers and a small population of higher order oligomers of viral building blocks were observed in the absence and presence of streptavidin in varying concentrations, which may be due to the spontaneous dimerization of TMV upon preparation for analysis by TEM. Due to this observation, it is difficult to discern if the binding of streptavidin facilitates the formation of 1D nanoarrays.

4.1 Materials and Methods

4.1.1 Materials

Biocytin hydrazide used in the biotinylation of the 3' end of RNA was purchased from Thermo Scientific Pierce Protein Research Products (Rockford, IL). 5'-Biotin-GMP used in the biotinylation of the 5' end of RNA was purchased from Trilink Biotechnolgies (San Diego, CA). Streptavidin was purchased from New England Biolabs (Ipswich, MA). The α-^{32}P used to radiolabel RNA transcripts was purchased from Perkin Elmer (Boston, MA). Scintiverse BD Cocktail from Thermo Fisher Scientific (Waltham, MA) was used for liquid scintillation counting. All chemicals were used without further purification.

4.1.2 Synthesis of Doubly Biotinylated RNA

To biotinylate the 5' end of RNA, 5' Biotin GMP was incorporated in the *in vitro* transcription reaction mixture of RNA transcripts. DNA template (2 pmoles) was mixed with 1x T7 RNA Polymerase Reaction buffer, ribonucleotides (1.5 mM each), 10 mM 5' Biotin GMP, DTT (5 mM) and 200 units T7 RNA Polymerase. When necessary, radiolabeled RNA was prepared with the addition of ATP [α-^{32}P] to incorporate ^{32}P throughout the transcript. The reagents were incubated at 42°C for 2 hours. The transcription reaction product was purified by resolution on a 4% native PAGE gel in 0.5x TBE running buffer. The bands of RNA were cut from the gel and electroeluted using the Elutrap electroelution system. The

RNA was then concentrated by ethanol precipitation and stored at -20°C until further use.

The biotinylation of the 3' end of RNA was achieved by conjugation of biocytin hydrazide via periodate oxidation. RNA transcript (~ 100 pmol), 5' biotinylated or not, was incubated with 5 mM sodium meta-periodate ($NaIO_4$) in 50 mM sodium acetate buffer, pH 5.5 in a total volume of 100 uL for 2 hrs at room temperature in the dark. The reaction was quenched by the addition of 100 uL 50% ethylene glycol. The 3' oxidized RNA was purified by ethanol precipitation. The pelleted 3' oxidized RNA was washed with cold 70% ethanol and allowed to dry. To biotinylate the 3' end of the RNA, the pellet of 3' oxidized RNA was resuspended in a solution of 0.5 umole biocytin hydrazide in 100 mM 2-(N-morpholino)ethanesulfonic acid (MES) buffer and incubated overnight at room temperature. The 3' biotinylated RNA was then ethanol precipitated and stored at -20°C until needed.

4.1.3 Gel Shift Assay with Biotinylated RNA and Streptavidin

Incorporation of biotin at the 3' end and 5' end of the RNA was verified using a gel shift assay with radiolabeled singly biotinylyated RNA and streptavidin (Figure 4.3). 20 pmol of 5' biotinylated RNA or 3' biotinylated RNA was incubated at room temperature with varying amounts of streptavidin: 0 pmol, 80 pmol (RNA:SA = 1:4), 5 pmol (RNA:SA = 4:1), or

20 pmol (RNA:SA = 1:1) in phosphate buffered saline for two hours. The resulting products were resolved on a 6% native PAGE gel for 2 hrs in 0.5x TBE running buffer at 24 W. The gel was imaged using a phosphoimager to obtain an autoradiograph image.

4.1.4 Liquid Scintillation Counting

To quantify the yield of biotinylation for the 3' end and 5' end of the RNA transcript, liquid scintillation counting was employed. Singly biotinylated radiolabeled RNA was incubated with streptavidin agarose resin for 2 hrs at room temperature in phosphate buffered saline. After incubation, the streptavidin agarose resin was washed 3 times with phosphate buffered saline to remove any unbound RNA. The wash supernatants were collected and along with the agarose beads, were subjected to liquid scintillation counting to quantify the amount of singly biotinylated radiolabeled RNA bound to the streptavidin agarose resin. 200 uL of the sample was mixed with 5 mL of Scintiverse BD Cocktail and analyzed using a Perkin Elmer TriCarb 2900 Liquid Scintillation Counter (Perkin Elmer, Boston, MA). The data was analyzed using QuantaSmart computer software.

4.1.5 Assembly of Doubly Biotinylated Viral Building Blocks

Doubly biotinylated viral building blocks were synthesized from RNA transcripts biotinylated at the 5' and 3' ends and viral coat proteins. For

this, coat proteins were equilibrated in 40 mM sodium phosphate buffer, pH 7 overnight at 20°C. Doubly biotinylated RNA was added to the equilibrated coat proteins in a ratio of 20:1 by mass and incubated for 2 hrs at 20°C.

4.1.6 Assembly of 1 Dimensional Arrays of Doubly Biotinylated Viral Building Blocks with Streptavidin

To study the assembly of 1D nanoarrays of doubly biotinylated viral building blocks with streptavidin, the doubly biotinylated viral building blocks were first purified from unassembled doubly biotinylated RNA by incubation with diethylaminoethyl cellulose beads. The purified doubly biotinylated viral building blocks were incubated with varying concentrations of streptavidin at 4°C overnight with rotating.

4.2 Results and Discussion

4.2.1 Synthesis of Biotinylated RNA

As seen in Figure 4.3, I first investigated the biotinylation of the 3' and 5' ends of RNA transcripts used for the assembly of doubly biotinylated viral building blocks. To accomplish biotinylation of the 5' end of RNA, 5'-Biotin-GMP was added to the *in vitro* transcription reaction[77]. Because 5'-Biotin-GMP is a nucleotide with only one phosphate group, 5'-Biotin-GMP can only be incorporated into the RNA transcript at the 5' end. 5'-Biotin-GMP does not possess the necessary leaving group to facilitate its

addition within the body of the RNA transcript by T7 RNA Polymerase. For the biotinylation of the 3' end of RNA, the 3' end of the RNA transcript was first selectively oxidized by sodium meta-periodate to yield a reactive dialdehyde, which is highly susceptible to nucleophilic attack. The 3' oxidized RNA is then reacted with a biotinylated hydrazide (EZ-Link Hydrazide-Biocytin) to complete the biotinylation of the 3' end of the RNA.

Figure 4.3a shows an autoradiograph image of a gel shift assay with 349 b 5' biotinylated radiolabeled RNA and streptavidin resolved on a 6% native PAGE gel. For this, 5' biotinylated RNA was transcribed with the incorporation of 5'-Biotin-GMP in the *in vitro* transcription reaction of 349 b radiolabeled RNA. Purified 5' biotinylated RNA was then incubated with varying amounts of streptavidin and the products were resolved on a PAGE gel. Lane 1 shows the resolved products of the incubation of 5' biotinylated RNA with streptavidin in 4 times mole excess. Lane 2 shows the resolved products of the incubation of 5' biotinylated RNA with streptavidin in equal mole amounts. Lane 3 shows the resolved products of the incubation of streptavidin with 5' biotinylated RNA in 4 times mole excess. Lane 4 shows 5' biotinylated RNA without the addition of streptavidin. In each lane for each ratio of streptavidin reacted with the 5' biotinylated RNA, a band of RNA is observed corresponding to RNA that has not interacted with streptavidin. This finding suggests the 5' biotinylation reaction yield of RNA transcripts is less than 100%. The yield

of 5’ biotinylation of RNA transcripts quantified by liquid scintillation counting was found to be greater than 86%. In lanes 1-3, the additional bands at lower mobility (i.e. bands resolved higher than 5’ biotinylated RNA on the gel) are the products of 5’ biotinylated RNA binding with streptavidin in addition to the formation of subsequent oligomers. As expected, when streptavidin is in excess (Lane 1), a limited number of bands at lower mobility are observed due to the excess streptavidin capping all the 5’ biotinylated RNA and preventing further assembly into oligomers. When streptavidin is present in ratios equal to or less than the amount of 5’ biotinylated RNA (Lane 2-3), multiple bands are observed at lower mobility, representing the multiple oligomers formed from the binding of 5’ biotinylated RNA with streptavidin. Collectively, these results show that the 5’ end of the RNA transcript was successfully biotinylated with the incorporation of 5’-Biotin-GMP in the *in vitro* transcription reaction and further able to interact with streptavidin.

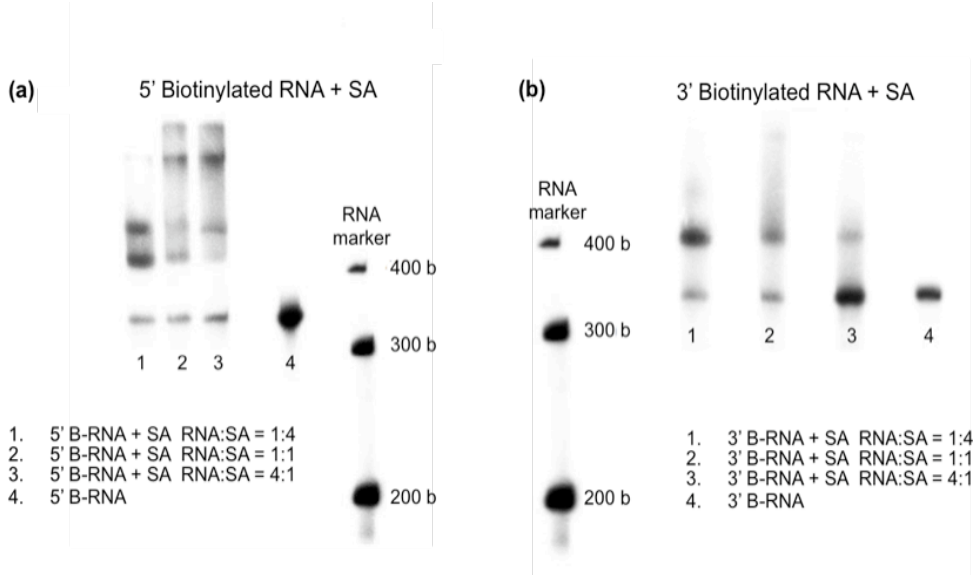

Figure 4.3 Gel shift assay of singly biotinylated RNA with streptavidin. Radiolabeled singly biotinylated RNA was incubated with streptavidin in excess (1:4), in equal amounts (1:1) and in deficit (4:1). Reactions were resolved by polyacrylamide gel electrophoresis and visualized using a phosphoimager. (a) 5' biotinylated RNA (b) 3' biotinylated RNA

Figure 4.3b shows an autoradiograph image of a gel shift assay with 349 b 3' biotinylated radiolabeled RNA and streptavidin resolved on a 6% PAGE gel. For this, purified 349 b radiolabeled RNA transcripts were selectively oxidized at the 3' end with sodium meta-periodate and then biotinylated by the reaction of hydrazide functionalized biotin[78-79]. Purified 3' biotinylated RNA was incubated with varying amounts of streptavidin and the products were then resolved on a PAGE gel. Lane 1 shows the resolved products of the reaction of 3' biotinylated RNA with 4 times mole excess of streptavidin. Lane 2 shows the resolved products of the reaction of 3' biotinylated RNA with streptavidin present in an equal amount. Lane 3 shows the resolved products of the incubation of streptavidin with 4 times mole excess of 3' biotinylated RNA. Lane 4 shows the band corresponding to 349 b 3' biotinylated RNA that was not incubated with streptavidin. In each lane for every ratio of streptavidin reacted with the 3' biotinylated RNA, a band of RNA is observed corresponding to RNA that has not interacted with streptavidin. Because not all of the 3' biotinylated RNA has interacted with the streptavidin, this suggests that the reaction yield of 3' biotinylated of the RNA transcript is less than 100%. Using liquid scintillation counting, the yield of biotinylation at the 3' end of RNA transcripts was found to be greater than 74%. As observed with the reaction of 5' biotinylated RNA and streptavidin, lanes 1-3 show the presence of additional bands of RNA at lower mobility which are the products of 3' biotinylated RNA binding to streptavidin. When streptavidin

is present in excess (Lane 1), the results show the presence of only one band of higher mobility. This finding suggests the 3' biotinylated RNA has interacted with the excess streptavidin such that the excess streptavidin has capped the RNA preventing the formation of oligomers as expected. When streptavidin is present in the same mole ratio as 3' biotinylated RNA (Lane 2), the formation of oligomers due to the streptavidin linking 3' biotinylated RNA molecules is observed as indicated by the presence of bands of lower mobility. For the binding of streptavidin to an excess of 3' biotinylated RNA (Lane 3), the results show a significant band of RNA corresponding to the mobility of 3' biotinylated RNA that has not interacted with streptavidin. As expected, because not enough streptavidin is present to interact with the 3' biotinylated RNA, bands of lower mobility are not observed. Together these results represent the successful biotinylation of the 3' end of RNA. Additionally, these findings demonstrate the ability of 3' biotinylated RNA to bind streptavidin, which will be instrumental in the assembly of 1D nanoarrays via biotin-streptavidin binding.

4.2.2 Synthesis of Doubly Biotinylated Viral Building Blocks

Next, as seen in Figure 4.4, I examined the assembly of doubly biotinylated viral building blocks to be used in the assembly 1D nanoarrays. For this, I first prepared RNA biotinylated at both the 5' and 3' end. This was achieved by incorporating biotin at the 5' end of the RNA

transcript during *in vitro* transcription with the addition of 5'-Biotin-GMP to the transcription reaction and then selectively oxidizing and conjugating a derivative of biotin hydrazide to the 3' end of the purified 5' biotinylated RNA transcript to yield doubly biotinylated RNA. Next, I equilibrated WT TMV coat proteins in sodium phosphate buffer to form the 20S disk structures necessary for assembly of the viral building blocks. To assemble doubly biotinylated viral building blocks, equilibrated coat proteins were mixed with RNA biotinylated at both the 5' and 3' ends and incubated together for 2 hrs. The assembly of doubly biotinylated viral building blocks was observed by TEM. Figure 4.4a shows a representative TEM image of the doubly biotinylated viral building blocks assembled from 602 b RNA transcripts biotinylated at both the 5' and 3' ends and equilibrated WT coat proteins. Importantly, the functionalization of the RNA transcripts with biotin did not affect the assembly of viral building blocks as a substantial population of doubly biotinylated viral building blocks was observed by TEM. As observed with the unbiotinylated viral building blocks, doubly biotinylated viral building block monomers and dimers are observed in the TEM image. Additionally, the length of the doubly biotinylated viral building blocks is dependent upon the length of RNA transcript employed for assembly, with no assembled products of alternative length being observed. The length of the 602 b doubly biotinylated viral building blocks is uniform and reproducible. These results signify that the addition of biotin to both ends of the RNA

transcript does not inhibit the readily controlled assembly of doubly biotinylated viral building blocks.

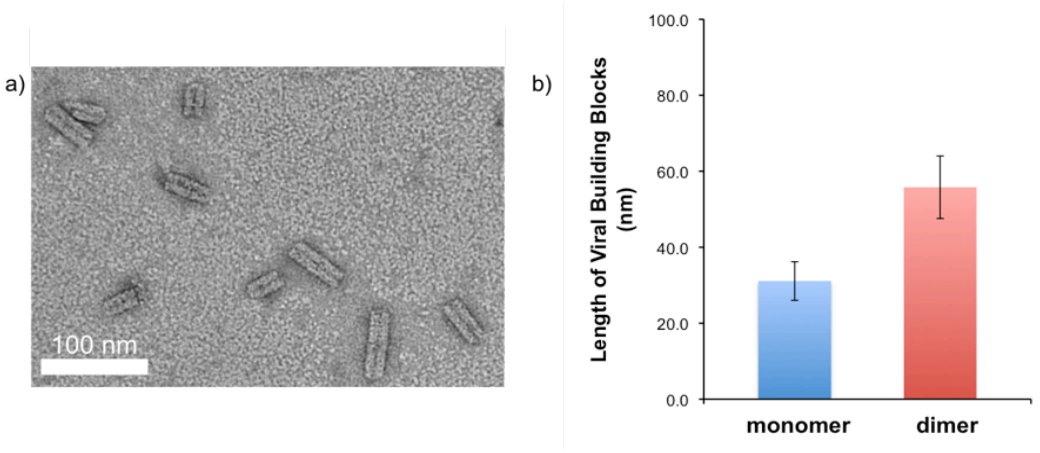

Figure 4.4 Assembly of doubly biotinylated viral building blocks. (a) Representative TEM image of 602 b (28 nm) doubly biotinylated viral building blocks. (b) Quantification of the lengths measured for the population of 600 b monomer and dimer doubly biotinylated viral building blocks observed. The mean length of the monomer was found to be 31.1 nm. The mean length of the dimer was found to be 55.8 nm.

Next, in Figure 4.4b I further examined the assembly of 602 b doubly biotinylated viral building blocks and found it to be highly reproducible and predictable as observed for viral building blocks assembled without functionalized RNA transcripts. For this, I measured the length of each doubly biotinylated viral building block from 10 or more TEM images to fully represent the population of doubly biotinylated viral building blocks observed. I measured the length of 303 doubly biotinylated viral building block monomers and 164 doubly biotinylated viral building block dimers. Using these data, I calculated the mean length for each 602 b doubly biotinylated viral building block monomer and dimer. Figure 4.4b shows the oligomer form of doubly biotinylated viral building block plotted against the calculated mean length of the doubly biotinylated viral building blocks. Although measuring the lengths of the doubly biotinylated viral building blocks by TEM provided limited resolution, the lengths of the doubly biotinylated viral building blocks correlate well with the expected values. The calculated mean length of the 602 b doubly biotinylated viral building block was found to be 31.1 nm in comparison to the expected value of 28 nm. The calculated mean length of the 602 b doubly biotinylated viral building block dimers observed was found to be 55.8 nm while the expected length is 56 nm. This finding demonstrates that the addition of biotin to both ends of the RNA transcript employed in assembly of viral building blocks does not inhibit the consistent and predictable assembly of doubly biotinylated viral building blocks. Together these results illustrate

that the assembly of doubly biotinylated viral building blocks is consistent and reproducible, such that the length of the assembly is governed by the length of the RNA transcript employed, in addition to being unaffected by the biotinylation of the ends of the RNA transcript employed.

4.2.3 Assembly of 1 Dimensional Nanoarrays using Doubly Biotinylated Viral Building Blocks and Streptavidin

Next, I investigated the assembly of 1D nanoarrays using doubly biotinylated viral building blocks and streptavidin. For this, I first removed any RNA biotinylated at the 5' and 3' ends that was not incorporated in the assembly of doubly biotinylated viral building blocks using equilibrated diethylaminoethyl (DEAE) beads. Then, to fabricate 1D nanoarrays of viral building blocks, I reacted doubly biotinylated viral building blocks with varying amounts of streptavidin and investigated the concentration dependence of streptavidin on the assembly of the 1D arrays. The assembled 1D nanoarrays of doubly biotinylated viral building blocks and streptavidin was analyzed by TEM. The TEM images of doubly biotinylated viral building blocks incubated with streptavidin showed many doubly biotinylated viral building block monomers, while only a small population of the viral building blocks observed assembled as dimers and higher order oligomers. As previously observed, even without the presence of streptavidin, doubly biotinylated viral building blocks were observed to exist as monomers and dimers. The formation of TMV dimers

has been well documented and known to occur spontaneously in solution due to hydrophobic interactions exhibited between the dipolar ends of the virus structure[20]. Additionally, aggregation resulting from TEM sample preparation may also contribute to the observation of viral building block oligomers. Because viral building block dimers are observed without the presence of streptavidin, this phenomenon makes it difficult to discern if the doubly biotinylated viral building blocks that are observed as dimers or higher order oligomers is due to the binding of streptavidin to form 1D nanoarrays or due to the spontaneous arrangement of the viral building blocks binding end-to-end driven by hydrophobic interactions.

As seen in Figure 4.5, I further examined the fabrication of 1D nanoarrays using doubly biotinylated viral building blocks and streptavidin by quantifying the lengths of the oligomers observed by TEM. For this, I measured the length of doubly biotinylated viral building block oligomers observed after incubation of streptavidin from 10 or more TEM images to ensure that a significant population of each oligomer was observed. Using these data, I then plotted the length of doubly biotinylated viral building blocks observed against the frequency by which they were observed. For each concentration of streptavidin tested, the highest frequency of doubly biotinylated viral building blocks observed exists around 30 nm as indicated by the large peak centralized at this length for each sample, as seen in Figure 4.5. Since the doubly biotinylated viral building blocks have

a calculated mean length of 31.1 nm, this finding signifies that most of the doubly biotinylated viral building blocks exist as monomers, independent of the presence of streptavidin or its concentration. Also, Figure 4.5 shows that when streptavidin was absent (control) a smaller peak is observed at 50-60 nm which signifies that a smaller frequency of doubly biotinylated viral building blocks was observed at this length. Additionally, this same small peak at 50-60 nm is observed when streptavidin was added to the doubly biotinylated viral building blocks in excess (RNA:SA = 1:4) or equal mole amounts (RNA:SA = 1:1). The calculated mean length of the dimeric form of doubly biotinylated viral building blocks was found to be 55.8 nm. These results illustrate that in the absence or presence of equal or excess amounts of streptavidin doubly biotinylated viral building block dimers are observed. Interestingly, when streptavidin was present in only excess of two (RNA:SA = 1:2), two peaks of similar frequency of doubly biotinylated viral building block lengths are observed at the monomer length of 30 nm and the dimer length of 50-60nm. This result demonstrates that a relatively equal amount of doubly biotinylated viral building block monomers and dimers were observed when the excess of streptavidin added to the doubly biotinylated viral building blocks was only double. Finally, Figure 4.5 shows that when the doubly biotinylated viral building blocks were incubated in excess of streptavidin (RNA:SA = 4:1), a broad peak for the frequency of the lengths of doubly biotinylated viral building blocks is observed, extending from 20-80 nm. This illustrates that

when the doubly biotinylated viral building blocks are in excess of streptavidin, the length of viral building block oligomers observed is disperse. Additionally, for each concentration of streptavidin tested, sparse frequency peaks exist at higher lengths of doubly biotinylated viral building block measured. This signifies that a small population of higher order oligomers (trimer and tetramer) was observed. Collectively, these results show that in the addition and absence of streptavidin, dimers of doubly biotinylated viral building blocks are observed. Because dimers are observed when no streptavidin is present due to the spontaneous end-to-end arrangement of viral building blocks and possible aggregation upon preparation of the sample for analysis by TEM, it is difficult to conclude that the addition of streptavidin facilitated the assembly of 1D nanoarrays.

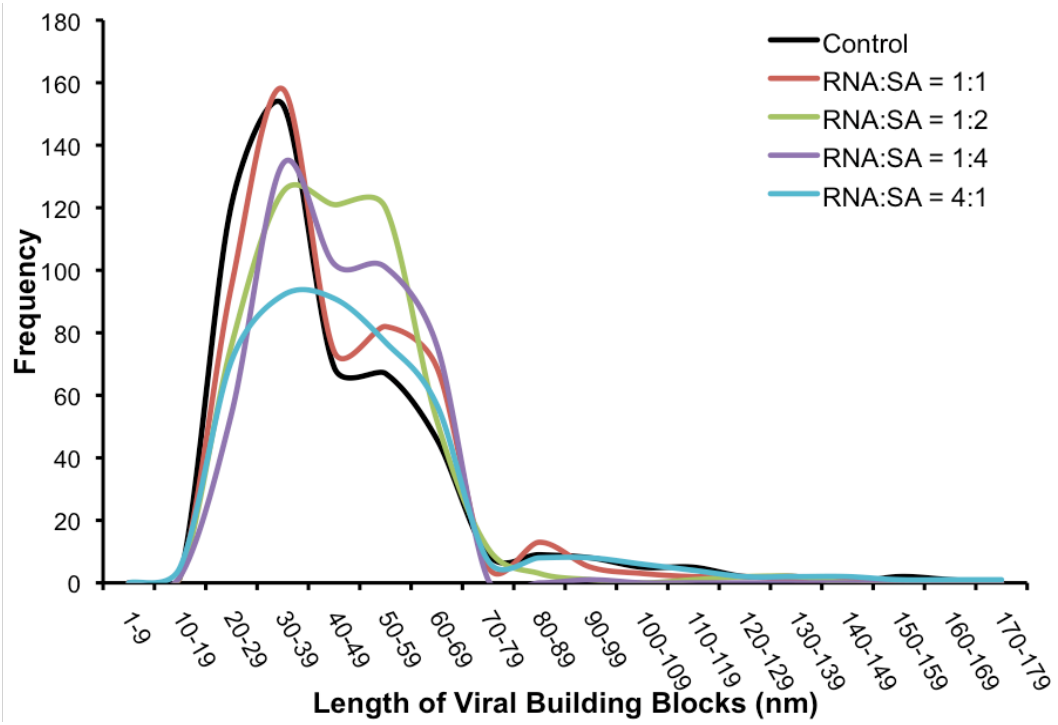

Figure 4.5 Quantification of 602 b doubly biotinylated viral building block lengths after reaction with streptavidin.

4.3 Conclusions

In this chapter, I investigated the assembly of doubly biotinylated viral building blocks and their employment in the formation of 1D nanoarrays with the addition of streptavidin. As shown in Figure 4.3a, I successfully synthesized 5' biotinylated RNA by the addition of 5' Biotin GMP in the *in vitro* transcription reaction of RNA transcripts of specified length and observe the binding of the 5' biotinylated RNA to streptavidin in a gel shift assay. Additionally, I biotinylated the 3' end of RNA transcripts by the selective oxidation with sodium meta-periodate and subsequent reaction with biotin hydrazide and observed the reaction of 3' biotinylated RNA with streptavidin as seen in Figure 4.3b. Next, doubly biotinylated viral building blocks were synthesized by assembling RNA transcripts biotinylated at both the 3' and 5' ends with equilibrated coat proteins, such that the length of the doubly biotinylated viral building block was governed by the length of the doubly biotinylated RNA transcript used in the assembly, as seen in Figure 4.4. Importantly, the functionalization of the ends of the RNA transcript did not inhibit the assembly of doubly biotinylated viral building blocks. For the investigation of the formation of 1D nanoarrays with doubly biotinylated viral building blocks, Figure 4.5 shows that dimers were observed in the absence and presence of varying amounts of streptavidin. The viral building blocks derived in this study were observed to exhibit the same spontaneous end-to-end alignment driven by hydrophobic interactions as the full-length TMV. In conclusion, while I was

able to confirm that RNA transcripts biotinylated at both the 5' and 3' ends could assemble with equilibrated coat proteins to form doubly biotinylated viral building blocks, I was unable to conclude that the addition of streptavidin to the doubly biotinylated viral building blocks facilitated the assembly of 1D nanoarrays as observed by the formation of higher order oligomers of doubly biotinylated viral building blocks.

4.4 Future Directions

The studies in this chapter were directed at utilizing the viral building blocks of a tunable length to fabricate biologically inspired 1D nanoarrays via streptavidin-biotin binding. Due to the spontaneous end-to-end arrangement of viral building blocks driven by hydrophobic interactions between ends of the viral building blocks and the possible aggregation of viral building blocks upon TEM sample preparation, it was not possible to contribute the formation of the doubly biotinylated viral building blocks oligomers observed to the addition of streptavidin to promote the assembly of 1D nanoarrays. Thus, an alternative method of analysis may be required. One such method may be the resolution of the products resulting from the addition of streptavidin to doubly biotinylated viral building blocks on a vertical agarose gel. The oligomers formed via biotin-streptavidin binding would be visualized as individual bands of varying mobility on the gel after staining. This solution based method for analysis of the products resulting from doubly biotinylated viral building blocks

binding streptavidin to form dimers, trimers and higher oligomers will circumvent the spontaneous aggregation observed upon TEM sample preparation and yield a suitable method for determining the results of streptavidin binding to doubly biotinylated viral building blocks. Additionally, chemical reagents, such as Tween 20, could be added to the assembly of 1D nanoarrays with doubly biotinylated viral building blocks and streptavidin to inhibit the hydrophobic interactions, which direct the end-to-end alignment of the viral building blocks. Also, increasing the pH used in the assembly of 1D nanoarrays would facilitate the repulsion exhibited by the amino acid residues Glu50 and Asp77 by deprotonating the carboxylate groups of these amino acids displayed by the viral coat protein[20, 80].

5 ALTERNATIVE APPLICATIONS OF VIRAL BUILDING BLOCKS WITH CONTROLLED DIMENSIONS

In this chapter, I study several alternative applications of viral building blocks with controlled dimensions that exploit the chemically reactive thiol groups displayed on the 1cys mutant viral building blocks. I first investigated the use of 1cys viral building blocks as a template for the synthesis of metal nanoparticles[18], as seen in Figure 5.1, to form nanocatalysts[10]. I studied the hypothesis that the number of metal nanoparticles synthesized on the surface of the viral building blocks will be dependent upon the number of cysteine residues displayed on the 1cys viral building blocks, which is directly governed by the length of the building block employed. As application as a nanocatalyst, the length of the viral building block will govern the number of metal nanoparticles synthesized and thus the extent of catalytic activity of the nanocatalyst. My results show the successful synthesis of platinum nanoparticles on 1cys viral building blocks, but aggregation of the metalized viral building blocks prevent the exact number of nanoparticles synthesized per viral building block to be obtained.

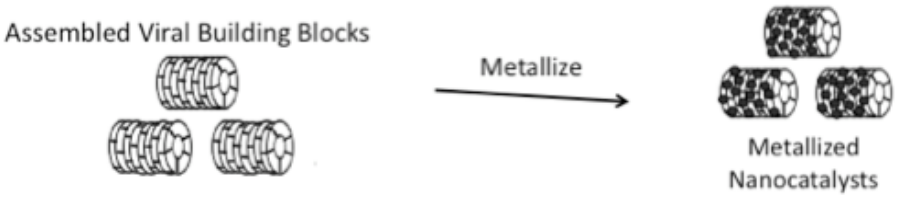

Figure 5.1 Schematic representation of the metallization of viral building blocks to form metallized nanocatalysts. Platinum nanoparticles are synthesized on 1cys viral building blocks by the reduction of platinum precursor.

Next, I studied the vertical assembly of 1cys viral building blocks on gold surfaces as seen in Figure 5.2. For this, I explored the exploitation of the position of the cysteine residues displayed on the 1cys viral building blocks. Along the length of the 1cys viral building blocks, the reactive thiol groups of the cysteine residues are recessed within a groove provided by the C-terminal end of the coat protein (Figure 5.2a)[81]. To preferentially assemble the 1cys viral building blocks vertically, I predicted that at the 3' end of the 1cys viral building blocks, the cysteine residues are more accessible and should preferentially bind to the gold surface to form a vertically patterned assembly of 1cys viral building blocks. Based on this hypothesis, the length of viral building blocks employed should determine the height of the vertical assembly, which can be readily tuned. Vertically patterned viral building blocks of controllable length could be further functionalized by metallization[5, 81] or conjugation[35, 82] by small molecules to promote the synthesis of novel biomaterials. My results show that under the reaction conditions studied, the vertical assembly of 1cys viral building blocks was not achieved but these studies yielded important insights which can be applied to alternative methods to achieve vertically patterned 1cys viral building blocks.

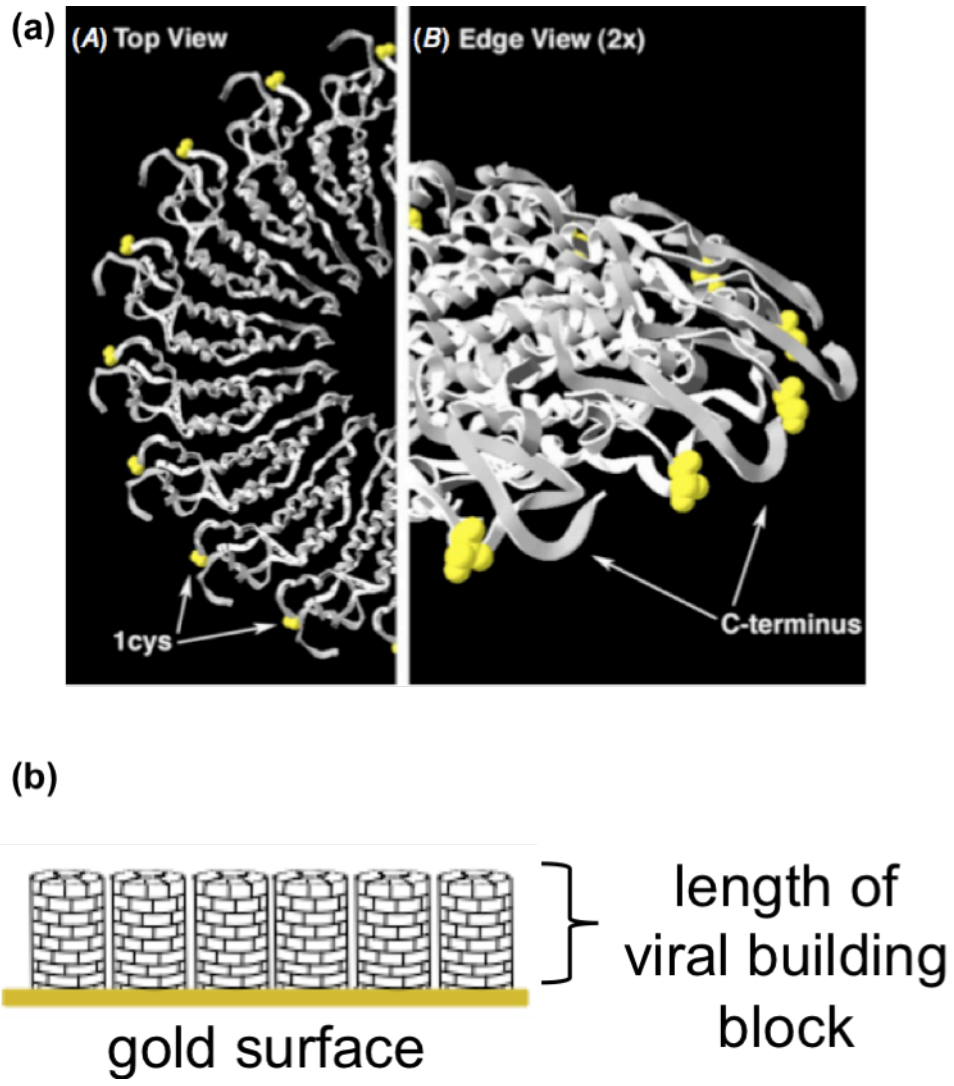

Figure 5.2 Display of 1cys mutation on 1cys viral building blocks and their vertical assembly on a gold surface. (a) Schematic depiction of the cysteine mutation in 1cys viral building blocks as adapted from Culver *et al*.[81] (b) Schematic depiction of viral building blocks vertically assembled on a gold surface where the height of the assembly is dependent upon the length of the viral building blocks.

Finally, I explored the functionalization of viral building blocks with small molecules by exploiting the chemically reactive thiol groups displayed on the 1cys mutant viral building blocks, as seen in Figure 5.3. Three small molecules were studied: fluorescein, Nanogold and green fluorescent protein (GFP). In these studies, I investigated the relationship between the number of cysteine residues displayed on the 1cys viral building blocks, which is directly dependent upon the length of the 1cys viral building block, and the number of small molecules bound to the 1cys viral building blocks. The functionalization of viral building blocks could be applied toward the bottom up assembly of novel biomaterials[34-35] from individual components of controlled length. My results of these studies show the extent of fluorescein functionalization of viral building blocks is dependent upon the length of the viral building blocks employed, such that more fluorescein molecules are associated with longer viral building blocks (1200 b) in comparison to shorter viral building blocks (602 b). The thiol-specific functionalization of 1cys viral building blocks envisioned to yield attachment of the same number of small molecules as cysteine residues displayed on the 1cys viral building blocks was not conclusive because the small molecules studied were found to interact similarly with both 1cys and WT viral building blocks. While the length dependent functionalization of viral building blocks was achieved by the studies conducted in this chapter, these studies have also provided the necessary foundation for elucidating the appropriate conditions for exploiting the

chemically reactive thiol residues displayed by 1cys viral building blocks to readily tune the extent of functionalization by varying the length of viral building blocks employed.

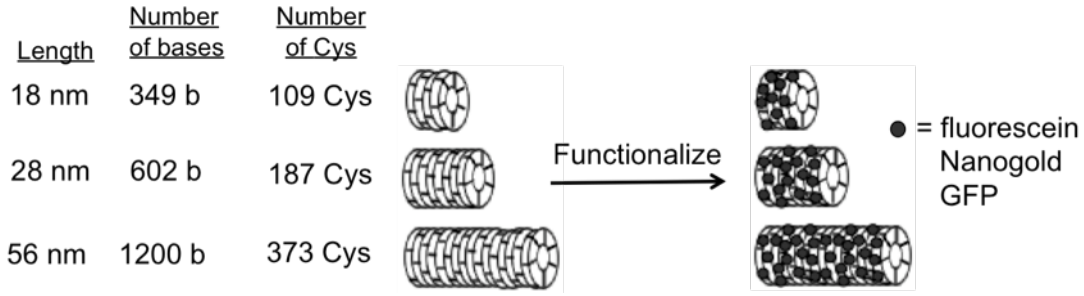

Figure 5.3 Schematic depiction of the length-dependent functionalization of viral building blocks. The table on the left shows the number of cysteine groups displayed for every length of 1cys viral building block studied. On the right is a schematic depiction of the length dependent functionalization of the 1cys viral building blocks with small molecules. The small molecules studied were fluorescein, Nanogold and green fluorescent protein (GFP). The number of small molecules attached to the 1cys viral building blocks should be dependent upon the number of cysteine groups displayed, which is directly dependent upon the length of the 1cys viral building block used for functionalization.

5.1 Materials and Methods

5.1.1 Materials

The fluorescein-5-maleimide used to functionalize viral building blocks with fluorescein was purchased from Thermo Scientific Pierce Protein Research Products (Rockford, IL). Gold-coated mica surfaces employed in the vertical assembly of viral building blocks were purchased from Platypus Technologies (Fitchburg, WI). Mono-maleimide Nanogold used in the functionalization of TMV with Nanogold was purchased from Nanoprobes, Inc. (Yaphank, NY). Maleimido-C3-NTA used to link GFP to 1cys full-length TMV and 1200 b viral building blocks was purchased from Dojindo Molecular Technologies, Inc. (Rockville, MD). Nanosep centrifugal devices with Omega^{TM} membrane filter used for purification by membrane filtration chromatography of functionalized full-length TMV or viral building blocks from excess, unreacted reagent were purchased from Pall Life Sciences (Ann Arbor, MI).

5.1.2 Metallization of Viral Building Blocks

The synthesis of platinum nanoparticles on 1cys viral building blocks was performed by Cuixian Yang. 602 b 1cys viral building blocks (~0.15 mg/mL) were incubated with 5 mM platinum precursor ($Na_2PtCl_6 \bullet 6H_2O$) and 0.5 mM $NaBH_4$ for 5 min at room temperature. The products of the metallization reaction were deposited on a TEM grid, rinsed several times

in distilled water to removed excess, unbound reagents and analyzed by TEM.

5.1.3 Vertical Assembly of Viral Building Blocks on a Gold Surface

Gold-coated mica surfaces were prepared by hydrogen flame annealing. To vertically assemble viral building blocks, 1cys or WT viral building blocks were deposited on hydrogen-flame annealed gold surfaces either by pipetting the viral building block solution on the gold surface or incubating the gold surface in a solution of viral building blocks in a closed Eppendorf tube. The concentration dependence of viral building blocks toward their preferential vertical assembly was also examined. Viral building blocks were allowed to deposit on gold surfaces overnight at room temperature. Gold surfaces with assembled viral building blocks were dipped in water and dried by nitrogen gas before analysis by atomic force microscopy.

5.1.4 Atomic Force Microscopy

The assembly of viral building blocks on gold surfaces was examined using atomic force microscopy (AFM). AFM images were acquired using a Dimension 3100 series Scanning Probe Microscope (SPM) (Veeco, Woodbury, NY). Images were analyzed using NanoScope software. All AFM measurements were conducted in tapping mode, with TAP-Al-50 AFM tips (Budget Sensors, Sofia, Bulgaria).

5.1.5 Functionalization of Viral Building Blocks with Fluorescein

Viral building blocks (~25 ug) were reacted with 10x mole excess of fluorescein-5-maleimide based on the number of reactive cysteine residues available due to the length of viral building block employed. Reagents were incubated together at room temperature for 2 hrs. Purification of fluorescein-labeled viral building blocks from excess, unreacted fluorescein was achieved by implementing size exclusion chromatography with G-10 Sephadex resin or membrane filtration centrifugation using 3 kDa MWCO membrane filtration centrifugation columns. The resulting products were analyzed by UV/Vis spectrometry.

5.1.6 UV/Vis Spectrometry

The extent of fluroescein functionalization of viral building blocks was monitored using an Evolution^{TM} 300 UV/vis Spectrophotometer (Thermo scientific, Waltham, MA).

5.1.7 Functionalization of TMV with Nanogold

To elucidate the reaction conditions necessary for the reaction of mono-maleimide Nanogold with 1cys viral building blocks, 1cys full-length TMV was used as a suitable substitution. For the reaction of mono-maleimide Nanogold with full-length TMV, ~30 ug of full-length TMV (WT and 1cys) were incubated with 1.5 nmol mono-maleimide Nanogold in 20 mM sodium phosphate buffer pH 6.5, 1 mM EDTA ± 0.1% Tween 20 for 2 hrs

at room temperature. The reaction mixture was then purified using membrane filtration chromatography using membranes with a MWCO of 300 kDa. The reaction mixture retained on top of the membrane was washed 3 times or more with 50 uL of reaction buffer until the resulting eluate was clear. Purified reaction products collected from the top of the membrane filter were analyzed by TEM without additional staining.

5.1.8 Functionalization of TMV with Green Fluorescent Protein (GFP)

To label full-length 1cys TMV and 1200 b 1cys viral building blocks with GFP, first 25 ug of full-length TMV and 35 ug of 1200 b 1cys viral building blocks were reacted with 19 nmol maleimide-C3-NTA in 100 mM HEPES overnight at room temperature. Next, 190 nmol of $NiSO_4$ were added and incubated with the reaction mixture for 1 hr at room temperature. To functionalize with GFP, 0.6 nmol of His-tagged GFP were added to the reaction mixture and incubated for 1 hr at room temperature. Size exclusion chromatography with Sephadex G75 resin was used to purify the reaction mixture.

To elucidate the appropriate purification conditions for an increased amount of GFP for functionalization, bovine serum albumin (BSA) was utilized as a suitable analogue. Size exclusion chromatography was tested using Sephadex G75 resin. Membrane filtration chromatography

with membrane filters of MWCO 300 kDa was also tested. The resulting elutions were analyzing using UV/Vis spectrometry.

5.2 Results and Discussion

5.2.1 Metallization of Viral Building Blocks

I first examined the metallization of 1cys viral building blocks as seen in Figure 5.4. To accomplish this, platinum nanoparticles were synthesized on the viral building blocks by incubating 602 b 1cys viral building blocks with platinum precursor followed by reduction by sodium borohydride. As with the full-length cysteine mutated TMV[18], I expect the platinum precursor to selectively bind to the cysteine residues displayed by the coat proteins on the 1cys viral building blocks. Because of this, the number of platinum nanoparticles synthesized on the viral building blocks should be dependent upon the number of cysteine residues displayed by the viral building blocks, which is governed by the length of the viral building blocks. Thus, the number of platinum nanoparticles synthesized should be directly dependent upon the length of the viral building blocks employed. The platinum metalized viral building blocks were observed by TEM without additional staining.

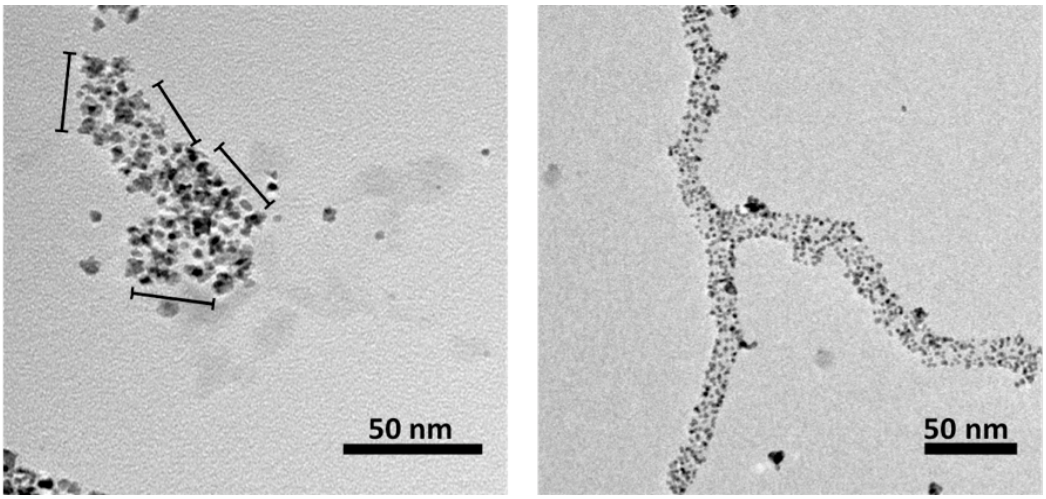

Figure 5.4 Representative TEM images of Pt metallized 602 b (28 nm) length viral building blocks. Brackets have been added to the image on the left to facilitate the distinction of individual viral building blocks.

Figure 5.4 shows representative TEM images of platinum metalized 602 b 1cys viral building blocks. As seen in this figure, platinum nanoparticles are observed and are confined to the dimensions of the viral building blocks as metal nanoparticles are not observed throughout the entire image. This result signifies that 1cys viral building blocks successfully functioned as a template for the synthesis of platinum nanoparticles. Additionally, the TEM image on the left in Figure 5.4 shows a cluster of viral building blocks. The brackets added to this TEM image assist to distinguish individual metalized viral building blocks. In all of the over 30 TEM images collected, the metalized viral building blocks are observed to aggregate which makes it difficult to discern individual metalized viral building blocks. This observed aggregation of metalized viral building blocks may result from sample preparation for analysis by TEM. Because individual metalized viral building blocks are not explicitly distinct in the TEM images collected, it is not possible to determine the number of metal nanoparticles formed on individual viral building blocks. This finding prevents correlation between the number of metal nanoparticles synthesized and the length of 1cys viral building blocks employed. Collectively, these results demonstrate that 1cys viral building blocks can be utilized as a biological template for the synthesis of platinum nanoparticles. In addition, the observed aggregation of metalized viral building blocks in the TEM images collected inhibited determination of the number of metal nanoparticles synthesized per individual viral building

block. The platinum nanoparticles were easily visualized by TEM and confined to the dimensions of the viral building blocks, which signified that the synthesis of platinum nanoparticles was limited to the surface of the viral building blocks such that extent of metal nanoparticles synthesized is governed by the length of the viral building block. Though due to the aggregation of the metalized viral building blocks, it was not possible to verify that the exact number of metal nanoparticles synthesized is dependent upon the number of cysteine residues displayed on the viral building blocks and thus, the length of the viral building blocks.

5.2.2 Vertical Assembly of Viral Building Blocks on a Gold Surface

Next, I examined the vertical assembly of 1cys viral building blocks on a gold surface. For this, I first prepared the gold surface by hydrogen flame annealing to ensure a clean binding surface. To vertically assemble the viral building blocks, 602 b 1cys viral building blocks were incubated with the freshly prepared gold surface overnight. The resulting assembly of viral building blocks was analyzed by AFM. I predicted that the viral building blocks would preferentially assemble vertically on the gold surface due to the arrangement of the cysteine groups displayed on the surface of the mutated form of the viral building blocks. The thiol moieties displayed on the 1cys viral building blocks are partially recessed within a groove created by the C-terminal arm of the coat protein as seen in Figure 5.2a. This arrangement permits the cysteine residues to be accessible to small

molecules in solution, but should prevent the reactive thiol residues from interacting with the gold surface to promote vertical assembly of the viral building blocks. As seen in Figure 5.2a, at the 3' end of the 1cys viral building blocks, the cysteine residues should not be hindered by the secondary structure of the coat protein and should be accessible for binding to the gold surface. The vertical assembly of full-length 1cys TMV on a gold surface has been observed previously by Culver and coworkers[5, 79] yielding precedence for this study. Importantly, the height of the vertically assembled viruses should be governed by the length of the viral building blocks used as seen in Figure 5.2b. Thus, I predicted that the height of vertically assembled viral building blocks could be tuned based on the length of the viral building blocks employed.

Figure 5.5 shows a representative AFM image of the resulting products of the assembly of 1200 b 1cys viral building blocks on a gold surface. The viral building blocks are horizontally arranged and not vertically arranged as predicted. Based on these findings, I arrived at several theories to elucidate the cause for horizontal assembly of the viral building blocks and implemented alternative methods to facilitate the vertical assembly of the 1cys viral building blocks. Firstly, I hypothesized that the shear force resulting from evaporation of the drop of viral building block solution on the gold surface resulted in the horizontal assembly of the 1cys viral building blocks. As the drop of solution evaporated, the force of the solution being

evaporated pushed the 1cys viral building blocks down into a horizontal arrangement or the 1cys viral building blocks did not have enough time to contact the gold surface in a vertical orientation before evaporation commenced. To test this hypothesis and facilitate the vertical assembly of 1cys viral building blocks, I modified the conditions used for the vertical assembly of the 1cys viral building blocks. To inhibit evaporation, a drop of the 1cys viral building blocks was incubated on a gold surface under a large glass Petri dish sealed with vacuum grease in a humidity chamber under constant humidity. Under these conditions, the drop of 1cys viral building block solution did not evaporate, but the AFM image of the resulting assembly of 1cys viral building blocks on the gold surface revealed them to be arranged horizontally. In another attempt to significantly reduce the affects of evaporation and promote the vertical assembly of the 1cys viral building blocks, I incubated the gold surface in a solution of 1cys viral building blocks in a closed Eppendorf tube. Again the resulting assembly of the 1cys viral building blocks under these conditions was also horizontal.

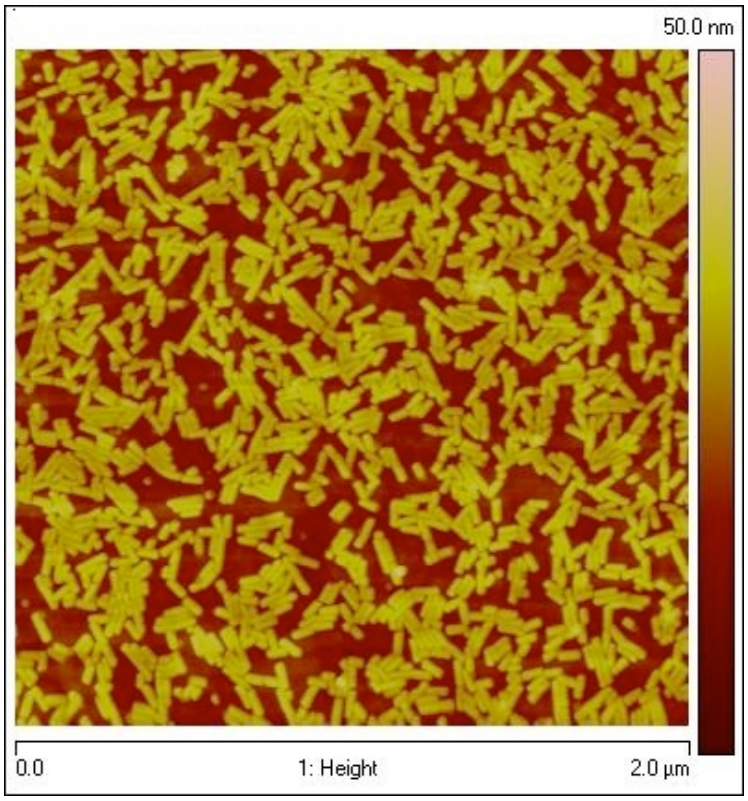

Figure 5.5 Representative AFM image of the results of 1cys viral building blocks assembled on a gold surface. A drop of 1.5 mg/mL of 1cys viral building blocks in 40 mM sodium phosphate buffer pH 7 was pipetted on a hydrogen flame annealed gold surface and incubated overnight under a sealed glass Petrie dish in a humidity chamber. The gold surface was then washed in distilled water and dried with nitrogen gas. The resulting assembly was analyzed by AFM.

I next examined the effects of the aspect ratio (i.e. length) of the viral building blocks and their concentration on the orientation of assembly on gold surfaces. I employed 602 b viral building blocks with a shorter aspect ratio than the 1200 b viral building blocks to examine if the shorter aspect ratio would promote the vertical assembly of the viral building blocks. Additionally, I investigated the concentration dependence of vertical assembly by increasing the concentration of 1200 b 1cys viral building blocks from 1 mg/mL to 6 mg/mL. Both the higher concentration and the shorter aspect ratio of 1cys viral building blocks did not result in the vertical assembly of the 1cys viral building blocks on a gold surface as illustrated in the AFM images collected of the resulting assembly products. Together, these results demonstrate that under the conditions examined vertical assembly of 1cys viral building blocks was not achieved. Further study of alternative methods for 1cys viral building block assembly on gold surfaces may reveal the appropriate conditions to achieve vertical assembly of 1cys viral building blocks on gold surfaces. Previously, I had been limited to minimal concentrations of 1cys viral building blocks (~1 mg/mL). By increasing the concentration of the 1cys viral building block solution and incubating it with the gold surface in a closed Eppendorf tube to concurrently minimize the effects of evaporation, I predict the observation of the assembly of vertically oriented 1cys viral building blocks.

5.2.3 Functionalization of Viral Building Blocks with Small Molecules

Next, I studied the functionalization of 1cys viral building blocks with three small molecules: fluorescein, Nanogold and green fluorescent protein (GFP). For this I exploited the thiol reactive groups displayed on the surface of the 1cys viral building blocks for conjugation with the maleimide-functionalized small molecules employed. Importantly, I investigated the relationship between the length of the viral building blocks, which governs the number of cysteine groups available for functionalization, and the number of small molecules associated with each viral building block as seen in Figure 5.3. Thus, I predicted that the extent of functionalization is dependent upon the length of the viral building block employed.

I first investigated the functionalization of 1cys viral building blocks with fluorescein maleimide. For this, I reacted 1200 b 1cys viral building blocks with fluorescein maleimide. I then used Sephadex G10 resin for size-exclusion chromatography to purify the unreacted, excess fluorescein maleimide from the fluorescein-functionalized viral building blocks. The products resulting from the reaction of fluorescein maleimide with 1200 b 1cys viral building blocks were analyzed by UV/Vis spectrometry. Figure 5.6 shows the UV/Vis spectra obtained from the products of the reaction of 1200 b 1cys viral building blocks with fluorescein maleimide after purification. Peaks at 260 nm/280 nm for 1200 b viral building blocks (WT

& 1cys) represent the presence of RNA and proteins that comprise the viral building blocks. The peak at 495 nm represents the presence of fluorescein. Importantly, the peak for fluorescein at 495 nm is greater for the reaction of 1cys viral building blocks with fluorescein maleimide than for the reaction of WT viral building blocks with fluorescein maleimide. This result illustrates that more of the fluorescein maleimide is associated with the 1cys vial building blocks than the WT viral building blocks, which signifies that the fluorescein maleimide has reacted specifically with the reactive thiols displayed on the 1cys mutated form of the viral building blocks and not with the WT form of the viral building blocks.

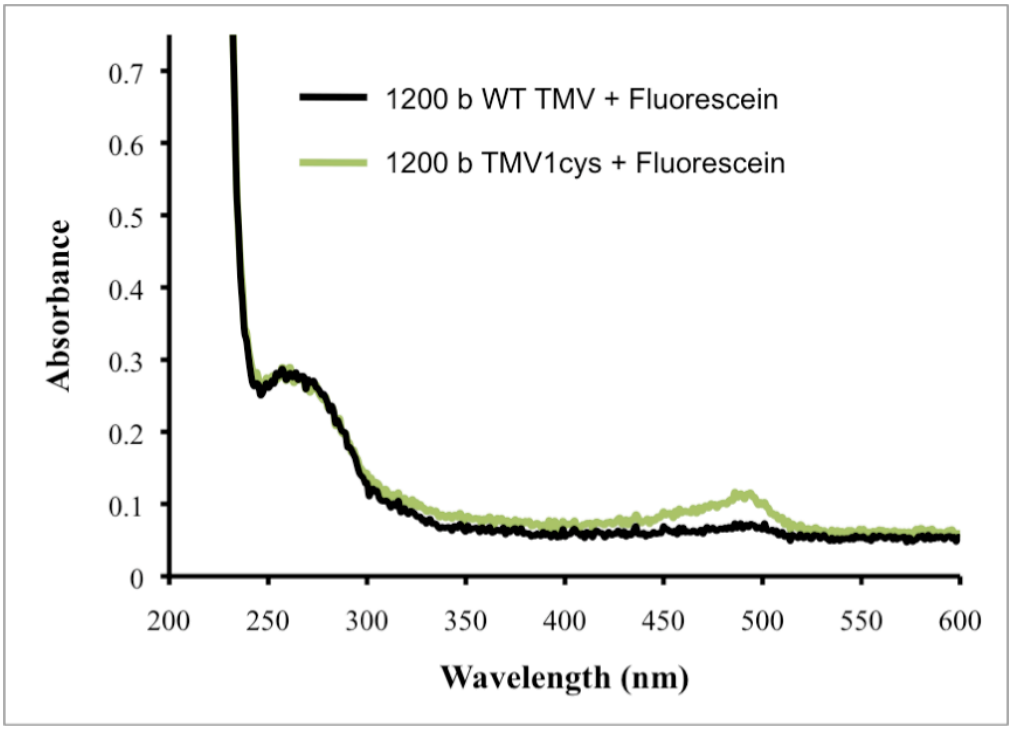

Figure 5.6 UV/Vis spectra obtained for the products of the fluorescein functionalization of 1200 b WT and 1cys viral building blocks.

Next, I applied fluorescein functionalization to 602 b viral building blocks to further examine the length dependence of viral building blocks on the extent of functionalization with small molecules. For this, I reacted the same number of moles of 602 b and 1200 b 1cys viral building blocks with fluorescein maleimide so that the same number of viral building blocks of each length was studied. Because the number of chemically reactive cysteine residues is dependent upon the length of the viral building block, the same number of 602 b 1cys viral building blocks (28 nm) will display one half the number of cysteine residues as the same number of 1200 b 1cys viral building blocks (56 nm). Thus, the same number of 602 b 1cys viral building blocks will conjugate one half the number of fluorescein molecules as the same number of 1200 b 1cys viral building blocks will. To purify 602 b and 1200 b fluorescein-functionalized viral building blocks from excess, unreacted fluorescein, I utilized membrane filtration chromatography. Using this purification method, the fluorescein maleimide should move through the membrane filter leaving behind the fluorescein-functionalized viral building blocks, which can be collected and analyzed.

Figure 5.7 shows the UV/Vis spectra of the purified products of the reaction of the same number of 602 b and 1200 b viral building blocks with fluorescein maleimide. A peak at 260 nm/280 nm for both the 602 b and 1200 b viral building blocks represents the presence of the RNA and coat

proteins that compose the viral building blocks. Notably, the 260 nm/280 nm peak is higher for the 1200 b viral building blocks when compared to the 602 b viral building blocks. This finding confirms that the same number of 1200 b viral building blocks includes more coat protein and RNA than the same number of 602 b viral building blocks. This is because the 1200 b viral building block is two times the length of the 602 b viral building block and thus will display more reactive cysteines for functionalization. Additionally, the peaks observed at 495 nm in Figure 5.7 represents the absorbance peak of fluorescein. Importantly, for both the 602 b and 1200 b viral building blocks, fluorescein is present in both the WT and 1cys samples. In addition, the absorbance peak for fluorescein is greater for the 1200 b viral building blocks than the 602 b viral building blocks. This result demonstrates that at the higher concentrations studied, fluorescein is not reacting specifically with the chemically reactive thiol residues displayed on the 1cys mutants of the viral building blocks but is also reacting with the WT viral building blocks as well. Additionally, the results also illustrate that the amount of fluorescein associated with the viral building blocks is dependent upon the length of the viral building block. Collectively these results demonstrate that the same number of 1200 b viral building blocks displays more cysteine residues to be targeted for fluorescein functionalization in comparison to 602 b viral building blocks because the 1200 b viral building blocks are longer than 602 b viral building blocks. Furthermore, while the fluorescein functionalization was

not specific for conjugation to the chemically reactive thiol residues displayed on the 1cys viral building blocks, the number of fluorescein molecules associated with the viral building blocks is dependent upon the length of the viral building blocks employed.

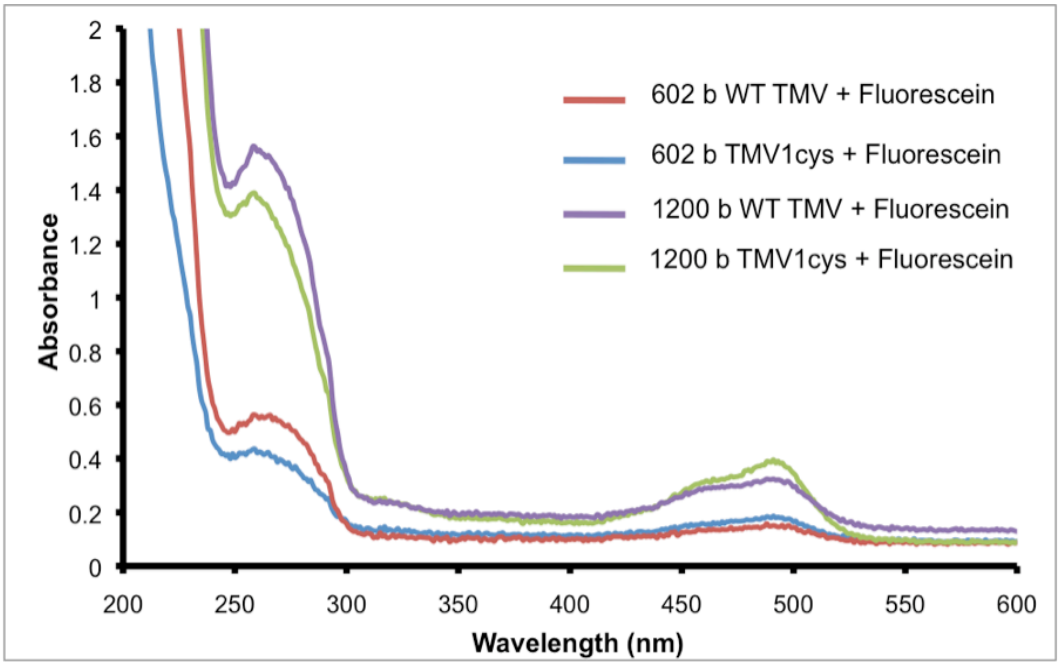

Figure 5.7 UV/Vis spectra of the resulting products from the fluorescein functionalization of 602 b and 1200 b viral building blocks.

Next, to promote the cysteine-specific conjugation of fluorescein to the viral building blocks, I modified the reaction conditions to inhibit fluorescein from being associated with the WT viral building blocks. I first hypothesized that fluorescein maleimide, a hydrophobic molecule, was interacting with the hydrophobic residues displayed on the surface of the viral building blocks[83]. In addition, I also predicted that the benzene rings of fluorescein maleimide were interacting with the aromatic side chains displayed on the surface of TMV, such as that of tyrosine, by pi-pi stacking[84]. To inhibit these interactions between fluorescein maleimide and the viral building blocks, during purification via membrane filtration chromatography, I used a solution of 60% DMSO to wash the fraction of the sample retained by the membrane filter, specifically the fluorescein-functionalized viral building blocks. I predicted that the addition of DMSO to the wash solution during purification would disrupt the hydrophobic or pi-pi stacking interactions to eliminate the association of fluorescein maleimide from the WT viral building blocks[85]. To test my hypothesis, I reacted 1200 b WT viral building blocks and full-length WT TMV with fluorescein maleimide and while purifying the reactions via membrane filtration chromatography, used 60% DMSO to wash the fluorescein-functionalized viral building blocks and TMV respectively. The resulting UV/Vis spectra of the purified products of the fluorescein maleimide reaction with 1200 b WT viral building blocks and full-length WT TMV showed absorbance peaks at 260 nm/280 nm demonstrating the presence

of coat proteins and RNA (i.e. 1200 b viral building blocks and full-length TMV). In addition, a significant absorbance peak at 495 nm, representing the presence of fluorescein, was also present for both the 1200 b WT viral building block and full-length WT TMV samples. This result demonstrates that washing WT viral building blocks or full-length TMV after incubation with fluorescein maleimide with 60% DMSO during purification by membrane filtration chromatography is not sufficient enough to inhibit the association of fluorescein maleimide with the WT coat proteins of viral building blocks or even the full-length virus. Alternative reaction conditions and/or methods of purification should be explored to further reduce the interaction of WT viral building blocks and fluorescein maleimide in order to exploit the cysteine-specific conjugation of fluorescein to the viral building blocks, whose extent of functionalization should be length dependent.

Next, I explored the functionalization of viral building blocks with mono-maleimide Nanogold to demonstrate the length dependence of the viral building blocks on the extent of functionalization by small molecules targeting the cysteine groups displayed on the 1cys mutant viral building blocks. Mono-maleimide Nanogold is a 1.4 nm diameter gold particle that will covalently bind to 1cys viral building blocks by maleimide-thiol conjugation. Again, I predicted the number of Nanogold particles that bind to the 1cys viral building blocks should be governed by the length of the

viral building block employed and thus, the number of cysteine residues displayed for conjugation. To elucidate the appropriate reaction and purification conditions for the reaction of mono-maleimide Nanogold with 1cys viral building blocks, I first employed full-length TMV as an analogue of the viral building blocks. For this, I reacted both WT and 1cys full-length virus with mono-maleimide Nanogold. The reactions were purified by membrane filtration chromatography and analyzed by TEM without further staining. In the TEM images collected for both the WT and 1cys full-length TMV reacted with mono-maleimide Nanogold, full-length TMV is observed. This result illustrates that the Nanogold has interacted with both the WT and 1cys TMV because without the electron dense Nanogold particles associated with the TMV, the TMV would not be visible by TEM since no further staining was employed during TEM sample preparation. Because of this, the results suggest that the mono-maleimide Nanogold did not specifically conjugate to the reactive thiol groups displayed on the 1cys mutant of TMV and instead interacted with both the 1cys and WT forms of TMV.

To promote the cysteine-specific conjugation of mono-maleimide Nanogold to TMV and reduce the interaction with WT TMV, I hypothesized that the hydrophobic polymer coating used on the Nanogold particles to prevent their aggregation in solution was interacting with the hydrophobic residues displayed on the surface of the virus. To inhibit this interaction, I

added 0.1% Tween 20 to the reaction mixture and used a solution of 60% DMSO to wash the Nanogold-labeled TMV's during purification by membrane filtration chromatography. The addition of Tween 20 to the reaction mixture in conjunction with the addition of DMSO to the purification method did not prevent the Nanogold from interacting with the WT TMV as the TEM images collected for both WT and 1cys TMV reacted with mono-maleimide Nanogold revealed the presence of TMV without additional staining. This result demonstrates that the addition of 0.1% Tween 20 to the reaction mixture and 60% DMSO to the purification method is not sufficient to inhibit the interaction of mono-maleimide Nanogold with WT TMV. As such, based on the conditions used in this study, it was not advantageous to attempt to functionalize the viral building blocks with Nanogold to demonstrate the predicted cysteine-specific functionalization of viral building blocks, the extent of which should be governed by the length of viral building block employed. Further studies are necessary to elucidate the appropriate reaction and purification conditions to eliminate the interaction of mono-maleimide Nanogold with WT virus and viral building blocks in order to demonstrate the cysteine-specific maleimide conjugation of Nanogold to the 1cys mutant of virus and viral building blocks, such that the number of Nanogold particles covalently bound to the viral building block will be dependent upon the length of viral building block employed.

Finally, I examined the conjugation of green fluorescent protein (GFP) to viral building blocks to demonstrate that the extent of functionalization of viral building blocks should be dependent upon the number of reactive thiol groups displayed on the 1cys mutant, which is governed by the length of viral building blocks employed. For this, I followed the reaction scheme detailed in Figure 5.8. First, I reacted TMV 1cys with maleimide-C3-NTA. Once the NTA functionality was attached to the virus, I then incorporated Ni^{2+} ions to be chelated by NTA. His-tagged GFP was then added to the Ni^{2+}-NTA-functionalized TMV to chelate the metal ions and functionalize the virus with GFP. Excess, unreacted GFP was removed by membrane filtration chromatography. The resulting products were visualized by TEM after uranyl acetate staining. Figure 5.9 shows representative TEM images collected of the resulting products from the reaction of GFP conjugation to full-length 1cys TMV and 1200 b 1cys viral building blocks when GFP is not in excess. Figure 5.9a shows the presence of GFP associated with the full-length 1cys TMV. Figure 5.9b shows the presence of 1200 b 1cys viral building blocks without any GFP observed. This result demonstrates that under the reaction conditions employed, GFP did not conjugate to the 1200 b 1cys viral building blocks.

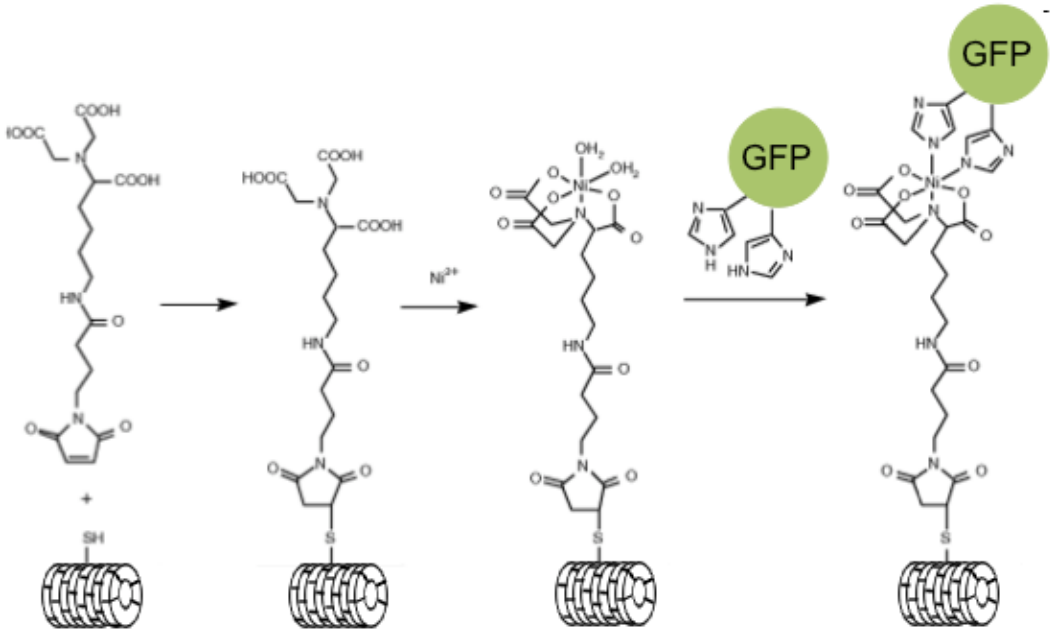

Figure 5.8 Schematic representation of the functionalization of viral building blocks with green fluorescein protein (GFP) via a NTA linker followed by chelation of nickel and binding of His-tagged GFP

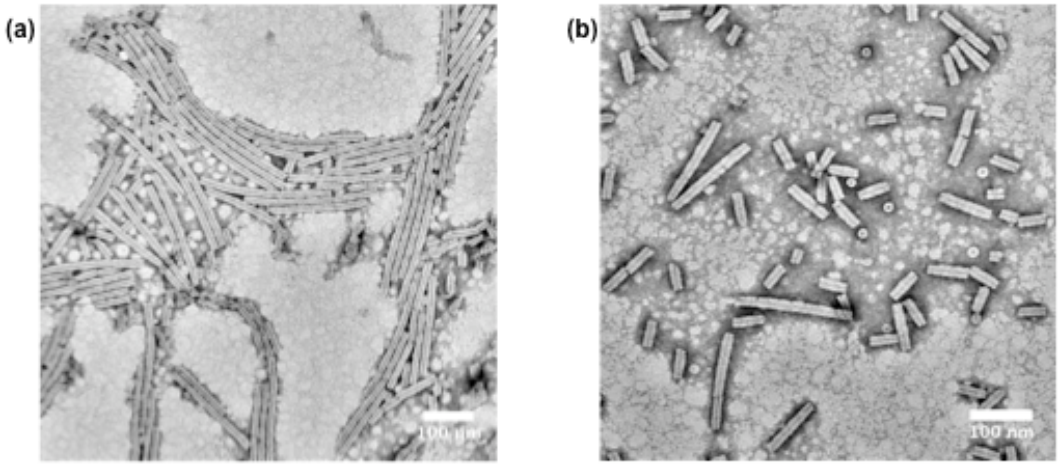

Figure 5.9 TEM images of GFP functionalization. (a) Full-length 1cys TMV conjugated with GFP (b) 1200 b 1cys viral building blocks conjugated with GFP

To facilitate the conjugation of GFP to 1200 b 1cys viral building blocks, I next hypothesized that increasing the concentration of GFP used in the functionalization of the viral building blocks would increase the reaction yield of GFP-conjugated 1cys viral building blocks. I first studied the method of purification for separating excess, unreacted GFP from the GFP-conjugated viral building blocks. For this, I employed bovine serum albumin (BSA) as an analogue of GFP. BSA (6.6×10^4 Da) has a similar molecular weight as GFP (2.7×10^4 Da), which makes BSA a suitable substitution for GFP in the purification method studies. I examined the use of size exclusion chromatography using Sephadex G75 resin and membrane filtration chromatography using a membrane with MWCO of 300 kDa. With both size exclusion chromatography and membrane filtration chromatography, BSA and the 1200 b viral building blocks eluted at the same time. This result illustrates that under the purification conditions tested, the separation of unreacted, excess GFP from GFP-conjugated 1200 b viral building blocks would not be possible. Further purification methods should be explored to elucidate the appropriate conditions necessary to eliminate excess, unreacted GFP from GFP-conjugated viral building blocks in order to demonstrate the length dependent functionalization of 1cys viral building blocks.

5.3 Conclusions

In this chapter, I examined the application of 1cys viral building blocks by targeting the chemically reactive cysteine residues displayed by the mutant form of the viral building blocks. As seen in Figure 5.4, I first studied the metallization of 1cys viral building blocks. In this study, I investigated my prediction that the number of metallic nanoparticles formed on the surface of the 1cys viral building blocks is limited to the number of cysteine residues displayed on the 1cys mutant viral building block, which is directly dependent upon the length of the viral building block. Although the 1cys viral building blocks successfully functioned as a biological template for the synthesis of metallic nanoparticles, it was not possible to determine the number of platinum metal nanoparticles synthesized per viral building block due to the aggregation of the metalized viral building blocks following preparation for TEM analysis. Next, as seen in Figure 5.2, I examined the vertical assembly of 1cys viral building blocks on gold surfaces to form a vertically patterned template of viral building blocks, which could later be functionalized, where the height of the vertical assembly could be specifically tuned based on the length of viral building blocks employed. Despite the myriad of assembly conditions tested, the vertical assembly of 1cys viral building blocks was not observed (Figure 5.5). Next, I investigated the functionalization of 1cys viral building blocks using small molecules, including fluorescein, Nanogold and GFP, as seen in Figure 5.3. The labeling of viral building

blocks with these small molecules all exploited the chemically reactive thiol moieties displayed on the 1cys mutant of viral building blocks for reaction with a maleimide-functionalized small molecule. I hypothesized that the number of small molecules bound to a 1cys viral building block is dependent upon the number of cysteine residues displayed, which is directly governed by the length of the viral building block. While the results show that the extent of functionalization of viral building blocks is length dependent by the association of fluorescein with 602 b and 1200 b viral building blocks as seen in Figure 5.6, I was unable to demonstrate the cysteine-specific conjugation of small molecules to the 1cys viral building blocks. Additional exploratory studies of functionalization with Nanogold and GFP employing full-length virus as an analogue of viral building blocks also did not yield satisfactory results for the cysteine-specific binding of these small molecules. Further studies are necessary to elucidate the necessary reaction and purification conditions to exploit the number of cysteine groups displayed on the surface of the viral building blocks for the cysteine-specific functionalization of viral building blocks.

5.4 Future Directions

The results of my studies concerning the application of viral building blocks obtained in this chapter offer the opportunity for additional investigation of alternative methods for exploring the hypothesis that the extent of functionalization of 1cys viral building blocks will be dependent upon the length of the 1cys viral building blocks and thus the number of cysteine residues displayed. When studying the metallization of 1cys viral building blocks, TEM sample preparation lead to the aggregation of 1cys viral building blocks with platinum nanoparticles synthesized on their surface. Dilution of the metalized viral building block sample will reduce the number of metalized viral building blocks present, which may reduce the ability of the metalized viral building blocks to aggregate with one another. The observation of individual metalized viral building block would permit the number of platinum nanoparticles synthesized per viral building block to be obtained. Additionally, the studies concerning the vertical assembly of 1cys viral building blocks revealed that the 1cys viral building blocks arranged horizontally on gold surfaces under the reaction conditions studied. To achieve the vertically patterned 1cys viral building blocks on a gold surface, the concentration of the 1cys viral building blocks could be substantially increased by using membrane filtration chromatography before vertical assembly. The increased concentration of 1cys viral building blocks coupled with their incubation with the gold surface in a closed Eppendorf tube will minimize the effects of evaporation

as well as promote the vertical assembly of the 1cys viral building blocks. Finally, the functionalization of viral building blocks with small molecules (fluorescein, Nanogold and GFP) was demonstrated to be length dependent for fluorescein, such that the length of the viral building block determined the extent of functionalization. My attempts at exploiting the number of chemically reactive thiols displayed on the surface of the 1cys viral building blocks to tune the number of small molecules bound to the viral building blocks was unsuccessful as both WT and 1cys forms of the viral building blocks exhibited the same extent of functionalization (Figure 5.7). An alternative method of purification, specifically by sucrose gradient, may establish the conditions necessary to inhibit the thiol-reactive small molecules intended for functionalization of the 1cys viral building blocks from interacting with the WT viral building blocks. Collectively, these proposed studies offer alternative methods to establish the application of viral building blocks by exploiting the cysteine-specific chemical reactivity of 1cys viral building blocks. Furthermore, these proposed studies facilitate the exploration of the hypothesis that the extent of functionalization of the viral building blocks is dependent upon the number of cysteine residues displayed by the viral building blocks employed, which is directly governed by the length of the viral building block.

6 CONCLUSIONS

In summary, the studies presented in this work show the fabrication of viral building blocks with controlled dimensions derived from both WT and genetically engineered 1cys TMV and the exploration of these viral building blocks as individual components and biological templates toward the synthesis of novel nanomaterials from a bottom-up assembly approach.

First, in Chapter 3, I demonstrated the assembly of viral building blocks of controlled dimensions using RNA transcripts of desired length and equilibrated coat proteins from either WT or 1cys TMV. For both WT and 1cys viral building blocks assembled, the lengths of the viral building blocks were consistent and reproducible. This signifies that the length of the viral building block assembled is governed by the length of the RNA transcript employed for assembly and can be readily controlled. Additionally, the synthesis of 1cys viral building blocks indicates that the presence of the chemically reactive thiol groups displayed on the 1cys coat proteins do not inhibit the assembly of 1cys viral building blocks with controlled dimensions.

Next, in Chapter 4, I examined the application of doubly biotinylated WT viral building blocks as components for the assembly of 1D nanoarrays via biotin-streptavidin binding. I first demonstrated the synthesis of 5'

biotoinylated RNA by the incorporation of 5'-Biotin-GMP to the *in vitro* transcription reaction. The synthesis of 3' biotinylated RNA was achieved by the 3' selective oxidation of purified RNA transcripts followed by reaction with hydrazide-functionalized biotin. The resulting RNA transcripts biotinylated at both the 5' and 3' ends were shown to readily assemble with equilibrated coat proteins to form doubly biotinylated viral building blocks. In the presence and absence of streptavidin, oligomers of doubly biotinylated viral building blocks were observed toward the assembly of 1D nanoarrays. Due to the spontaneous end-to-end aggregation of viral building blocks, the assembly of 1D nanoarrays driven by biotin-streptavidin could not be conclusively determined.

Finally, in Chapter 5, I explored alternative applications of viral building blocks of controlled dimensions. Specifically, I studied the use of 1cys viral building blocks to exploit the cysteine residues displayed on the surface of the mutated form of viral building blocks for thiol-specific conjugation chemistry. Additionally, I examined the hypothesis that the length of the 1cys viral building block and hence the number of cysteine residues displayed by the viral building block will govern the number of small molecules to be conjugated to the 1cys viral building blocks. First, I showed the application of 1cys viral building blocks for the synthesis of platinum metal nanoparticles, such that metal nanoparticles were observed to be synthesized only on the surface of 1cys viral building

blocks and not in the bulk solution. But due to aggregation of the metalized viral building blocks, the number of metal nanoparticles synthesized per 1cys viral building block could not be resolved. Next, I examined the preferential vertical assembly of 1cys viral building blocks on gold surfaces by exploring the spatial orientation of the cysteine groups displayed on the 1cys viral building blocks. Through my examination, I show numerous conditions that were explored to promote the preferential vertical assembly of 1cys viral building blocks, though only the horizontal assembly of viral building blocks was achieved. Lastly, I studied the application of 1cys viral building blocks for functionalization by small molecules and examined the prediction that the extent of functionalization will be dependent upon the length of the 1cys viral building block employed. Here I demonstrated the length dependent fluorescein functionalization of 1cys viral building blocks. Additionally, using full-length TMV, I examined conditions for the functionalization of 1cys viral building blocks by mono-maleimide Nanogold and conjugation by maleimide-C3-NTA followed by chelation of Ni^{2+} ions and then GFP.

While the complete application of viral building blocks was not fully realized in this study, significant progress was made toward the elucidation of the conditions necessary to exploit the controlled dimensions of the viral building blocks for components of novel nanomaterials. Additionally, alternative methods are proposed and

discussed, based on the results garnered in this study, to overcome the obstacles encountered and achieve the objection of this study. For example, although the length dependent functionalization of viral building blocks was observed by reaction with fluorescein, the cysteine-specific functionalization of 1cys viral building blocks was not observed as the maleimide derived small molecules employed for thiol-specific conjugation with 1cys viral building blocks interacted similarly with both the WT and 1cys viral building blocks. Further study of the reaction and/or purification conditions should assist toward realizing the cysteine-specific and thus length dependent functionalization of 1cys viral building blocks.

In conclusion, I believe the assembly of viral building blocks of controlled dimensions derived from TMV offers a novel approach to fabricate a biological unit in the nanoscale whose dimensions are precise and can be readily tuned. These viral building blocks are robust and can be functionalized to perform as a biological template or be employed as the individual components of hierarchical nanoarchitectures for the bottom-up assembly of nanomaterials. Furthermore, I anticipate that the applications for the viral building blocks examined in this thesis has established the foundation for further studies which will result in the realization of the viral building blocks of controlled dimensions as functional biologically templated nanocatalysts and nanomaterials.

7 REFERENCES

[1] B. R. Cuenya, *Thin Solid Films*, *518*, 3127.

[2] G. Drummen, *International Journal of Molecular Sciences* **2010**, *11*, 154.

[3] L. Lee, Z. Niu, Q. Wang, *Nano Research* **2009**, *2*, 349.

[4] N. F. Steinmetz, D. J. Evans, *Organic & Biomolecular Chemistry* **2007**, *5*, 2891.

[5] E. Royston, A. Ghosh, P. Kofinas, M. T. Harris, J. N. Culver, *Langmuir* **2008**, *24*, 906.

[6] K. T. Nam, D.-W. Kim, P. J. Yoo, C.-Y. Chiang, N. Meethong, P. T. Hammond, Y.-M. Chiang, A. M. Belcher, *Science* **2006**, *312*, 885.

[7] T. L. Schlick, Z. Ding, E. W. Kovacs, M. B. Francis, *Journal of the American Chemical Society* **2005**, *127*, 3718.

[8] Y.-Z. Ma, R. A. Miller, G. R. Fleming, M. B. Francis, *The Journal of Physical Chemistry B* **2008**, *112*, 6887.

[9] Y. S. Nam, A. P. Magyar, D. Lee, J.-W. Kim, D. S. Yun, H. Park, T. S. Pollom, D. A. Weitz, A. M. Belcher, *Nat Nano*, *5*, 340.

[10] C. Yang, A. K. Manocchi, B. Lee, H. Yi, *Applied Catalysis B: Environmental*, *93*, 282.

[11] C. M. Niemeyer, *Angewandte Chemie International Edition* **2001**, *40*, 4128.

[12] E. R. Ballister, A. H. Lai, R. N. Zuckermann, Y. Cheng, J. D. Mougous, *Proceedings of the National Academy of Sciences* **2008**, *105*, 3733.

[13] F. F. Miranda, K. Iwasaki, S. Akashi, K. Sumitomo, M. Kobayashi, I. Yamashita, J. R. H. Tame, J. G. Heddle, *Small* **2009**, *5*, 2077.

[14] A. Klug, *Philosophical Transactions of the Royal Society of London. Series B: Biological Sciences* **1999**, *354*, 531.

[15] J. N. Culver, *Annual Review of Phytopathology* **2002**, *40*, 287.

[16] H. Yi, S. Nisar, S.-Y. Lee, M. A. Powers, W. E. Bentley, G. F. Payne, R. Ghodssi, G. W. Rubloff, M. T. Harris, J. N. Culver, *Nano Letters* **2005**, *5*, 1931.

[17] H. Yi, G. W. Rubloff, J. N. Culver, *Langmuir* **2007**, *23*, 2663.

[18] A. K. Manocchi, N. E. Horelik, B. Lee, H. Yi, *Langmuir* **2009**, *26*, 3670.

[19] S-Y. Lee, J. Choi, E. Royston, D. B. Janes, J. N. Culver, M. T. Harris *J. Nanosci. Nanotech.* **2006**, *6*, 974.

[20] W. Shenton, T. Douglas, M. Young, G. Stubbs, S. Mann, *Advanced Materials* **1999**, *11*, 253.

[21] Y. Okada *Adv. Biophys.*, **1986**, *22*, 95.

[22] D. Zimmern *Cell*, **1977**, *11*, 463.

[23] P. J. G. Butler, *J Gen Virol* **1984**, *65*, 253.

[24] G. Lebeurier, A. Nicolaieff, K. E. Richards *Proc. Natl. Sci. Acad. USA*, **1977**, *74*, 149.

[25] T. M. Schuster, R. B. Scheele, M. L. Adams, S. J. Shire, J. J. Steckert, M. Potschka *Biophys. J.*, **1980**, *10*, 313.

[26] D. R. Turner, C. J. McGuigan, P. J. G. Butler, *J. Mol. Biol.*, **1989**, *209*, 407.

[27] G. P. Lomonossoff, P. J. G. Butler, *FEBS Lett.*, **1980**, *113*, 271.

[28] A. S. Blum, C. M. Soto, C. D. Wilson, T. L. Brower, S. K. Pollack, T. L. Schull, A. Chatterji, T. Lin, J. E. Johnson, C. Amsinck, P. Franzon, R. Shashidhar, B. R. Ratna, *Small* **2005**, *1*, 702.

[29] M. Fischlechner, E. Donath, *Angewandte Chemie International Edition* **2007**, *46*, 3184.

[30] C. Yang, A. K. Manocchi, B. Lee, H. Yi, *Journal of Materials Chemistry*, *21*, 187.

[31] P. J. G. Butler, *Philosophical Transactions of the Royal Society of London. Series B: Biological Sciences* **1999**, *354*, 537.

[32] K. Namba, G. Stubbs, *Science* **1986**, *231*, 1401.

[33] M. Knez, A. M. Bittner, F. Boes, C. Wege, H. Jeske, E. Mail, K. Kern, *Nano Letters* **2003**, *3*, 1079.

[34] T. L. Schlick, Z. Ding, E. W. Kovacs, M. B. Francis, *J. Am. Chem. Soc.,* **2005**, *127*, 3718.

[35] M. A. Bruckman, G. Kaur, L. A. Lee, F. Xie, J. Sepulveda, R. Breitenkamp, X. Zhang, M. Joralemon, T. P. Russell, T. Emrick, Q. Wang, *ChemBioChem* **2008**, *9*, 519.

[36] Z. Niu, J. Liu, L. A. Lee, M. A. Bruckman, D. Zhao, G. Koley, Q. Wang, *Nano Letters* **2007**, *7*, 3729.

[37] E. Dujardin, C. Peet, G. Stubbs, J. N. Culver, S. Mann, *Nano Letters* **2003**, *3*, 413.

[38] M. Knez, M. Sumser, A. M. Bittner, C. Wege, H. Jeske, T. P. Martin, K. Kern, *Adv. Funct. Mater.* **2004**, *14*, 116.

[39] M. Knez, M. Sumser, A. M. Bittner, C. Wege, H. Jeske, S. Kooi, M. Burghard, K. Kern, *J. Electroanal. Chem.* **2002**, *522*, 70.

[40] S. Balci, A. M. Bittner, K. Hahn, C. Scheu, M. Knez, A. Kadri, C. Wege, H. Jeske, K. Kern, *Electrochimica Acta* **2006**, *51*, 6251.

[41] S-Y. Lee, E. Royston, J. N. Culver, M. T. Harris, *Nanotechnology* **2005**, *16*, S435.

[42] C. Yang, A. K. Manocchi, B. Lee, H. Yi, *Applied Catalysis B: Environmental*, *93*, 282.

[43] F. Sainsbury, M. C. Caizares, G. P. Lomonossoff, *Annual Review of Phytopathology* **2010**, *48*, 437.

[44] G. P. Lomonossoff, J. E. Johnson, *Progress in Biophysics and Molecular Biology* **1991**, *55*, 107.

[45] T. Lin, J. E. Johnson, F. A. M. Karl Maramorosch, J. S. Aaron, in *Advances in Virus Research, Vol. Volume 62*, Academic Press, **2003**, pp. 167.

[46] J. A. Speir, S. Munshi, G. Wang, T. S. Baker, J. E. Johnson *Structure* **1995**, *3*, 63.

[47] Q. Wang, T. Lin, L. Tang, J. E. Johnson, M. G. Finn, *Angewandte Chemie International Edition* **2002**, *41*, 459.

[48] S. Meunier, E. Strable, M. G. Finn, *Chemistry & Biology* **2004**, *11*, 319.

[49] E. Strable, J. E. Johnson, M. G. Finn, *Nano Letters* **2004**, *4*, 1385.

[50] N. F. Steinmetz, G. P. Lomonossoff, D. J. Evans, *Langmuir* **2006**, *22*, 3488.

[51] N. Steinmetz, G. Lomonossoff, D. Evans, *Small* **2006**, *2*, 530.

[52] N. F. Steinmetz, S. N. Shah, J. E. Barclay, G. Rallapalli, G. P. Lomonossoff, D. J. Evans, *Small* **2009**, *5*, 813.

[53] T. Douglas, M. Young, *Nature* **1998**, *393*, 152.

[54] M. T. Klem, M. Young, T. Douglas, *Journal of Materials Chemistry* **2008**, *18*, 3821.

[55] G. P. Smith, *Science* **1985**, *228*, 1315.

[56] S. S. Sidhu, *Biomolecular Engineering* **2001**, *18*, 57.

[57] D. A. Marvin, *Current Opinion in Structural Biology* **1998**, *8*, 150.

[58] G. P. Smith, V. A. Petrenko, *Chemical Reviews* **1997**, *97*, 391.

[59] A. Merzlyak, S.-W. Lee, *Current Opinion in Chemical Biology* **2006**, *10*, 246.

[60] S. R. Whaley, D. S. English, E. L. Hu, P. F. Barbara, A. M. Belcher, *Nature* **2000**, *405*, 665.

[61] C. Mao, C. E. Flynn, A. Hayhurst, R. Sweeney, J. Qi, G. Georgiou, B. Iverson, A. M. Belcher, *Proc. of the Natl. Acad. Sci. USA* **2003**, *100*, 6946.

[62] Y. S. Nam, A. P. Magyar, D. Lee, J.-W. Kim, D. S. Yun, H. Park, T. S. Pollom, D. A. Weitz, A. M. Belcher, *Nat. Nano.* **2011**, *5*, 340.

[63] Y. Huang, C. Y. Chiang, S. K. Lee, Y. Gao, E. L. Hu, J. De Yoreo, A. M. Belcher *Nano Lett.*, **2005**, *5*, 1429.

[64] A. Merzlyak, S. Indrakanti, S.-W. Lee, *Nano Lett.,* **2009**, *9*, 846.

[65] W.-J. Chung, A. Merzlyak, S. Y. Yoo, S.-W. Lee, *Langmuir*, **2010**, *26*, 9885.

[66] A. Mueller, F. J. Eber, C. Azucena, A. Petershan, A. M. Bittner, H. Gliemann, H. Jeske, C. Wege, *ACS Nano*, **2011**, *5*, 4512.

[67] H. Inoue, Y. Hayase, S. Iwai, E. Ohtsuka, *FEBS Lett* **1987**, *215*, 327.

[68] B. S. Sproat, A. I. Lamond, B. Beijer, P. Neuner, U. Ryder, *Nucleic Acids Res.* **1989**, *17*, 3373.

[69] J. L. Oakley, J. E. Coleman *Proc. Natl. Sci. Acad. USA*, **1977**, *74*, 4266.

[70] K. E. Richards, R. C. Williams, *Proc. Natl. Acad. Sci. USA*, **1972**, *69*, 1121.

[71] U. T. Ruegg, J. Rudinger, *Methods Enzymol.*, **1977**, *47*, 111.

[72] A. C. H. Durham, J. T. Finch, A. Klug, *Nature New Biology,* **1971**, *229*, 37.

[73] R. A. McMillan, C. D. Paavola, J. Howard, S. L. Chan, N. J. Zaluzec, J. D. Trent, *Nature Materials*, **2002**, *1*, 247.

[74] H. Bui, C. Onodera, C. Kidwell, Y. Tan, E. Graugnard, W. Kuang, J. Lee, W. B. Knowlton, B. Yurke, W. L. Hughes, *Nano Lett.*, **2010**, *10*, 3367.

[75] N. M. Green, *Methods Enzymol*. **1990**, *184*, 51.

[76] Q. Wang, T. Lin, J. E. Johnson, M. G. Finn, *Chem. Biol.*, **2002**, *9*, 813.

[77] C. Pitulle, R. G. Kleineidam, B. Sproat, G. Krupp, *Gene*, **1992**, *112*, 101.

[78] F. Hansske, F. Cramer, *Methods Enzymol*. **1979**, *59*, 172.

[79] D. K. Willkomm & R. K. Hartmann in *RNA Biochemistry Handbook* (R. K. Hartmann, A. Bindereif, A. Schon, E. Westhof, ed.) **2005**, Wiley-VHC Verlag GmbH & Co., Weinheim, 86.

[80] B. Lu, G. Stubbs, J. N. Culver, *Virology*, **1996**, *225*, 11.

[81] K. Gerasopoulos, M. McCarthy, E. Royston, J. N. Culver, R. Ghodssi, *J. Micromech. Microeng.* **2008**, *18*, 104003

[82] R. A. Miller, A. D. Presley, M. B. Francis, *J. Am. Chem. Soc.,* **2007**, *129*, 3104.

[83] A. C. Bloomer, J. N. Champness, G. Bricogne, R. Staden, A. Klug, *Nature* **1978**, *276*, 362.

[84] K. Namba, R. Pattanayek, G. Stubbs, *J. Mol. Biol.* **1989**, *208*, 307.

[85] L. Ramirez-Silva, J. O-H. S. Uribe in *Encyclopedia of Surface and Colloid Science* (P. Somasundaran, ed). **2006**, Taylor & Francis Group, Boca Raton, FL 5299.